PB-236 675

HEAT TRANSFER AND FLOW FRICTION PERFORMANCE OF HEATED PERFORATED FLAT PLATES

Wen-Jei Yang

Michigan University

Prepared for:

Environmental Protection Agency

June 1973

DISTRIBUTED BY:

NTIS

National Technical Information Service
U. S. DEPARTMENT OF COMMERCE

TECHNICAL REPORT DATA
(Please read Instructions on the reverse before completing)

1. REPORT NO. APTD-1554	2.	PB 236 675
4. TITLE AND SUBTITLE Heat Transfer and Flow Friction Performance of Heated Perforated Flat Plates		5. REPORT DATE June 1973
		6. PERFORMING ORGANIZATION CODE
7. AUTHOR(S) Dr. Wen-Jei Yang		8. PERFORMING ORGANIZATION REPORT NO.
9. PERFORMING ORGANIZATION NAME AND ADDRESS University of Michigan Department of Mechanical Engineering Ann Arbor, Michigan 48105		10. PROGRAM ELEMENT NO.
		11. CONTRACT/GRANT NO. 68-04-0019
12. SPONSORING AGENCY NAME AND ADDRESS U.S. Environmental Protection Agency Office of Air and Water Programs Office of Mobile Source Air Pollution Control Ann Arbor, Michigan 48105		13. TYPE OF REPORT AND PERIOD COVERED Final
		14. SPONSORING AGENCY CODE
15. SUPPLEMENTARY NOTES		

16. ABSTRACT

A large scale modelling technique is developed to examine the effects of perforation geometry on the heat transfer and friction loss performance of compact heat exchanger fins. The test core consists of an electrically heated matal plate and several unheated dummy plates forming flow channels. Both test and dummy plates are identically perforated in a staggered pattern. The cores were tested in a subsonic wind tunnel designed specifically for testing automobile radiators, environmental system condensers, and liquid-to-air heat exchangers. The plate surface porosity, the core frontal porosity, and the perforation size and arrangement were varied. The Reynolds numbers ranged from those corresponding to both laminar and turbulent flow. The heat transfer factor (j), friction factor (f) and their ratio (f/j) for a single plate-channel system are obtained as functions of the Reynolds number, the plate surface porosity and the core frontal porosity. These results represent qualitatively those of a compact plate-fin heat exchanger having the same geometric scaling factors when these systems are represented by appropriate geometric, dynamic and thermodynamic similarity parameters. The technique can be used to understand the performance of compact fin surfaces in order to determine an optimum performation geometry and to form a basis for rational design of compact-heat exchangers.

It is found that under certain circumstances plate perforation will produce significant improvement in heat transfer for the same pressure drop. These studies are directed to the design of air-cooled condensers for Rankine cycle automotive engines, marine power propulsion systems and the dry cooling towers of extra-high capacity electric power plants.

17. KEY WORDS AND DOCUMENT ANALYSIS

a. DESCRIPTORS	b. IDENTIFIERS/OPEN ENDED TERMS	c. COSATI Field/Group

Reproduced by
NATIONAL TECHNICAL
INFORMATION SERVICE
U S Department of Commerce
Springfield VA 22151

18. DISTRIBUTION STATEMENT Unlimited	19. SECURITY CLASS *(This Report)* Unclassified	21. NO. OF PAGES 141
	20. SECURITY CLASS *(This page)* Unclassified	22. PRICE 4.75 - 2.25

i.

EPA Form 2220-1 (9-73)

APTD-1554

HEAT TRANSFER AND FLOW FRICTION PERFORMANCE OF HEATED PERFORATED FLAT PLATES

Prepared By

Dr. Wen-Jei Yang

University of Michigan
Department of Mechanical Engineering
Ann Arbor, Michigan 48105

Contract No. 68-04-0019

EPA Project Officers:

William B. Zeber, Paul Kerwin

Prepared For

U.S. ENVIRONMENTAL PROTECTION AGENCY
Office of Air and Water Programs
Office of Mobile Source Air Pollution Control
Advanced Automotive Power Systems Development Division
Ann Arbor, Michigan 48105

June 1973

1a

The APTD (Air Pollution Technical Data) series of reports is issued by the Office of Air Quality Planning and Standards, Office of Air and Water Programs, Environmental Protection Agency, to report technical data of interest to a limited number of readers. Copies of APTD reports are available free of charge to Federal employees, current contractors and grantees, and non-profit organizations - as supplies permit - from the Air Pollution Technical Information Center, Environmental Protection Agency, Research Triangle Park, North Carolina 27711 or may be obtained, for a nominal cost, from the National Technical Information Service, 5285 Port Royal Road, Springfield, Virginia 22151.

This report was furnished to the U.S. Environmental Protection Agency by The University of Michigan in fulfillment of Contract No. 68-04-0019 and has been reviewed and approved for publication by the Environmental Protection Agency. Approval does not signify that the contents necessarily reflect the views and policies of the agency. The material presented in this report may be based on an extrapolation of the "State-of-the-art." Each assumption must be carefully analyzed by the reader to assure that it is acceptable for his purpose. Results and conclusions should be viewed correspondingly. Mention of trade names or commercial products does not constitute endorsement or recommendation for use.

Publication No. APTD - 1554

ACKNOWLEDGMENTS

The support of the Advanced Automotive Power Systems Development Division, Office of Air Programs, Environmental Protection Agency for this work is gratefully acknowledged. The study was carried out under contract number 68-04-0019. The author wishes to express his appreciation to Messrs. W.B. Zeber and Paul Kerwin, Contract Monitors, for their assistance and encouragement.

During the first phase of the study, Dr. I.C. Macedo designed and tested the experimental apparatus and Dr. J.W. Ou developed a computer program for correlating test data. Professor John A. Clark and Mr. K.H. Choy had participated in the study. Messrs. C.Y. Liang and T.L. Tsai also helped take some test data. The author wishes to extend his thanks to them for having helped to complete this study.

TABLE OF CONTENTS

Page

LIST OF TABLES vi

LIST OF FIGURES vii

NOMENCLATURE ix

ABSTRACT 1

INTRODUCTION 2

EXPERIMENTAL APPARATUS AND PROCEDURE 5

TEST RESULTS AND DISCUSSION 10

CONCLUSIONS 20

REFERENCES 21

FIGURES

COMPUTER PROGRAM FOR CORRELATING TEST DATA

Preceding page blank

LIST OF TABLES

Table		Page
1	Geometrical Dimensions and Arrangement of Oval-Slotted Surfaces	13
2	Uncertainty Intervals	19

LIST OF FIGURES

Figure	Caption
1.	Heat exchanger test core and position of thermocouples
2.	Plate-rectangular perforated fin surface
3.	Wind tunnel
4.	Schematic of electric power supply loop
5.	Schematic of test core installation in wind tunnel
6.	Perforation geometry
7.	(a) f and j versus Re, (b) f/j versus σ_s, (c) f versus σ_s, (d) j versus σ_s, for t/b = 0.141, 1/2" (length) x 1/8" (width) slots in in-line arrangement
8.	for t/b = 0.0665, 1/2" x 1/8" slots in in-line arrangement
9.	for t/b = 0.0321, 1/2" x 1/8" slots in in-line arrangement
10.	for t/b = 0.141, 1/2" x 1/8" slots in overlap arrangement
11.	for t/b = 0.0665,1/2" x 1/8" slots in overlap arrangement
12.	for t/b = 0.0321, 1/2" x 1/8" slots in overlap arrangement
13.	for t/b = 0.141, 2" x 1/8" slots in in-line arrangement
14.	for t/b = 0.0665, 2" x 1/8" slots in in-line arrangement
15.	for t/b = 0.0321, 2" x 1/8" slots in in-line arrangement
16.	for t/b = 0.141, 2" x 1/8" slots in overlap arrangement
17.	for t/b = 0.0665, 2" x 1/8" slots in overlap arrangement
18.	for t/b = 0.0321, 2" x 1/8" slots in overlap arrangement
19.	for t/b = 0.141, 1/2" x 1/16" slots in in-line arrangement
20.	for t/b = 0.0665, 1/2" x 1/16" slots in in-line arrangement
21.	for t/b = 0.0321, 1/2" x 1/16" slots in in-line arrangement
22.	f and j versus Re for t/b = 0.141, slots; (a) through (e) for σ_s = 5.7, 12.8, 17.4, 22.8 and 28.8%, respectively.

LIST OF FIGURES (continued)

23. f and j versus Re for $t/b = 0.0665$, slots; (a) through (e) for $\sigma_s = 5.7$, 12.8, 17.4, 22.8 and 28.8%, respectively.

24. f and j versus Re for $t/b = 0.0321$, slots; (a) through (e) for $\sigma_s = 5.7$, 12.8, 17.4, 22.8, and 28.8%, respectively.

25. (a) f versus Re, (b) f/j versus σ_s, (c) f versus σ_s, and (d) j versus σ_s for $t/b = 0.141$, staggered round holes

26. for $t/b = 0.0665$, staggered round holes

27. for $t/b = 0.0321$, staggered round holes

28. Performance parameters 22 FPI perforated fin [5]

NOMENCLATURE

A	total heat transfer area
A_c	free flow area inside test core
A_i	free flow area at core entrance
A_p	cross-sectional area of test plate in the flow direction
A_w	wetted surface area
a	slot spacing, see Fig. 6
A^*	slot overlap (in flow direction), see Fig. 6
b	plate spacing
C_p	specific heat of air
D_h	hydraulic diameter of the flow channel, $=4A_cL/A_w$; D_{hf}, for friction loss; D_{hj} for heat transfer
d	diameter of round hole
d_s	slot width (in flow direction)
f	fanning friction factor
G	mass velocity
g_c	conversion factor
h	heat transfer coefficient
j	heat transfer factor
K	pressure drop coefficient; K_e, at core exit; K_i, at core entrance
k	thermal conductivity of test plate
L	flow length
ℓ	center-to-center distance between two adjacent holes, see Fig. 6
m	rate of air flow
ΔP	pressure drop; ΔP_{T-S}, total-to-static; ΔP_{s-s}, static-to-static
p	pitch; p_ℓ, longitudinal; p_t, transverse
q_e	rate of heat generation in test section

q	rate of heat conduction into test section
Re	Reynolds number based on hydraulic diameter; R_{ef}, based on D_{hf}; R_{ej}, based on D_{hj}
r_h	hydraulic radius
T	temperature; T_a, or air; T_{ae}, or air at core exit; T_{ai}, of air at core entrance; T_s, of plate surface
ΔT	temperature increase of air in test core
t	plate thickness
V	air flow velocity; V_c, inside core; V_i, at core entrance
w	plate width or height of rectangular fin
w_s	slot length (normal to flow direction)
μ	absolute viscosity of air
ρ	air density; ρ_e, at core exit; ρ_i, at core entrance, ρ_m, inside core
σ	porosity, σ_F, frontal; σ_s, surface (or percent open area)

Subscripts

F	core front
f	for friction loss
j	for heat transfer
s	plate surface or slot

ABSTRACT

A large scale modelling technique is developed to examine the effects of perforation geometry on the heat transfer and friction loss performance of compact heat exchanger fins. The test core consists of an electrically heated metal plate and several unheated dummy plates forming flow channels. Both test and dummy plates are identically perforated in a staggered pattern. The cores were tested in a subsonic wind tunnel designed specifically for testing automobile radiators, environmental system condensers, and liquid-to-air heat exchangers. The plate surface porosity, the core frontal porosity, and the perforation size and arrangement were varied. The Reynolds numbers ranged from those corresponding to both laminar and turbulent flow. The heat transfer factor (j), friction factor (f) and their ratio (f/j) for a single plate-channel system are obtained as functions of the Reynolds number, the plate surface porosity and the core frontal porosity. These results represent qualitatively those of a compact plate-fin heat exchanger having the same geometric scaling factors when these systems are represented by appropriate geometric, dynamic and thermodynamic similarity parameters. The technique can be used to understand the performance of compact fin surfaces in order to determine an optimum performation geometry and to form a basis for rational design of compact-heat exchangers.

It is found that under certain circumstances plate perforation will produce significant improvement in heat transfer for the same pressure drop. These studies are directed to the design of air-cooled condensers for Rankine cycle automotive engines, marine power propulsion systems and the dry cooling towers of extra-high capacity electric power plants.

INTRODUCTION

The cycle efficiency of a steam or gas turbine power plant may be considerably enchanced by the use of a waste heat exchanger. In order to exploit the small size and low weight advantages of the power plant, the compactness of the heat exchanger is an imperative objective in design, with proper considerations given to heat recovery and pressure drop. The need for compactness in such heat exchangers has prompted the use of extended surfaces, surface roughness, boundary layer promoters, and boundary layer interrupters to augment the heat transfer coefficient.

In recent years, a number of studies have been published on the heat transfer and friction loss performance of compact heat exchangers, notably the work of Kays and London [1]. Since this type of heat exchangers deals with low density fluids the friction characteristics of the surface is as important as the heat transfer behavior.

Among the extended surfaces of the plate-fin and tubular types, the louvered-plate-fin surface has been favored because of its high area-to-volume ratio and its higher heat transfer coefficient resulting from boundary layer interruptions. However, the high heat transfer performance is accompanied by high resistance to flow. The perforated-plate-fin surface has heat transfer and friction loss performance comparable to the louvered-plate fin surface. However, the compactness of the louvered fin type heat exchangers is limited by the geometry of the louvers. If very high compactness is required, such as for the condenser in the Rankine-cycle automotive steam power plant, perhaps only the plain-plate-fin surface or perforated-plate-fin surface can serve the purpose. The excellence of the latter surface over the former has been demonstrated in Reference [1].

By virtue of its high heat transfer and low friction loss performance, the perforated fin tubular heat exchangers can be made either in small size and light weight as air-cooled condensers in marine [2,3] and automotive [4] propulsion systems or in large size as air-cooled heat exchangers in dry cooling towers of extra-high capacity electric power plant [5]. Kays [6] has reported that perforation results in a substantial increase in heat transfer performance without introducing a pronounced form drag. This observation was later confirmed by Pucci _et al_. [2] and Shah and Osborn [3]. Wong _et al_. [4] have tested very compact (22 fins per in.) perforated-fin air-cooled condenser cores for Rankine-cycle automotive propulsion systems. Their test data supported the Kays observation. However, a recent work of Mondt and Siegla [7] have indicated some conflict in the generality of these observations. Over a range of area densities (heat transfer area divided by core volume), no significant improvement in heat transfer was observed for the same pressure drop. Miller and Leeman [8] have also concluded no beneficial effect due to perforations.

The present study serves two main purposes: (1) to determine the effects of the system parameters and the Reynolds number on the heat transfer and friction factors of perforated plate surfaces and to rationalize the conflicting performance data previously reported [1,4,7,8]; (2) to determine the system parameters for the optimum performance in the operating range of the Reynolds number. The system parameters include perforation geometry and arrangement, plate thickness-to-spacing ratio, channel length-to-hydraulic diameter ratio, plate surface porosity and frontal core porosity. In order to achieve fine detail, a large scale was chosen, with individual units approximately eight times larger than those fins used in compact condensers. The perforated test and dummy plates have been arranged in parallel to form a test core with rectangular channels for the flow of cooling air. The test plate can be considered a section of rectangular fins attached between two plates in a compact heat exchanger.

In the present study, only one out of four walls of the rectangular test channel is heated for studying heat transfer performance using the steady state method. As a result, some test results expressed in terms of the f/j ratio take values even less than the theoretical limit of 2 for a flow channel with all walls being heated. Detailed discussion is addressed to the question of very low f/j values. With the use of an appropriate Reynolds number for single-wall heated flow channels,the f/j ratios agree well with those for all-wall heated flow channel obtained by the single-blow(transient) method [9]. The effects of plate (or fin) thickness on the heat transfer and pressure drop performance are also discussed. The reasons for no beneficial effect due to perforations [7,8] are explained.

EXPERIMENTAL APPARATUS AND PROCEDURE

The experimental setup used to investigate the heat transfer and friction loss performance of perforated plates consisted of a heat exchanger test core situated in a subsonic wind tunnel.

The heat exchanger test core, as schematically illustrated in Fig. 1, was constructed for large scale testing of the plate-rectangular fin surface, Fig. 2. It consisted of an electrically heated aluminum plate and several dummy plates made of fiberglass. All the plates were 1/32-inch thick (t) and identically perforated with round or slotted holes of a staggered arrangement. The number and size of the round or slotted holes determine the surface porosity or percent open area. The plates were arranged in parallel with the test plate as the center piece. Wood slabs were used to space the plates for air flow passages. The thickness of the wood slabs was varied to have different values of the plate thickness-to-spacing ratio or the frontal porosity. The plates and wood slabs were stacked together by 1/4-inch bolts. The total number of the plates and slabs determines the frontal area of the test core: 6-inch width, w , by 4-inch height. Thus, the w/t ratio for the test core was 192. This may be compared with 80 , the w/t ratio, for a fin of 0.004-inch thickness and 0.320-inch height, which is that of a prototype heat exchanger used as a reference. For both systems, the ratios were large enough to warrent the neglect of side effects on the flows through the channels. The test core was 6 inches long in the flow direction.

Aluminum was selected as the material for the test plate mainly for several reasons: (i) its high thermal conductivity which tends to uniformize the temperature distribution, (ii) sufficiently high electric resistance to warrent for electrical heating, (iii) easy for perforation by drilling or punching, and (iv) the Garrett condenser for low-pollution potential steam engine is made of the same material. Fiberglas was used as the dummy plates. Only the test plate was heated for the investigation of convective heat transfer to the air, while the unheated dummy plates were used for the study of friction loss of air flow over the plates.

The wind tunnel consisted of a contraction section, test section, diffuser, fan, and discharge ducting as shown in Fig. 3. It was originally designed with the capability for testing both scale models and full size automotive radiators and condensers over a range of vehicle speeds and air-side pressure drops comparable to automotive application [10].

Three flow control methods may be used to meet the air flow requirements of the tunnel: (1) a 2:1 fan speed reduction by means of switching the voltage of the electric motor which reduces fan air flow by this same ratio; (2) variable inlet guide vane geometry capable of producing a continuous variation in fan air flow from 15% to 100% of maximum air flow; and (3) a bypass around the test section which can produce a continuous variation in test section air flow from 10 to 100% of maximum test section air flow. The change in fan speed and the inlet guide vane geometry produce changes in fan characteristics while the tunnel bypass alters the total system flow characteristic to vary the test section air flow. The bypass also allows the fan to operate in a surge-free region at all times. The bypass is accomplished by constructing the contraction section and the test section as a single unit and then translating this unit forward relative to the fixed diffuser and fan.

In order to obtain the information on the uniformity of the air flow in the test section of the wind tunnel, horizontal and vertical Pitot tube traverses were made in a plane normal to the tunnel longitudial axis and located near the middle of the test section. The traverses were made at 3-inch intervals except near the walls where the spacing was reduced to 1.5 and then to 0.25 inches from the walls. Using the velocity at the center of the tunnel as the reference velocity (at 77.1 ft/sec), it was found that at a distance of 1.5 inches velocities were generally within 1.5% of the reference value. These results indicated the uniformity of air flow in the test section of the wind tunnel.

The test core was installed in the test section of the wind tunnel. Electric power was supplied to the test plate through cables from a low-voltage M-G power supply (36 Kw, 0-12v, 0-3000 amp). In order to insure flexibility of operation, the power source and the test plate were arranged in series with a stainless steel pipe to form a power supply loop, Fig. 4. The pipe which was internally cooled by water from municipal supply was designed to dissipate excess electric power. By varying the length of the pipe and/or by adjusting the water flow rate through the pipe, the electric power dissipated in the test plate was adjusted so that the plate surface temperature was set in a desired range. Because of relatively low electrical resistance, only a fraction of electric power from the power supply was consumed by the test section. A shunt of known electrical resistance was installed in the power supply loop. The voltage drop across the shunt and the test plate (only the portion that was exposed to the air stream) were measured by a Weston Model 622 Millivoltmeter. The electric power that dissipated in the test section was transmitted to the air stream.

Since the frontal area of all of the test cores was considerably less than the wind tunnel test section area, the cores were mounted on a support which was fixed to the bottom of the test section, Fig. 5. Baffles of constant area section were installed immediately upstream as well as downstream of the core. A bellmouth in the inlet end of the constant area section was used to insure proper inlet flow conditions. Sealing was used to insure proper inlet flow conditions. Sealing was used around the core-baffle joint and also the baffle-test section wall joint to insure that all of the airflow which entered the constant area section flowed through the core.

Two Pitot tubes were inserted into the constant area sections, one at upstream and the other at downstream. The Pitot tubes were connected to a CGS 5-23-1 Type (Range 0.1 psi) Barocel pressure sensor. The following four pressure differences were read from a CGS Class I barocel electronic manometer: total to static pressure differences at both upstream and downstream and total to total and static to static pressure differences between upstream and downstream. The air velocities at the inlet and exit of the test core and the static, dynamic and total friction losses in the test core were measured by copper-constantan thermocouples and read on a L & N 8662 precision potentiometer. The inlet air temperature was read by a thermocouple located near the tip of the upstream Pitot tube. Nine thermocouples were mounted on the test plate surface at 1/2" back from the downstream edge, Fig. 1. One was on the center line of the test plate and the other eight were installed symmetrically, four on each side spaced at 0", 1/4", 1/2" and 1-1/2" from the wall. The tips of these thermocouples, electrically insulated from the test plate by very thin mica films, were cramped tightly on the plate surface. The readings of these nine thermo-couples were used to determine the temperature gradients of the test plate at the wall. Their geometrical average was used as the plate surface temperature. Two copper rods were erected vertically at 1-inch distance downstream from the edge of the test plate at 1.5-inch from the center of the constant area section on each side. Six thermocouples were mounted on the rods, two on the left rod and four on the right rod. They measured the distri-

bution of the outlet air temperatures at six different vertical locations downstream from the test plate, Fig. 1. One thermocouple was lined up with the test plate, while the vertical location of the other five thermocouples was varied: at 1/8", 1/4", 1/2", 1" downward and 1/4" upward from the test plate. The integrated mean value of the measured temperature distribution was employed as the average outlet temperature of the air stream from the channels heated by the test plate. During adiabatic runs for pressure drop measurements the copper rods were removed.

For testing, the fan was started. The desired air velocity through the test section was set by means of adjusting bypass opening. Water to the power dissipating tube was turned on. Power supply was turned on and adjusted to bring the plate surface temperature to about 200°F. When steady state values had been established, air and plate surface temperatures and voltage drops were recorded. After these measurements, the two copper rods with six air thermocouples were removed. The same test was repeated without heating the test plate and pressure drops were measured. This extra step was taken in order to eliminate the effect of the copper rods on the pressure drop readings. These steps were repeated for successive data points.

TEST RESULTS AND DISCUSSION

The electric power dissipated as heat (at the rate of q_e) in the test plate is equal to the product of the voltage drop across the test plate and the current flowing in the power supply loop. Because of high thermal conductivity of the aluminum test plate, a substantial amount of the heat being generated in the portions of the test plate which protruded out of the baffle was transmitted into the test core by conduction. The amount of heat q_k transferred into the test core by conduction is given as $q_k = kA_p[(\frac{\Delta T}{\Delta x})_1 + (\frac{\Delta T}{\Delta x})_2]$ where k is the thermal conductivity of aluminum, A_p is the cross sectional area of the test plate normal to air flow, and $(\Delta T/\Delta x)_1$ and $(\Delta T/\Delta x)_2$ are the temperature gradients at the baffle walls in the direction normal to air flow. These two components of heat q_e and q_k, were then transmitted to the air stream in the channels wetting the test plate by convection. Therefore, the heat transfer coefficient between the test plate and the air stream, h can be evaluated using the equation $q_e + q_k = hA(T_s - T_a)$, where A is the heat transfer surface area, T_s is the plate surface temperature and T_a is the mean bulk temperature (average of the inlet and the outlet) of the air stream. As a result of convective heat transfer, the enthalpy of the air streams has increased by $mC_p(T_{ae} - T_{ai})$, where m is the flow rate of the air streams in the channels wetting the test plate, C_p is the specific heat of the air at constant pressure and T_{ai} and T_{ae} are the air temperatures at the inlet and exit, respectively. Good agreement between the enthalpy change of the air stream and the power input was obtained in the tests.

All physical properties of the air were evaluated at the mean bulk temperture. The flow velocity entering the core V_i is calculated using the Bernoulli's equation:

$$V_i = [2g_c(\Delta P_{T-S})_i / \rho_i]^{1/2} \tag{1}$$

where $(\Delta P_{T-S})_i$ is the total-to-static pressure difference measured by the upstream Pitot tube, ρ_i is the density of the fluid entering the core and g_c is the conversion factor. The flow velocity is not different appreciably from that leaving the core based on $(\Delta P_{T-S})_e$ measured by the downstream Pitot tube. This indicates virtually no change in the fluid density from the core entrance to the core outlet, i.e., $\rho_i \cong \rho_m \cong \rho_e$ in which the subscripts i, m and e denote the core entrance, the average value in the core and the core outlet, respectively. Due to flow area change the flow velocity inside the core V_c is calculated from

$$V_c = \frac{A_i}{A_c} V_i \tag{2}$$

wherein A_i and A_c represent the free flow areas at the core entrance and inside the core, respectively.

The Reynolds number which indicates flow conditions in the test core is defined based on the hydraulic radius r_h of the flow channels in the core as

$$R_e = \frac{4 r_h G}{\mu} \tag{3}$$

where μ is the absolute viscosity and G is the mass velocity defined as $G = \rho_m V_c$ The hydraulic radius is defined as the minimum flow area inside the core A_c divided by the wetted perimeter. For the present system, it is equal to $\frac{wb}{2(w+b)}$ where b is the plate spacing and w is the width of the channel.

The friction factor f is defined based on the static pressure drop across the test core ΔP_{S-S} and determined by the pressure drop equation (2-26a) of Reference [1]:

$$f = \frac{r_h}{L}\left[\frac{2 g_c \rho_m \Delta P_{s\text{-}s}}{G^2} - (K_i + K_e)\right] \tag{4}$$

in which the effect of flow acceleration on pressure drop is neglected and the entrance and exit loss coefficients K_i and K_e are determined by Fig. 5-3 of Reference [1]. Both the j and f factors are functions of the frontal porosity of the test core, the plate surface porosity (percent open area) and the Reynolds number.

The heat transfer performance is expressed by the heat transfer factor j, which is defined as

$$j = \frac{h}{G C_p} P_r^{2/3} \tag{5}$$

in which Pr is the Prandtl number.

The frontal porosity σ_f is the ratio of the free flow to frontal area. It is related to the ratio of the plate thickness to spacing as

$$\sigma_f = \frac{1}{1 + t/b} \tag{6}$$

The plate surface porosity σ_s can be expressed as

$$\sigma_s = \frac{\pi}{2\sqrt{3}} \left(d/\ell\right)^2 \tag{7}$$

for the round hole pattern in a staggered arrangement, where d is the hole diameter and l is the center-to-center distance between two adjacent holes, Fig. 6. It is a function of only one dimensionless parameter d/l. In the case of the oval slotted pattern

$$\sigma_s = \frac{\frac{\pi}{4} d_s^2 + d_s(w_s - d_s)}{P_t P_\ell} = \frac{\frac{\pi}{4} + \left(\frac{w_s}{d_s} - 1\right)}{\left(\frac{P_t}{d_s}\right)\left(\frac{P_\ell}{d_s}\right)} = \frac{\frac{\pi}{4} + \left(\frac{w_s}{d_s} - 1\right)}{\frac{P_\ell}{d_s}\left(\frac{a}{d_s} + \frac{w_s}{d_s}\right)} \tag{8}$$

for $w_s/d_s \geq 1$, where w_s is the slot length, d_s is the slot width, p_ℓ is the longitudinal pitch (the center-to-center distance between two adjacent transverse rows measured in the flow direction), and p_t is the traverse pitch (the distance between centers of the slots in adjacent longitudinal rows measured perpendicularly to the direction of flow). It is functions of three dimensionless parameters: w_s/d_s, p_ℓ/d_s and p_t/d_s. For the case of $w_s/d_s = 1$, σ_s of the oval slotted pattern reduces to that of the round circle pattern. $a/d_s = 0$ corresponds to the case of an infinite slot.

Both the round hole patterns and the oval slotted patterns, each having five plate surface porosities of 5.7, 12.8, 17.4, 22.8, and 28.8%, were fabricated and tested. The round-hole surface was tested in the first phase of the project (from May, 1971 to December, 1971). In the second phase (from January, 1972 to August, 1972), five different oval-slotted surfaces were tested whose geometrical dimensions and arrangement are given in Table 1. The number of figures illustrating the test results for the slotted surfaces is also listed in Table 1.

Surface	w_s(in)	d_s(in)	a*(in)	Test Results in Figures
1	1/2	1/8	0	7 - 9
2	1/2	1/8	1/8	10 - 12
3	2	1/8	0	13 - 15
4	2	1/8	1/2	16 - 18
5	1/2	1/16	0	19 - 21

Table 1. Geometrical Dimensions and Arrangement of Oval-Slotted Surfaces

Here, a* is defined as the slot overlapping width in the flow direction. Surface 1 was tested during the first phase of the project and it was repeated in the second phase. The surface porosity was changed by varying the center-to-center distance d, or p_l .

Three plate spacings were tested: 0.974", 0.47" and 0.221". For the plate thickness of 1/32", the thickness-spacing ratios were 0.0321, 0.0665, and 0.141, respectively, or equivalently, σ_F = 0.970, 0.937 and 0.875, respectively. The t/b ratios for a plate-fin heat exchanger with rectangular fins of 0.004-in thickness are 0.046 and 0.0962 for the fin pitches of 11 and 22 fins per inch, respectively.

The test results were correlated for the j and f factors and their ratio against (i) the Reynolds number with plate porosity as parameter in the a series of Figs. 7 through 21, (ii) against the plate surface porosity with the Reynolds number as parameter in the b, c and d series, and (iii) the Reynolds number with a", w_s and d_s as parameters in Figs. 22 through 24. The test results for the round hole surface are included in the report in Figs. 25 through 27. These results were obtained by correlating the test results using the flow velocity at the core entrance.

The variables to be examined include hole or slot size (d_s, w_s or d), degree of slot overlapping a*, plate surface porosity σ_s and frontal porosity σ_F or t/b).

1) Effects of slot length

Two slot lengths had been studied, w_s = 2" and w_s = 1/2". Referring to Table 1, the comparisons were made between surfaces 1 and 3 for the in line arrangements and between surfaces 2 and 4 for the overlapping arrangements. In each case, w_s is the only variable with d_s being held constant at 1/8 inch. Figures 22 through 24 illustrate the effects of slot length on the f and j factor. It is disclosed that the f factor for the slot length of 2" is consistently lower than that for the slot length of 1/2". In general, the j factor for the slot length of 2" is higher than that for the slot length of 1/2". Consequently, the longer slots (w_s = 2") have lower f/j ratios than the shorter ones (w_s = 1/2") for both the in-line arrangement and the overlapping arrangement.

2) Effects of slot width

The effects of slot width (d_s) on the friction loss and heat transfer performance of the perforated plates were studied by comparing a slot width of 1/8" with that of 1/16". Referring to Table 1 again, this is a comparison between surfaces 1 and 5 both being the in-line arrangements with a* = 0 and w_s = 1/2". The results indicated that for the slot width of 1/16", the j factor is consistently higher than that of the slot width of 1/8", and the f factor is slightly lower for the narrower slot than that of the wider one. Consequently, the narrower slot (d_s = 1/16") has a lower f/j ratio than the wider one.

3) Effects of slot overlapping

Two overlapping arrangements were studied: surface 4 with a* = 1/2" and surface 2 with a* = 1/8". The effects of slot overlapping were evaluated by comparing the results for surfaces 2 and 4 with those for surfaces 1 and 3 with the in-line arrangements having identical slot width and slot length. An examination of these results shows that there is no appreciable difference in f, j, or f/j between the two slot arrangements. This is an indication that slot arrangement plays an insignificant role on both the heat transfer and flow friction performance.

4) Effects of Reynolds number

The effects of the Reynolds number on the f and j factors depend largely on the t/b ratio as can be seen by comparing Figs. 22, 23 and 24. For the value of t/b equal to 0.141, the f factor decreased with an increase in the Reynolds number until the latter reached the value of approximately 4,000 at which high-pitch noise generated in the test core was heard. A further increase in the Reynolds number was marked by a sudden upturn in the value of f which was evidenced by the generation of high-pitch noises (those test data encircled by a dotted line). This increase in the f factor had eventually resulted in a high f/j ratio when the Reynolds number exceeded 4,000. For the value of t/b equal to 0.0665, the value of f decreased with an increase in the Reynolds number. It reached a minimum value at the Reynolds number of approximately 8,000 and then increased for a further increase in the Reynolds number. However, noise was detected only at the highest Reynolds number in the test series, approximately 15,200. At the t/b ratio of 0.0321, no noise was ever detected up to the Reynolds number of approximately 3×10^4. The effect of the Reynolds number on the f factor was found to be very minor. For all values of the t/b ratio, the j factor was found to decrease with an increase in the Reynolds number.

5) Effects of plate surface porosity

A solid plate and five perforated plates were tested. The plate surface porosities correspond to 0, 5.7, 12.8, 17.4, 22.8 and 28.8%. Regardless of perforation size and geometry, generally, both the f and j factors increased with an increase in the plate surface porosity. But because of the problem of noise generation which becomes more severe as the surface is more perforated, the optimum plate surface porosity is taken to be between 15 to 22 percent.

As the surface porosity is increased beyond 22 percent, the problem of noise becomes quite serious. This can be realized in the plots of f versus Re for the surface porosity of 28.8 percent. Especially at the highest Reynolds number, the intensity of noise generated in the test core was very high, and the f factor increased sharply. These phenomena were especially pronounced at the t/b ratio of 0.141.

6) Effects of frontal porosity

A comparison of the test data for three t/b ratios 0.141, 0.0665 and 0.0321, revealed that the t/b ratio of 0.0665 gives the best f/j ratio. Noise generated by the test core is related to the t/b ratio. No noise was detected at the t/b ratio of 0.0321 even at high Reynolds number and high plate surface porosity. At the t/b ratio of 0.0665, noise was heard only when the Reynolds number exceeded approximately 11,400. Therefore, the optimum t/b ratio is between 0.0665 and 0.141.

7) Error analysis of test data

An error analysis was carried out to evaluate the uncertainty intervals for the experimental results using the method described in Reference [11]. The 95 percent confidence limits for both the f and j factors were evaluated at three representative Reynolds numbers and three t/b ratios: 0.141, 0.0665 and 0.0321, respectively. Only the test plate having $w_s = 1/2''$, $d_s = 1/8''$, $a^* = 0$ and surface porosity of 5.7 percent was used in the error analysis. However, the results which vary only with the Reynolds number apply to any test plates irrespective of their perforation size and geometry and surface porosity. The percentage of error for the f and j factors increases with a decrease in the Reynolds number. The average percentage of error for the j factor is around 14 percent and that for the f factor is about 13 percent. The results of the error analysis were tabulated in Table 2 and the uncertainty intervals were marked in Fig. 7a, 8a, and 9a.

It is important to note that the test results have confirmed the geometric and dynamic similarities through the following two observations. First, the "transition" of air flow patterns is delayed from Re=2,000 to about 3,500 as t/b decreases from 0.2 to 0.0964, as illustrated in Fig. 28. The same phenomenon is observed in the present results. The "transition" is delayed from Re of approximately 5,000 to 9,000 to 17,000 (which is disclosed from the plot of j versus Re) as t/b decreases from 0.141 to 0.0665 to 0.0321. Second, the values of f/j for the plate surface porosities of 12.5% and 25% in Reference [5] are practically the same. The equal values of f/j for the two porosities is confirmed in the present results for both perforated patterns.

Table 2. Uncertainty Intervals

$\sigma_s = 17.4\%$

Slot-Size: 1/2" x 1/8"

Perforation Geometry: in-line, a*=0

t/b	Re	j	$\pm\frac{\delta j}{j} \times 100\%$	f	$\pm\frac{\delta f}{f} \times 100\%$
0.141	7883	0.0066	12.0%	0.0140	5.0%
0.141	3153	0.0076	13.4%	0.0108	12.6%
0.141	788	0.0117	27.2%	0.0223	50.8%
0.0665	15156	0.0066	12.3%	0.0112	5.0%
0.0665	6062	0.0081	14.0%	0.0095	12.7%
0.0665	1516	0.0134	28.0%	0.0150	57.0%
0.0321	28137	0.0061	13.0%	0.0121	5.1%
0.0321	11255	0.0082	15.0%	0.0126	13.0%
0.0321	2814	0.0115	27.0%	0.0133	74.0%

DISCUSSION

Figure 2 shows the f/j ratio at some values less than two. This may appear at first to be at variance with certain established views. However, one may recall that for laminar flow inside tubes or ducts, the ratio $f/j=8.6\ (L/D_h/Re)$ may take any values depending upon the magnitude of L/D_h and Re. Hence, in this case there is no reason why a value of 2 is a lower limit for this ratio. The presence of perforated holes should not change the order of magnitude of f/j substantially. Secondly, the present study deals with the case of asymmetrical heating. That is heat transfer from one wall (of the test plate), while the flui flow wets all four channel walls. Therefore, the hydraulic diameter, defined as $4A_cL/A_w$, will have two different values: $D_{hj}=4b$ for heat transfer and $D_{hf}=2wb/(w+b)$ for friction loss. As a result, the characterizing Reynolds number takes two different forms: $Re_j=4bG/\mu$ for heat transfer and $Re_f=2wbG/\mu(w+b)$ for friction loss. For the same flow velocity, Re_j is about two times Re_f when the channel width is much greater than the channel height. Since both the j and f factors depend upon both the Reynolds number and the hydraulic diameter, the relationships of $j=j(Re_j, L/D_{hj})$ and $f=f(Re_f, L/D_{hf})$ should be employed in an asymmetrical heating case. Under this circumstance, the ratio of f/j will lead to a physical situation which is entirely different from that for a symmetrical heating case. For convenience, both f and j are plotted against Re_f here. . In the event all plates are heated (as indicated by the subscript 2), the hydraulic diameter D_{hj} will be exactly 2b, since the two vertical walls of a flow channel are unheated. Then, the corresponding Reynolds number is one half that of the one-plate heated case (as denoted by the subscript 1) for the same flow velocity. A preliminary result in [9] indicated that j_1 (in the present study) at Re_{j1} is approximately equal to j_2 (obtained by the Single Blow Technique) at Re_{j2} for the same flow velocity or for $Re_{j1}=2Re_{j2}$, see Fig. 7-a for j. With this approximation, all test results for j_1 for $\sigma=0$ case were recalculated in terms of j_2, when $f_1=f_2$ and $Re_f=Re_{j2}$. In so doing all f_2/j_2 ratios have become either equal to or greater than 2, within experimental uncertainty. Hence, it should be recognized that the f/j ratio has been employed merely for convenience to indicate the overall behavior of a symmetrically heated flow channel. One should not extend its implications, particularly the concept of $f/j=2$, to an asymmetrical heating case.

Another item of importance is the problem of noise generation in the perforated surfaces. As was noted in the previous section, noise intensity increases with an increase in the surface porosity at high Reynolds number. It is shown in [9] that noise is edge tone in nature and high intensity occurs when the vortex shedding frequency coincides with a natural frequency of either the plate or the air column in the test core. This noise may be removed or eliminated by inserting plate supports to increase the natural frequency of both the plates and the air column.

As disclosed by the visualization study in Reference [3], several different flow patterns are generated inside and downstream from the cavities (round holes and slots) depending upon the slot width (or the diameter in case of a round-hole cavity) to plate thickness ratio, d_s/t or d/t. As a result, both the pressure drop and heat transfer performance (also noise generation and plate vibration) are significantly affected by the ratio. For low values of the ratios as were the cases in References 7 and 8, the fluid produces neither circulation inside the cavity nor cross flow through the cavity into the stream on the other side of the plate. In other words, the fluid experiences very little or no disturbance when it flows over the cavities as if no cavities are there. This leads to no merit due to perforations as concluded in References [7] and [8]. On the other hand, when the d_s/t ratio exceeds a value of 2.00 in case of slot perforation or 2.75 in case of round-hole perforation, either a counterclockwise circulation inside the cavity and/or cross flow through the cavity into the stream on the other side of the plate occurs, resulting in a rigorous turbulence and mixing downstream from the cavity. Significant improvement in heat transfer accompanied by an increase in pressure drop is observed.

CONCLUSIONS

A large scale technique is developed to examine the effects of perforation geometry on the heat transfer and friction loss performance of compact heat exchangers of the plate-perforated rectangular fin surfaces. Through the comparison of the test results with those of the compact heat exchangers of different scale, the geometric and dynamic similarities of both systems are confirmed, thus establishing the validity of the large scale technique. The technique is simple and quick to carry out and may also be employed to determine the optimum perforation geometry and to understand or interpret the test data of the compact heat exchanger. It is concluded from the study

1. Plates perforated with smaller slots seem to give the better overall heat transfer-friction loss performance, i.e.lower f/j, than those with larger slots.
2. The optimum plate thickness to plate spacing ratio, t/b, is found to be between 0.0665 and 0.141.
3. With noise problems taken into consideration, the optimum surface porosity for all slotted plates appears to be between 15 and 22 percent.
4. Noise generation becomes a serious problem under the conditions of high Reynolds numbers when the plates with high surface porosity are arranged in a high t/b ratio.
5. An increase in the slot length results in a slight decrease in the f factor but an increase in the j factor.
6. The degree of slot overlapping in the flow direction has little effect on the f/j ratio.

REFERENCES

1. W. M. Kays and A. L. London, Compact Heat Exchangers, 2nd Ed., McGraw-Hill Book Co., New York (1964).

2. P. F. Pucci, C. P. Howard and C. H. Piersall, Jr., "The Single Blow Transient Testing Technique for Compact Heat Exchangers Surfaces," Journal of Engineering for Power, Trans. ASME, Ser. A, 89, pp. 29-40 (1967).

3. R. H. Shah and H. H. Osborn, "Final Report-Advanced Heat Exchanger Design of Compact Heat Exchangers When Operating in a Marine Environment," Air Preheater Company, Wellsville, New York (May 1967).

4. S. Wong, J. D. Duncan, D. W. Graumann, J. C. Gibson and J. J. Killackey, "Compact Condenser for Rankine Cycle Engine," Final Report 71-7464 (prepared for Office of Air Programs, Environmental Protection Agency, Ann Arbor, Michigan), AiResearch Manufacturing Co., Los Angeles, California (June 1971).

5. L. Forgo, "Some Extra High Capacity Heat Exchangers of Special Design," Proc. 1972 International Seminar on Recent Developments in Heat Exchangers, International Center for Heat and Mass Transfer, Trogir, Yugoslavia (1972).

6. W. M. Kays, "The Heat Transfer and Flow Friction Characteristics of a Wavy Fin, and a Perforated Fin Heat Transfer," TR No. 39, Department of Mechanical Engineering, Stanford University, Stanford, California (1958).

7. J. R. Mondt and D. C. Sigela, "Performance of Perforated Heat Exchanger Surfaces," ASME Paper No. 72-WA/HT-52 (1972).

8. H. L. Miller and C. A. Leeman, "Heat Transfer and Pressure Drop Characteristics of Several Compact Plate Surfaces," AIChE Preprint 9, 13th National Heat Transfer Conf., Denver, Colorado (1972).

9. C. Y. Liang, "Heat Transfer and Friction Loss Performance of Perforated Surfaces," Ph.D. thesis in progress, Department of Mechanical Engineering, University of Michigan, Ann Arbor, Michigan (1973).

10. J. A. Clark, C. A. Siebert, R. B. Keller, M. Borden, and J. C. Hoo, "Automotive Radiators Manufactured by the Electroforming Process," Final Report of ORA Project 05335 (under contract with International Copper Research Association, Inc., New York), University of Michigan, Ann Arbor, Michigan (December 1964).

11. S. J. Kline and F. A. McClintock, "Describing Uncertainties in Single-Sample Experiments," Mechanical Engineering, 75, pp. 3-8 (1953).

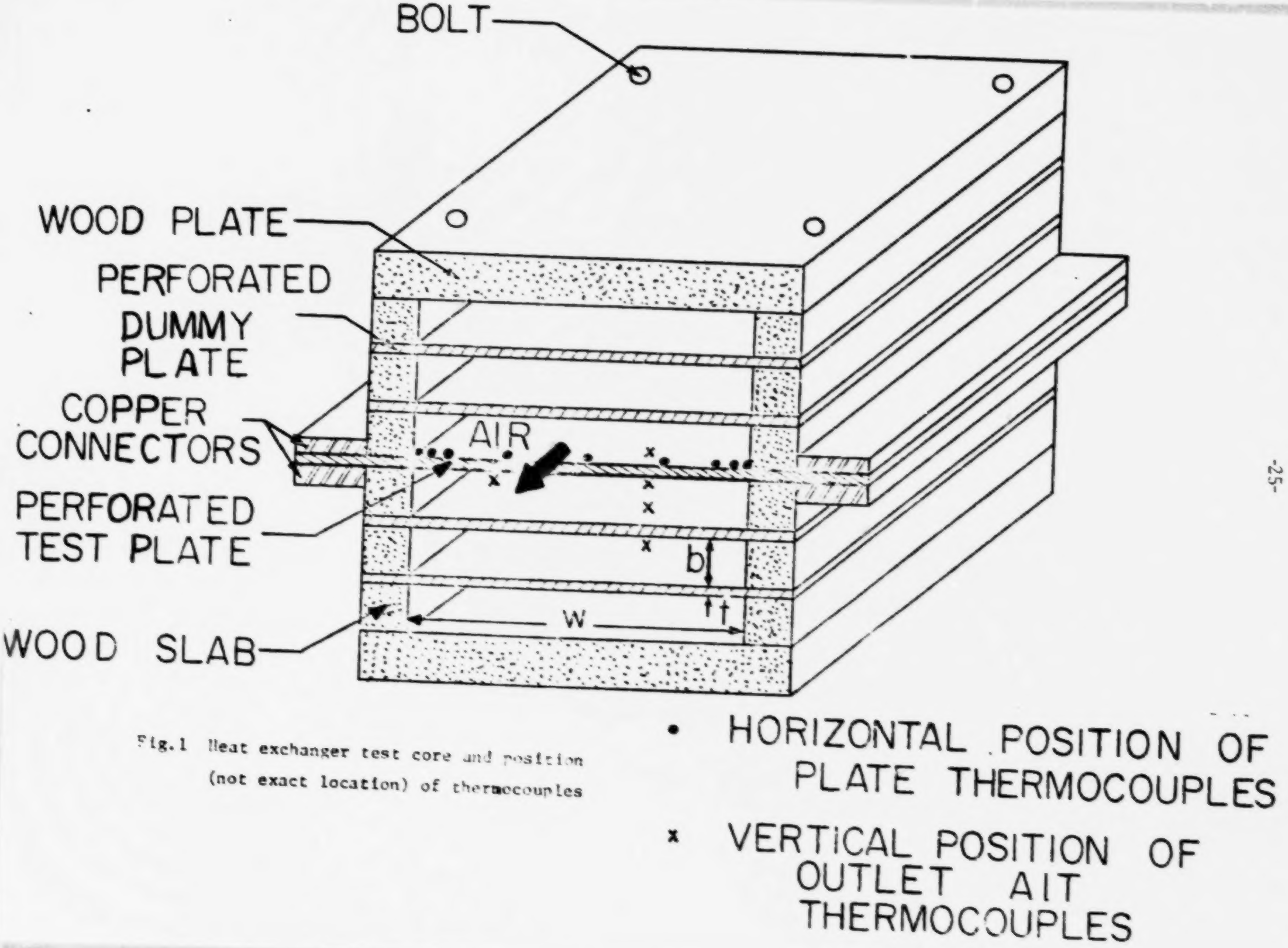
BOLT
WOOD PLATE
PERFORATED
DUMMY
PLATE
COPPER
CONNECTORS
PERFORATED
TEST PLATE
WOOD SLAB
AIR
b
t
w
• HORIZONTAL POSITION OF
PLATE THERMOCOUPLES
x VERTICAL POSITION OF
OUTLET AIT
THERMOCOUPLES

Fig.1 Heat exchanger test core and position
(not exact location) of thermocouples

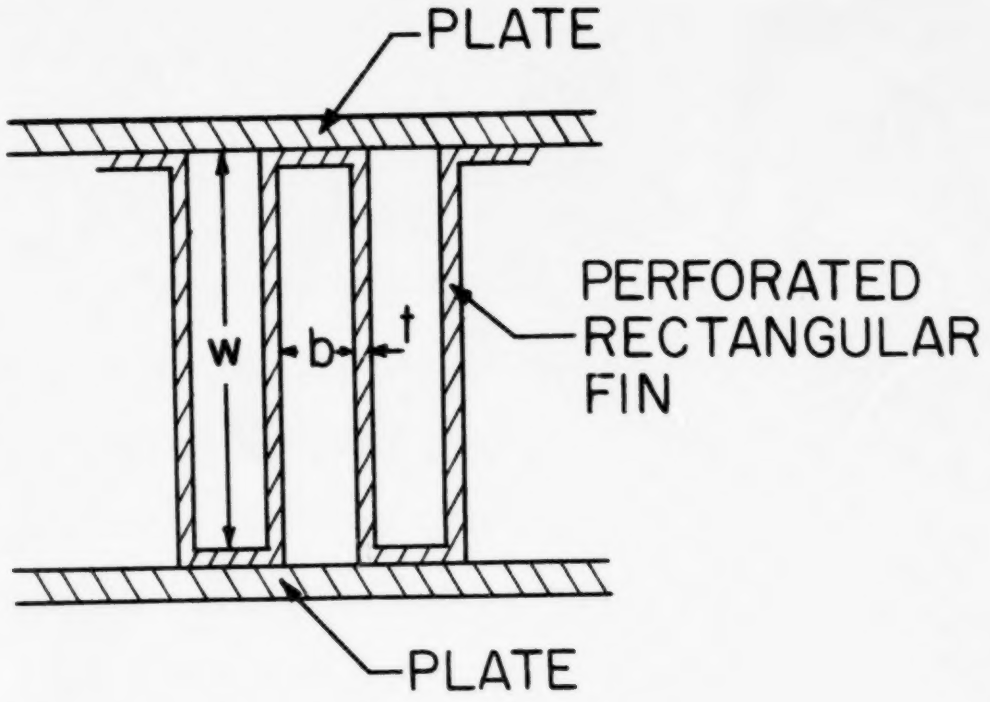
PLATE
PERFORATED RECTANGULAR FIN
w
b
t
PLATE

Fig.2 Plate-rectangular perforated fin surface

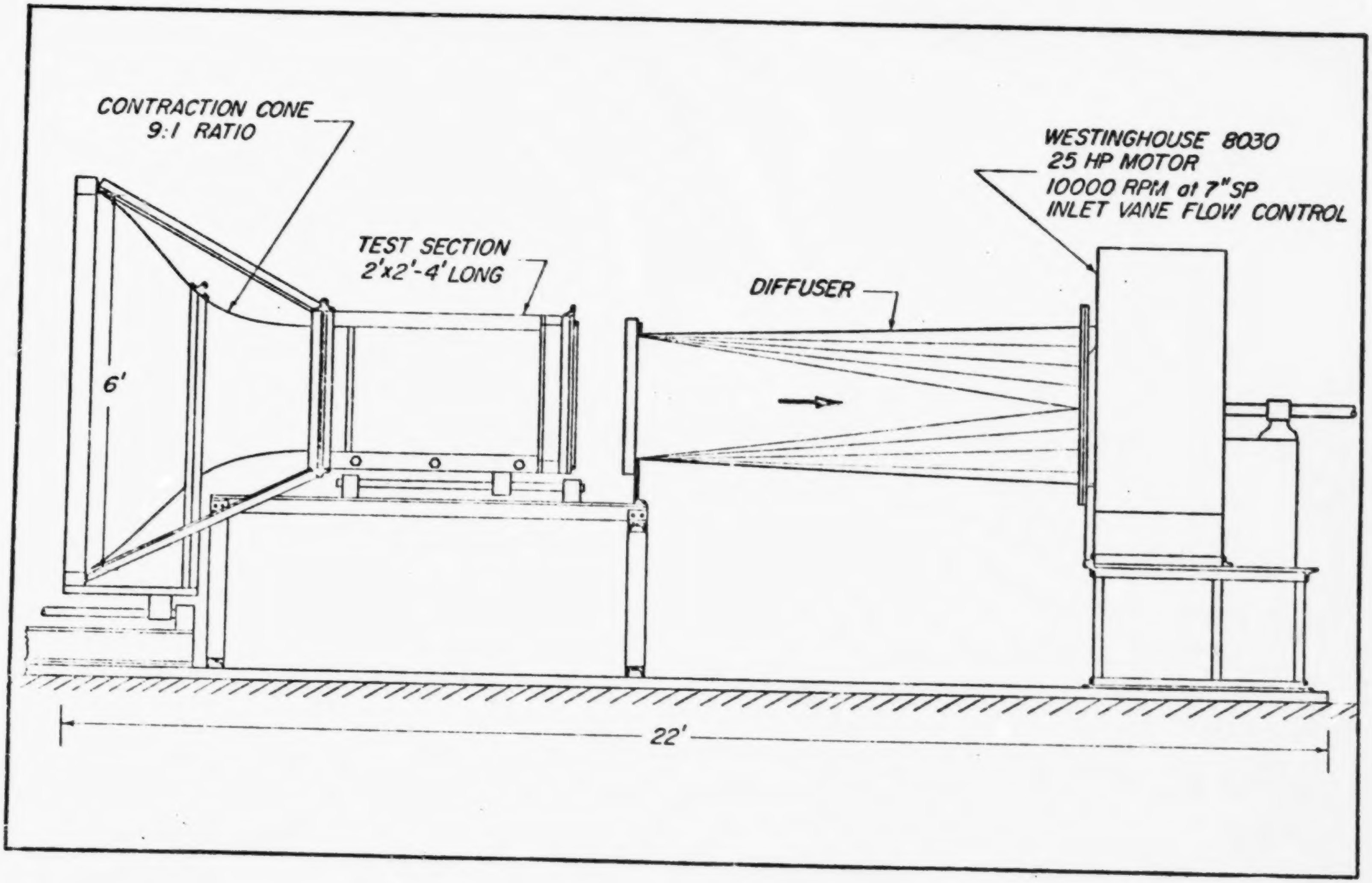
CONTRACTION CONE
9:1 RATIO
TEST SECTION
2'x2'-4' LONG
DIFFUSER
WESTINGHOUSE 8030
25 HP MOTOR
10000 RPM at 7"SP
INLET VANE FLOW CONTROL
6'
22'

Fig.3 Wind tunnel

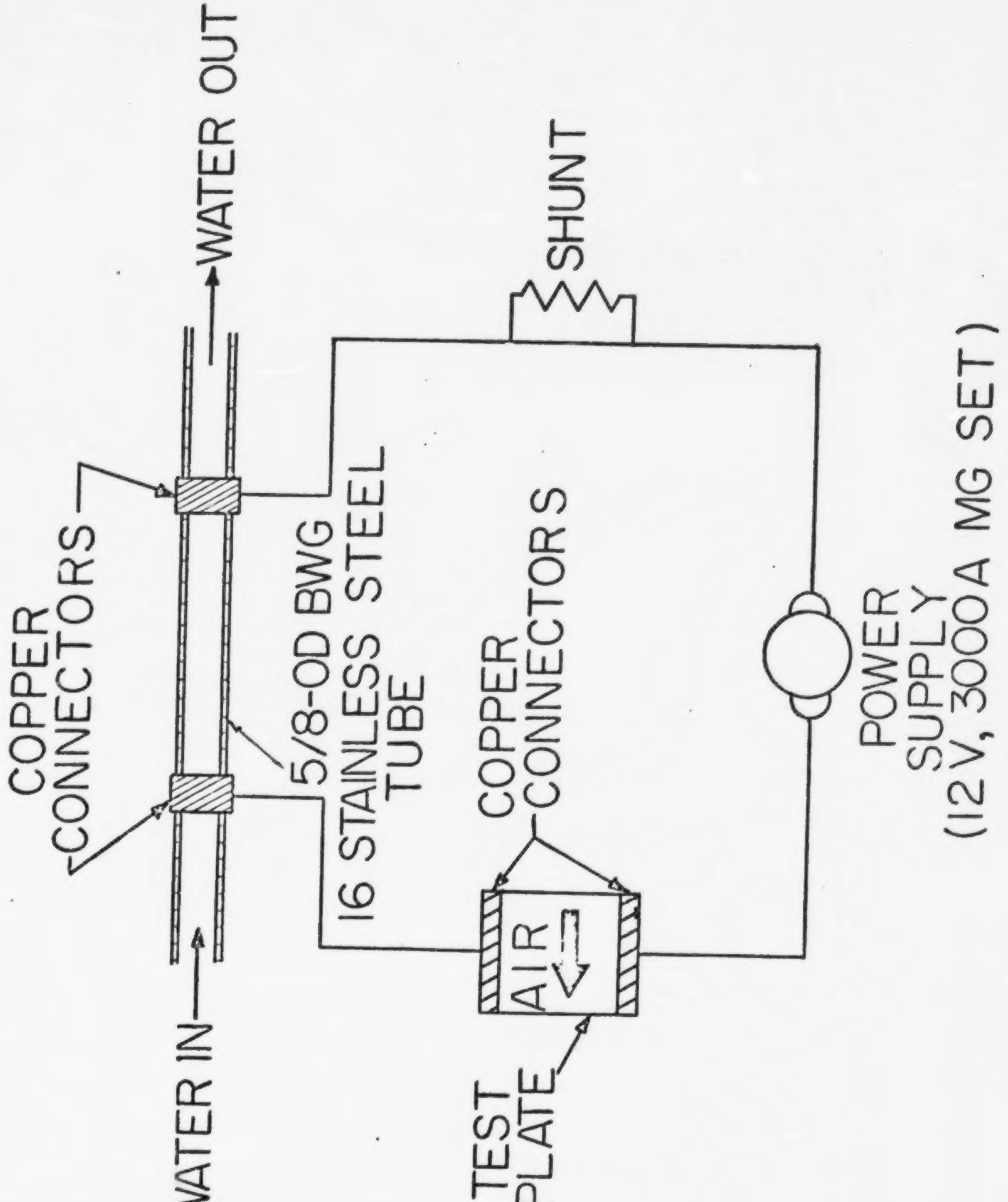
WATER IN
WATER OUT
COPPER CONNECTORS
5/8-OD BWG 16 STAINLESS STEEL TUBE
SHUNT
COPPER CONNECTORS
TEST PLATE
AIR
POWER SUPPLY (12 V, 3000 A MG SET)

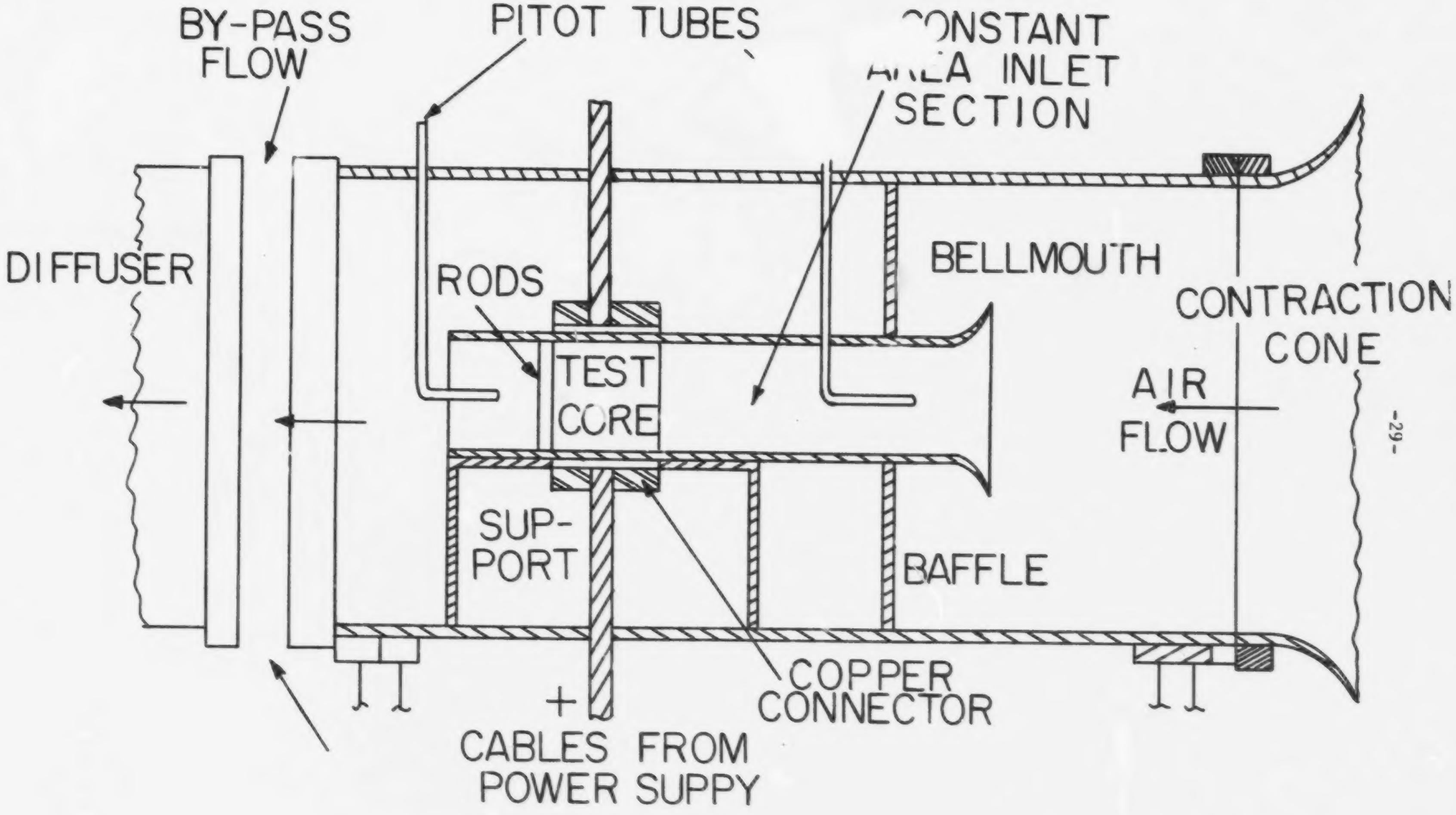
BY-PASS FLOW
PITOT TUBES
CONSTANT AREA INLET SECTION
DIFFUSER
RODS
BELLMOUTH
CONTRACTION CONE
TEST CORE
AIR FLOW
SUP-PORT
BAFFLE
COPPER CONNECTOR
+
CABLES FROM POWER SUPPY

Fig.5 Schematic of test core installation in wind tunnel (elevation view)

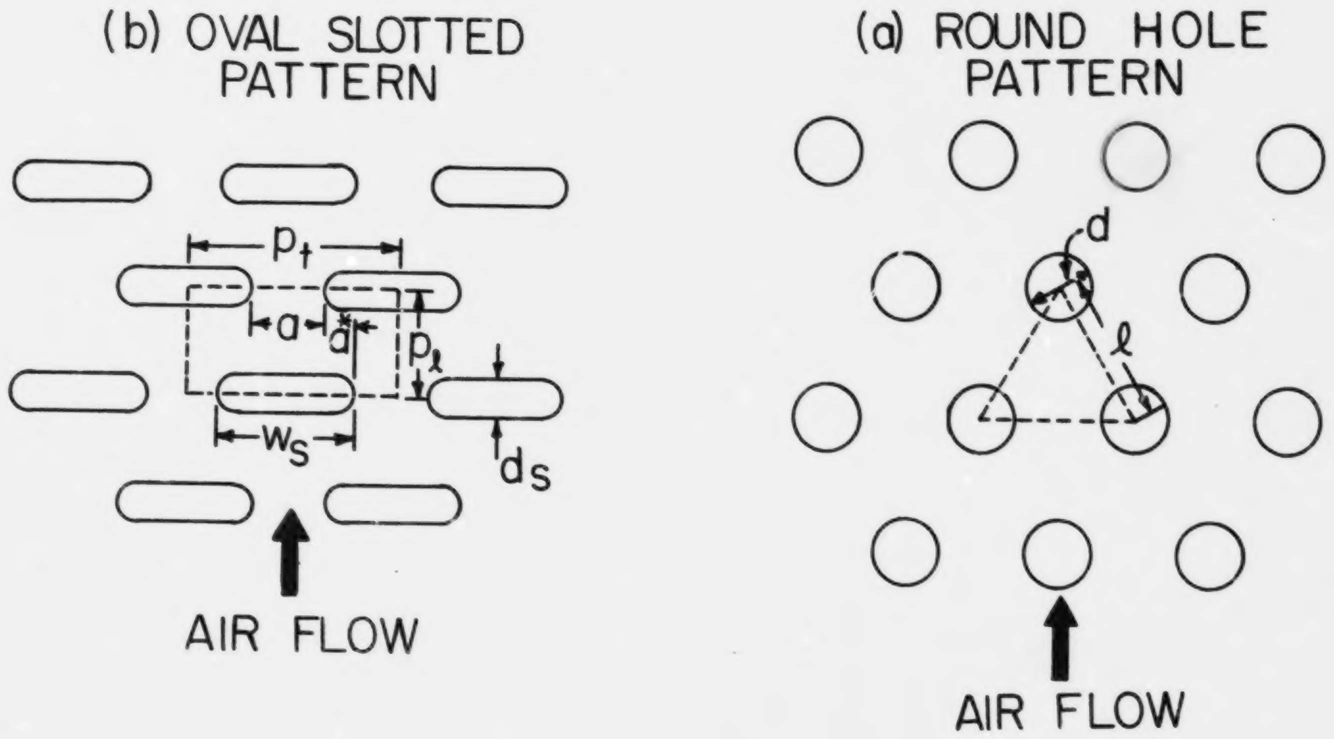
(b) OVAL SLOTTED PATTERN
p_t
a
d
p_ℓ
w_s
d_s
AIR FLOW
(a) ROUND HOLE PATTERN
d
ℓ
AIR FLOW

Fig.6 Perforation geometry

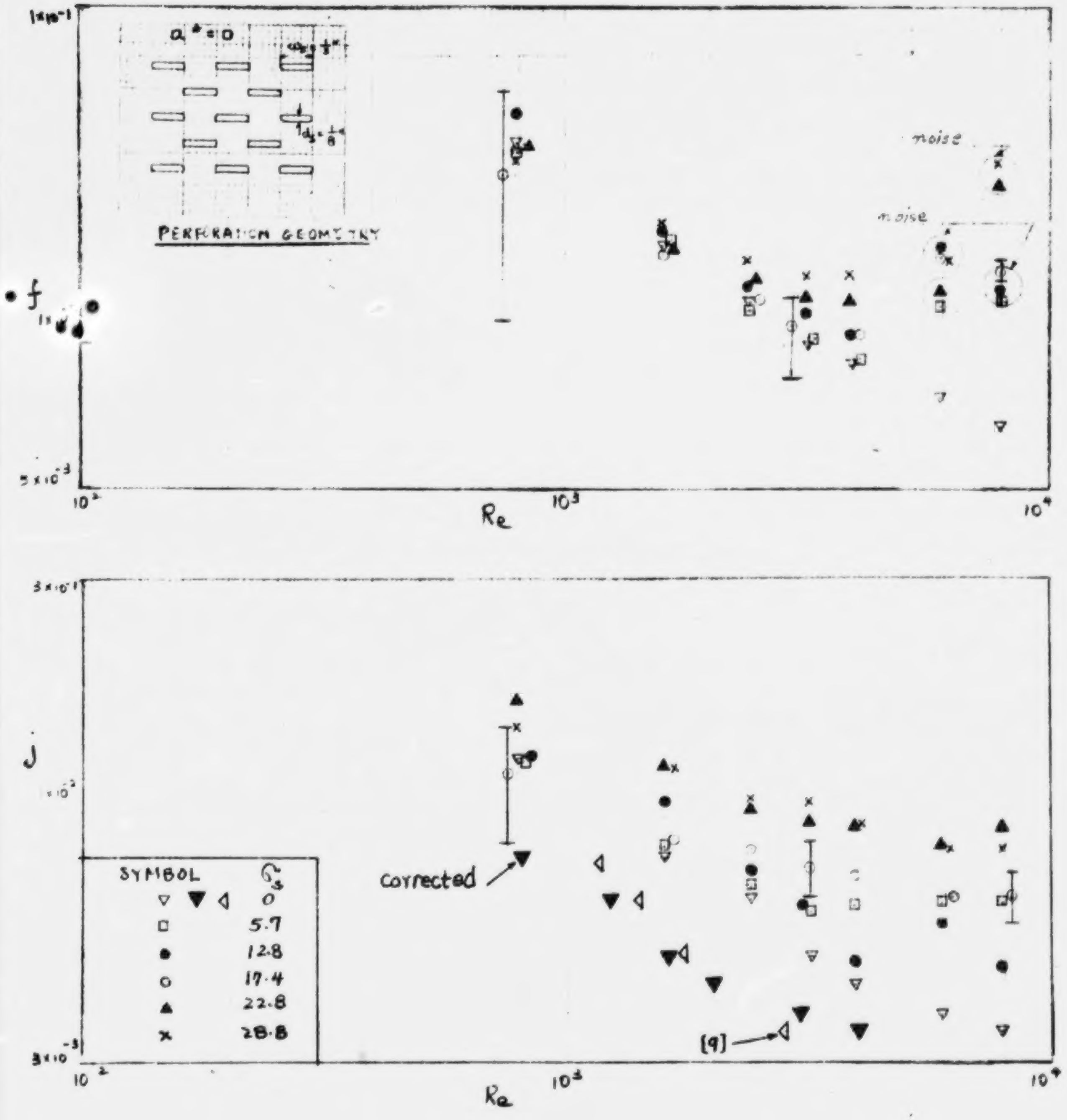

Fig. 7a. f and j versus Re, for t/b=0.141, 1/2" (length) x 1/8" (width) slots in in-line arrangement.

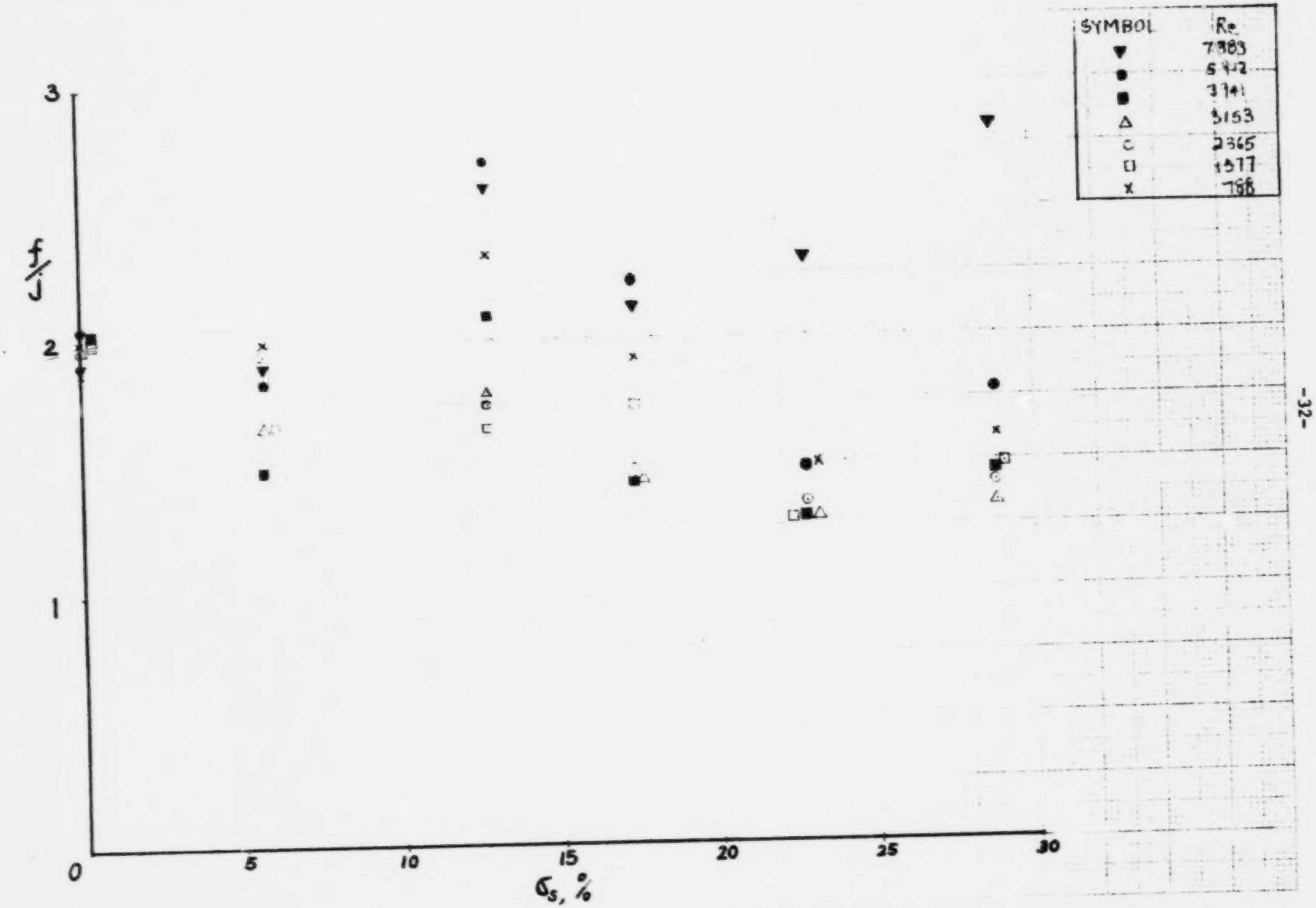
SYMBOL
Re
▼ 7883
● 5942
■ 3941
△ 3153
⊙ 2365
□ 1577
x 788
f/J
3
2
1
0
5
10
15
20
25
30
σ_s, %

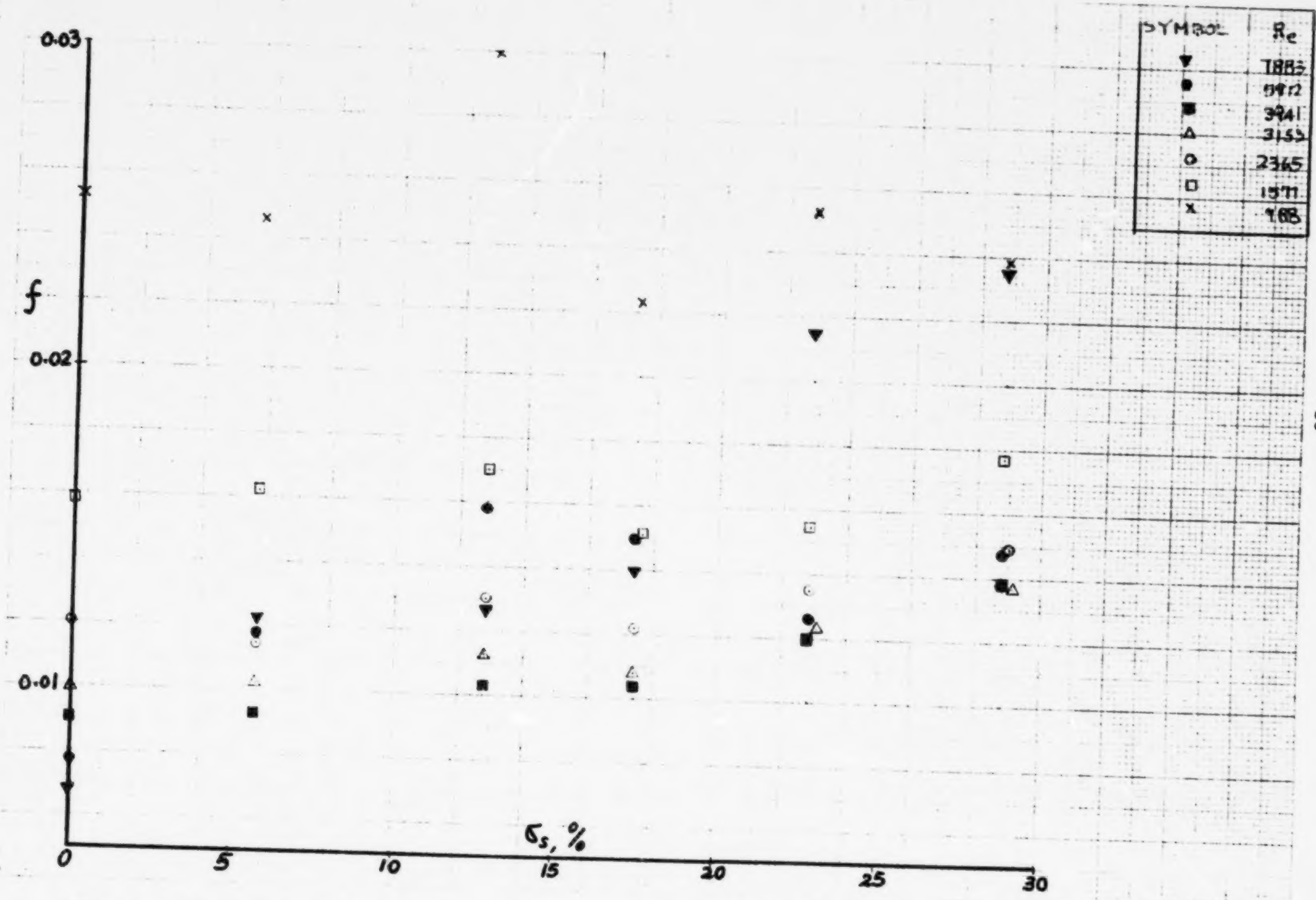

Fig. 7c. f versus σ_s, for t/b=0.141, 1/2" (length) x 1/8" (width) slots in in-line arrangement

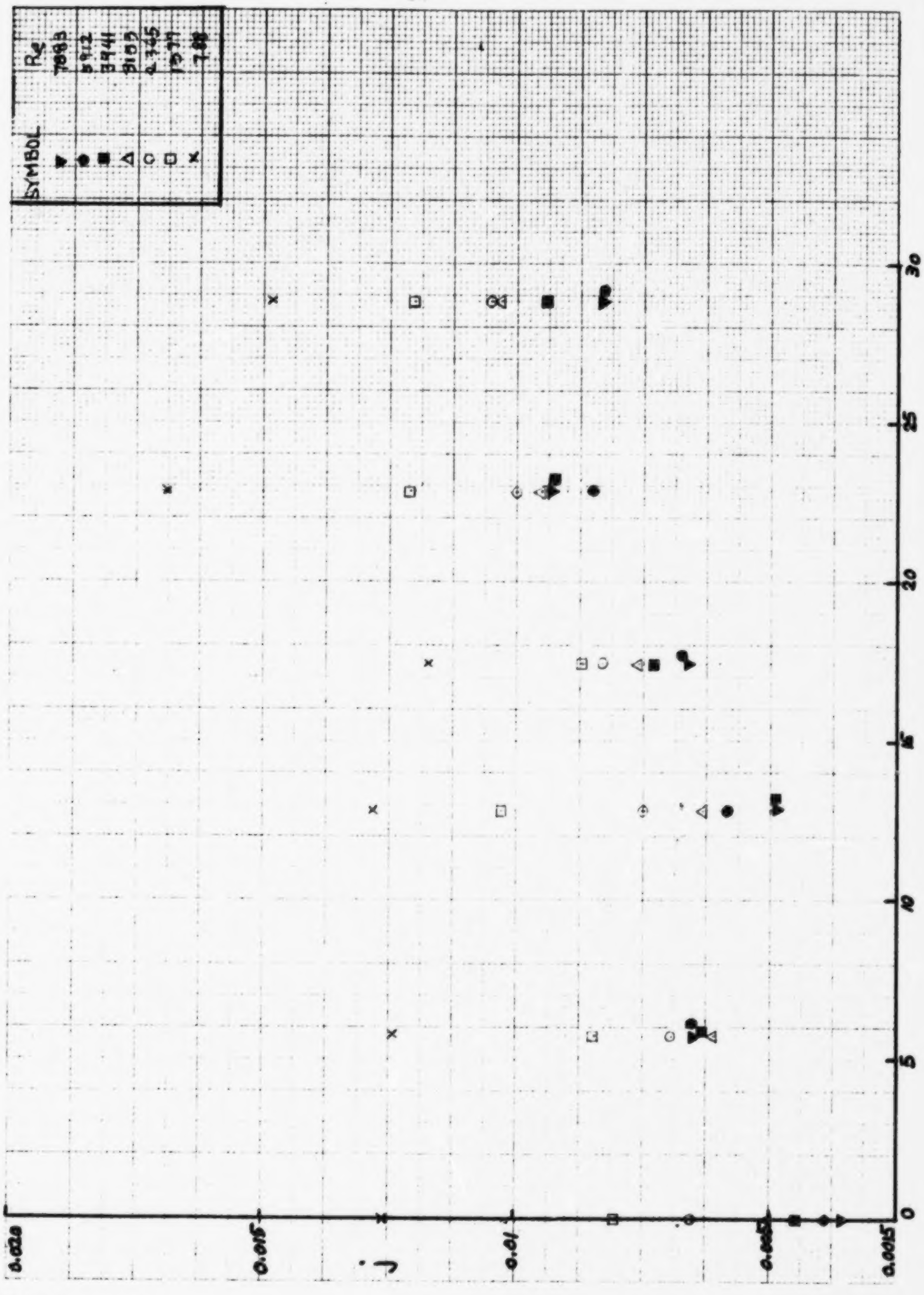

20 Squares to the Inch

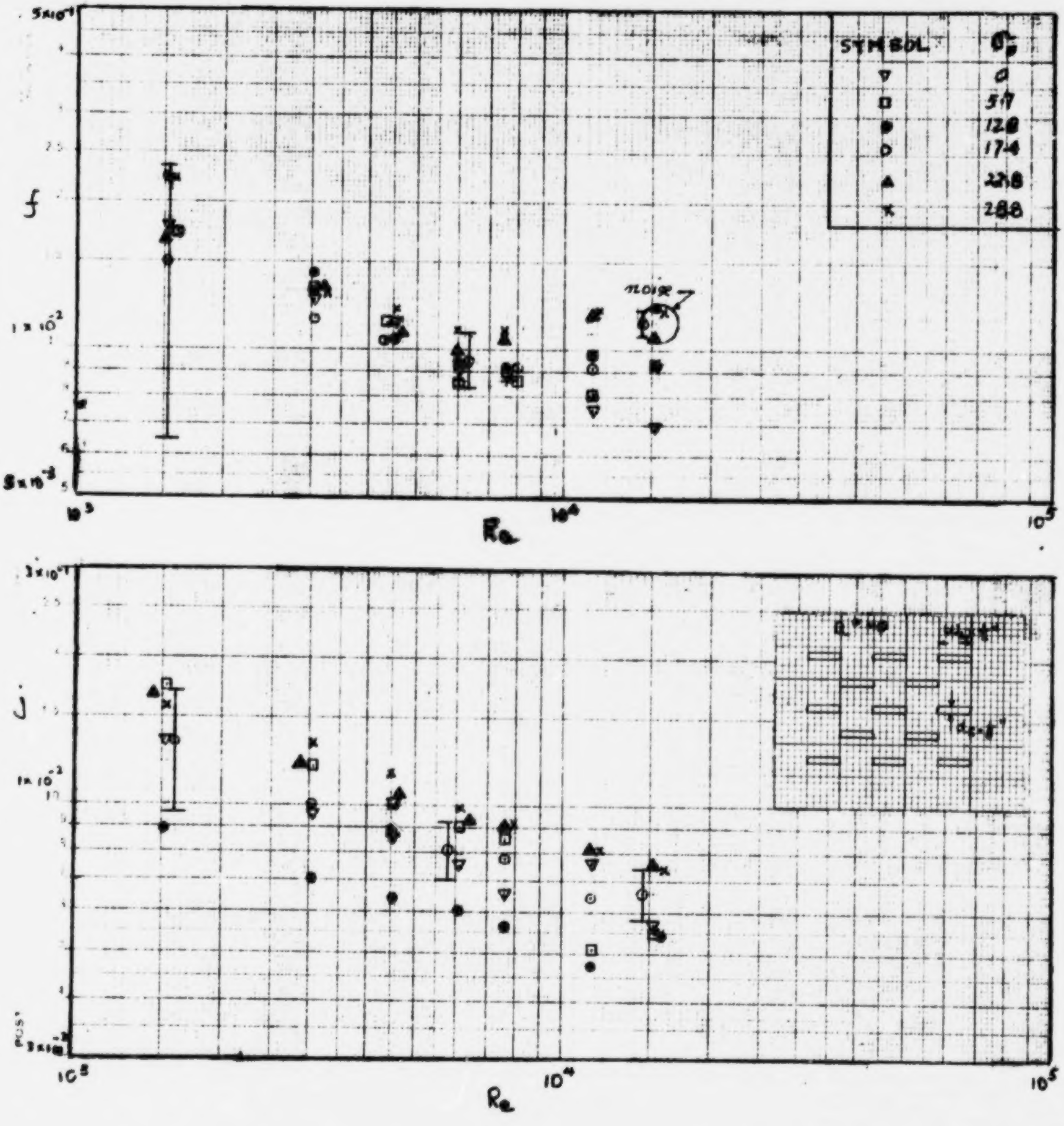

Fig. 8a. f and j versus Re, for t/b=0.0665, 1/2" x 1/8" slots in in-line arrangement

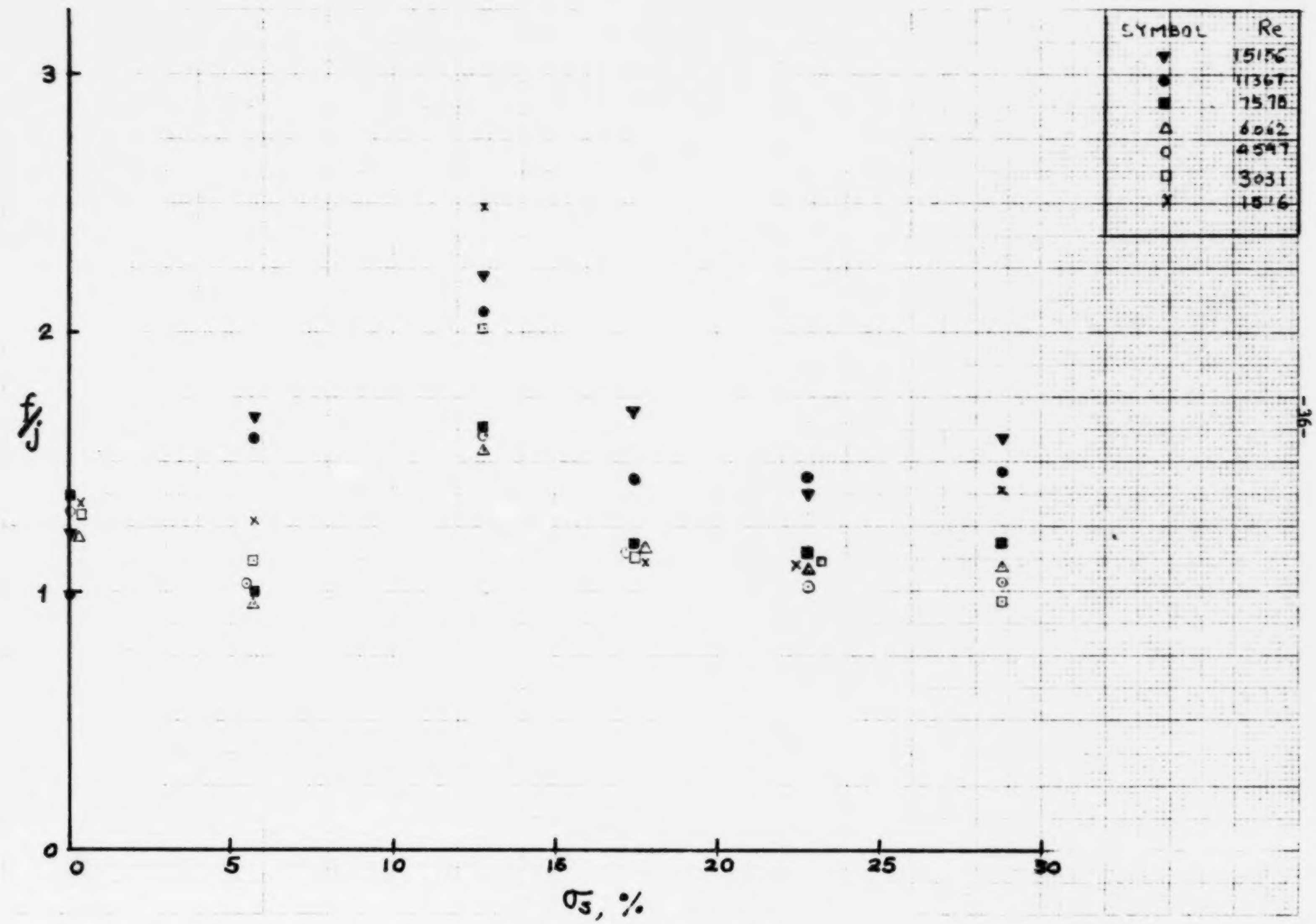

Fig. 8b. f/j versus σ_s, for t/b=0.0665, 1/2" x 1/8" slots in in-line arrangement

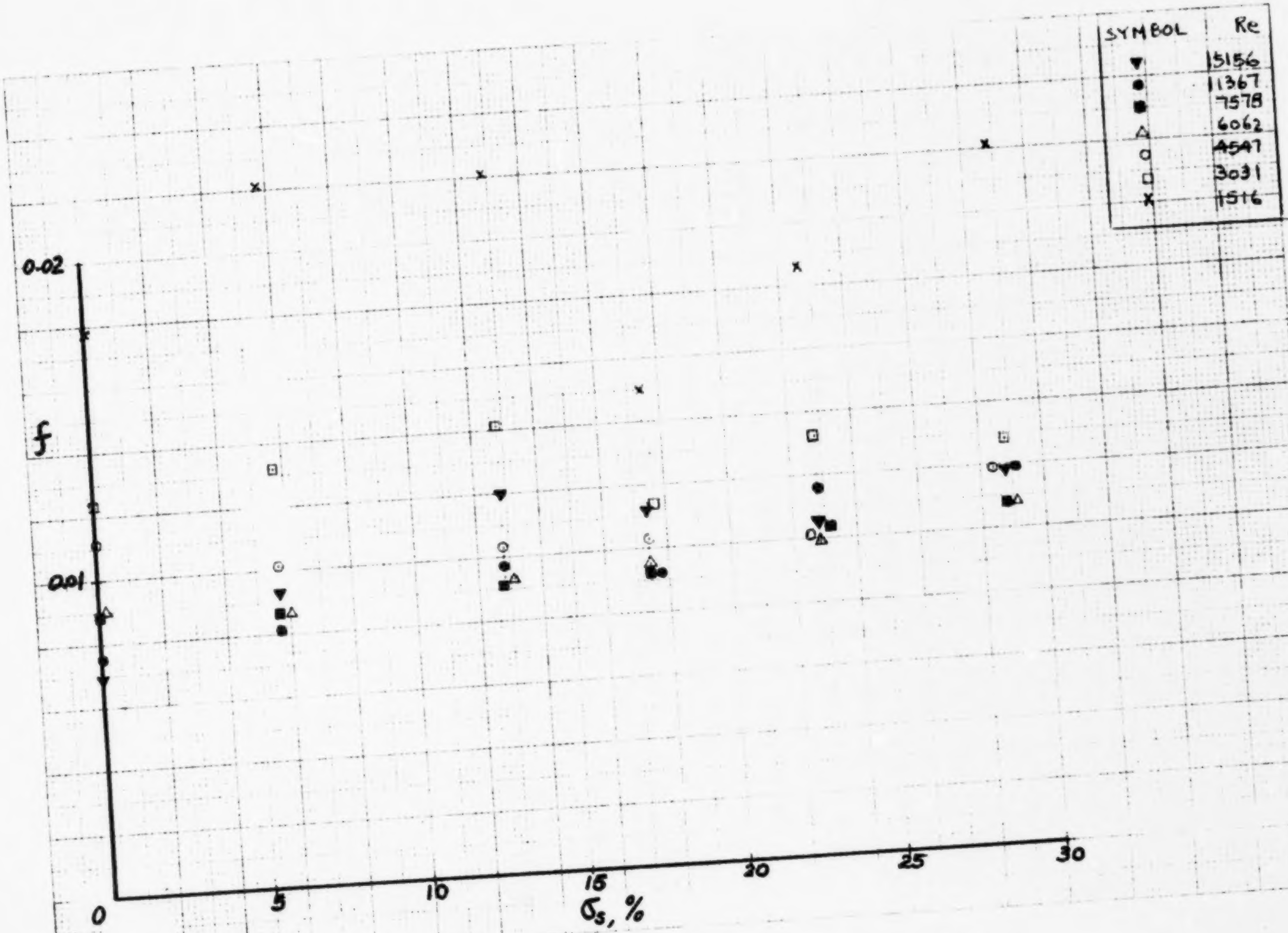

Fig. 8c. f versus σ_s, for t/b=0.0665, 1/2" x 1/8" slots in in-line arrangement

20 Squares to the Inch

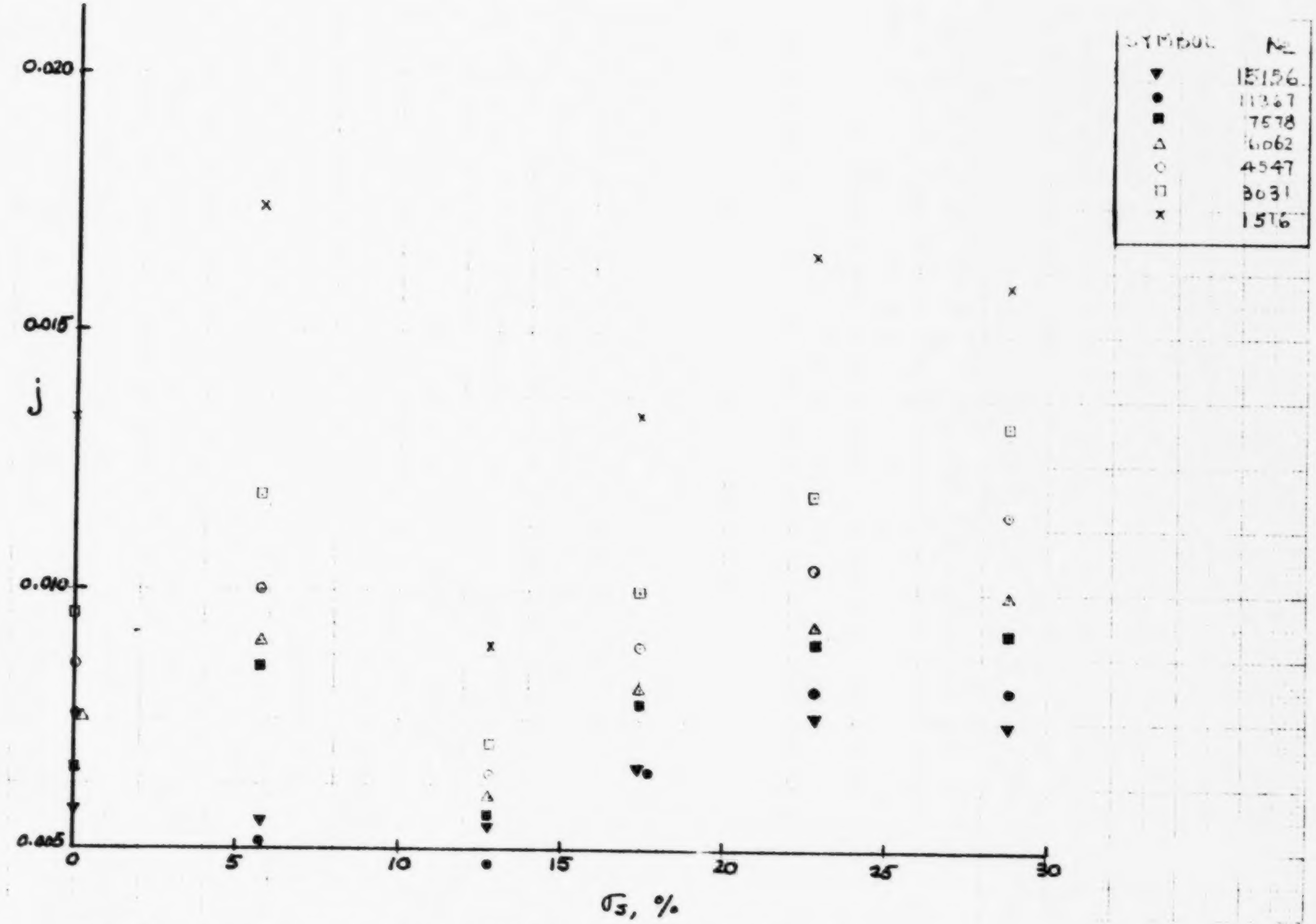

Fig. 8d. j versus σ_s, for t/b=0.0665, 1/2" x 1/8" slots in in-line arrangement

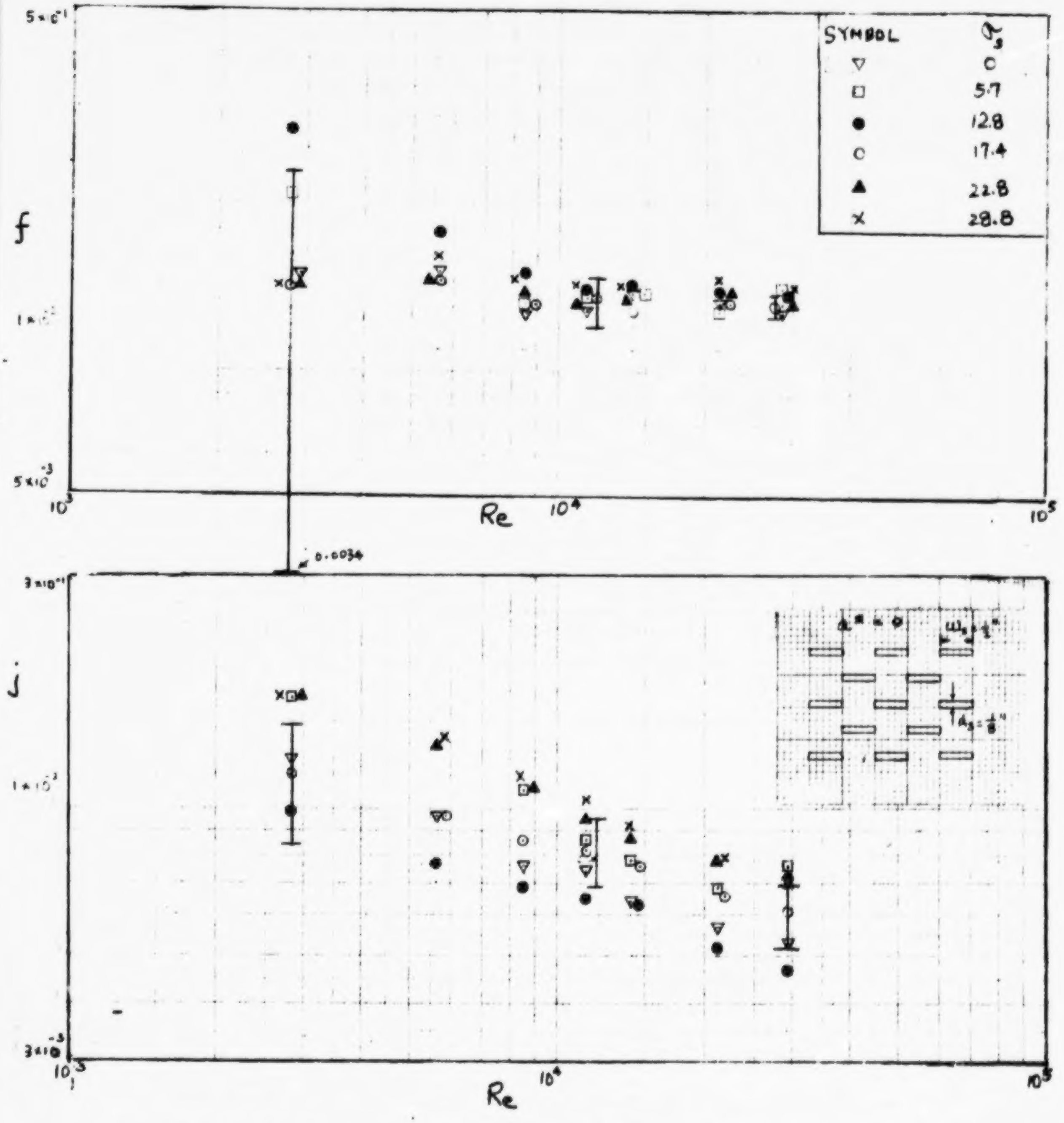

Fig. 9a. f and j versus Re, for t/b=0.0321, 1/2" x 1/8" slots in in-line arrangement

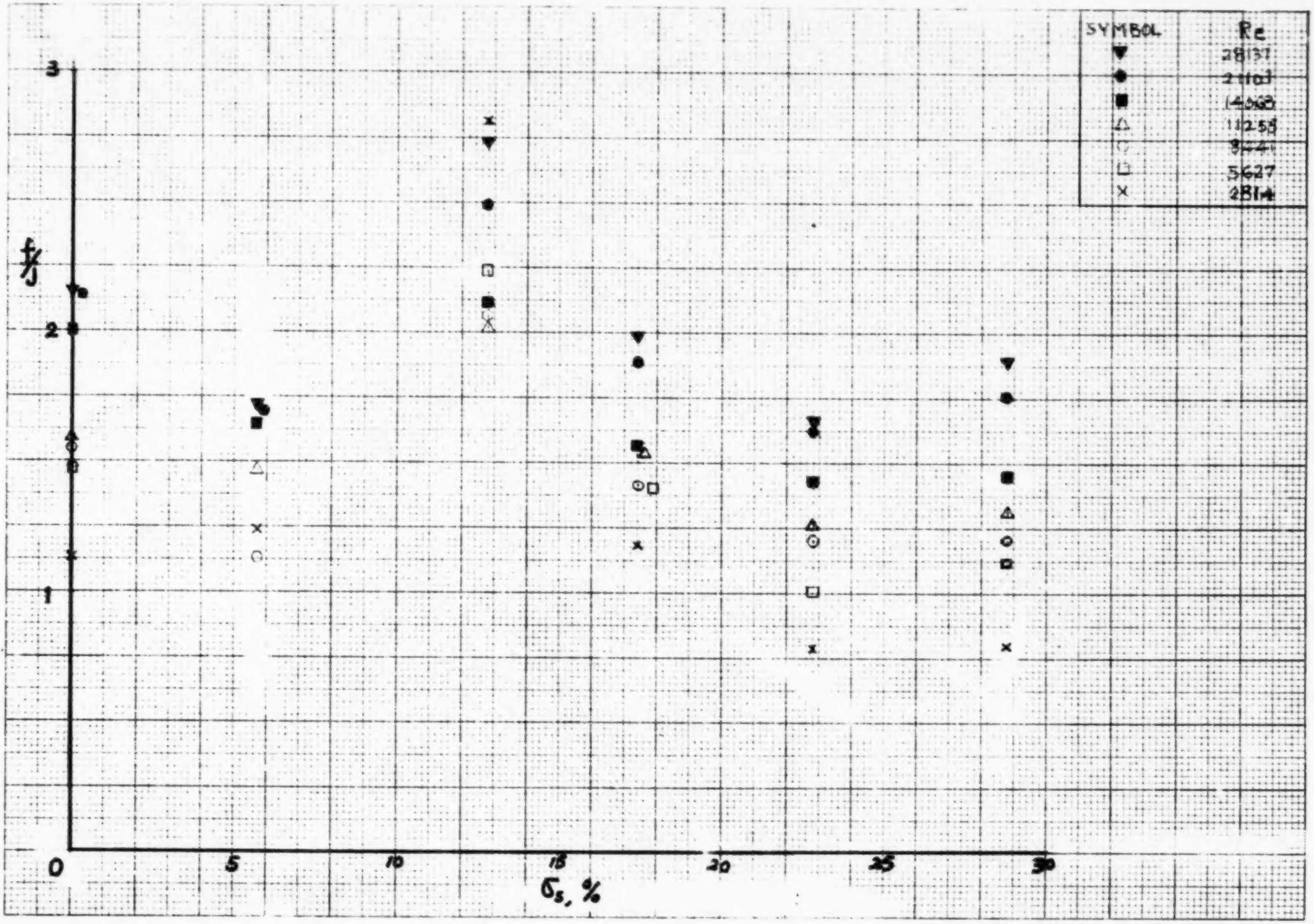

Fig. 9b. f/j versus σ_s, for t/b=0.0321, 1/2" x 1/8" slots in in-line arrangement

20 Squares to the inch

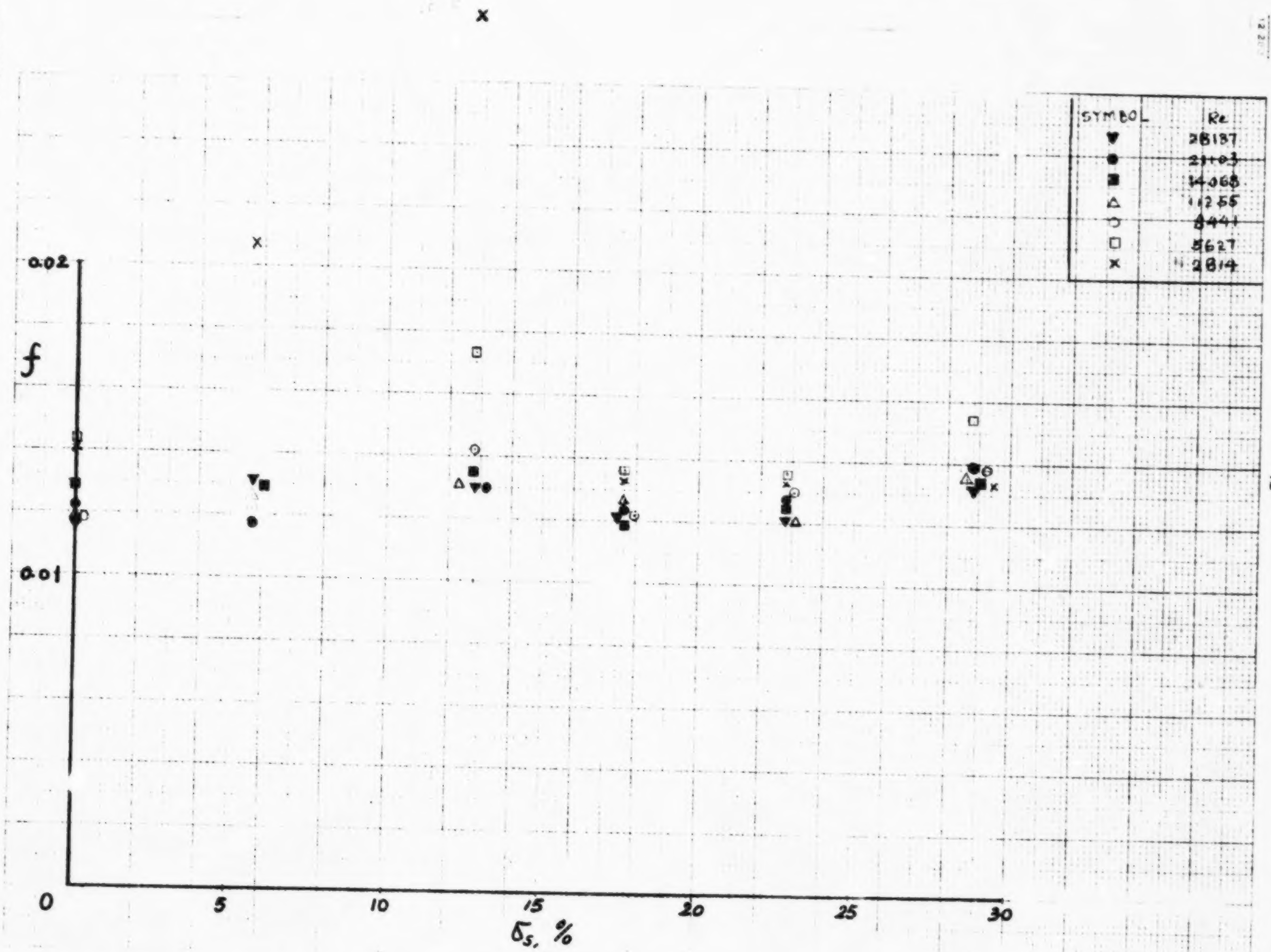

Fig. 9c. f versus σ_s, for t/b=0.0321, 1/2" x 1/8" slots in in-line arrangement

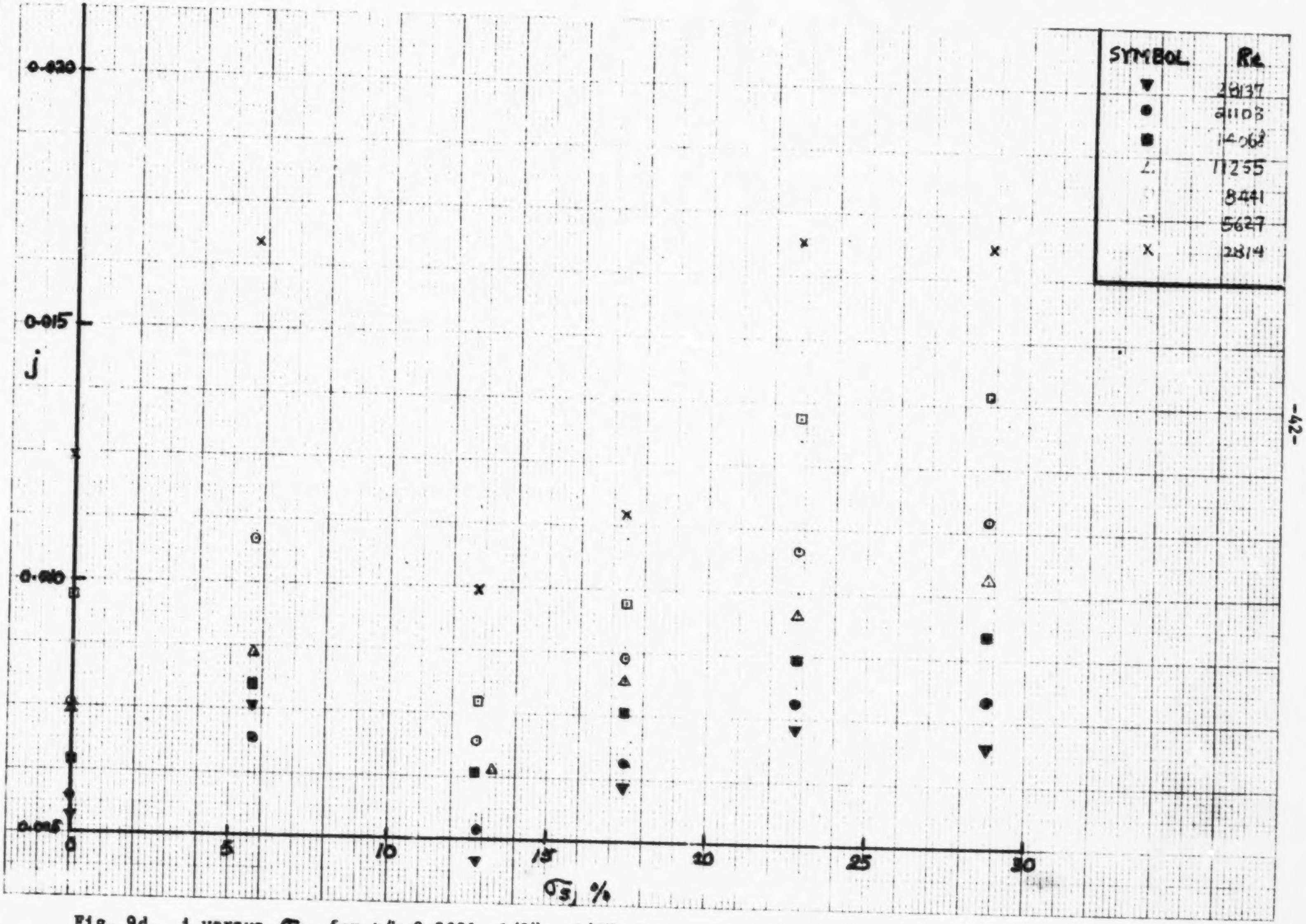

Fig. 9d. j versus σ_s, for t/b=0.0321, 1/2" x 1/8" slots in in-line arrangement

20 Squares to the Inch

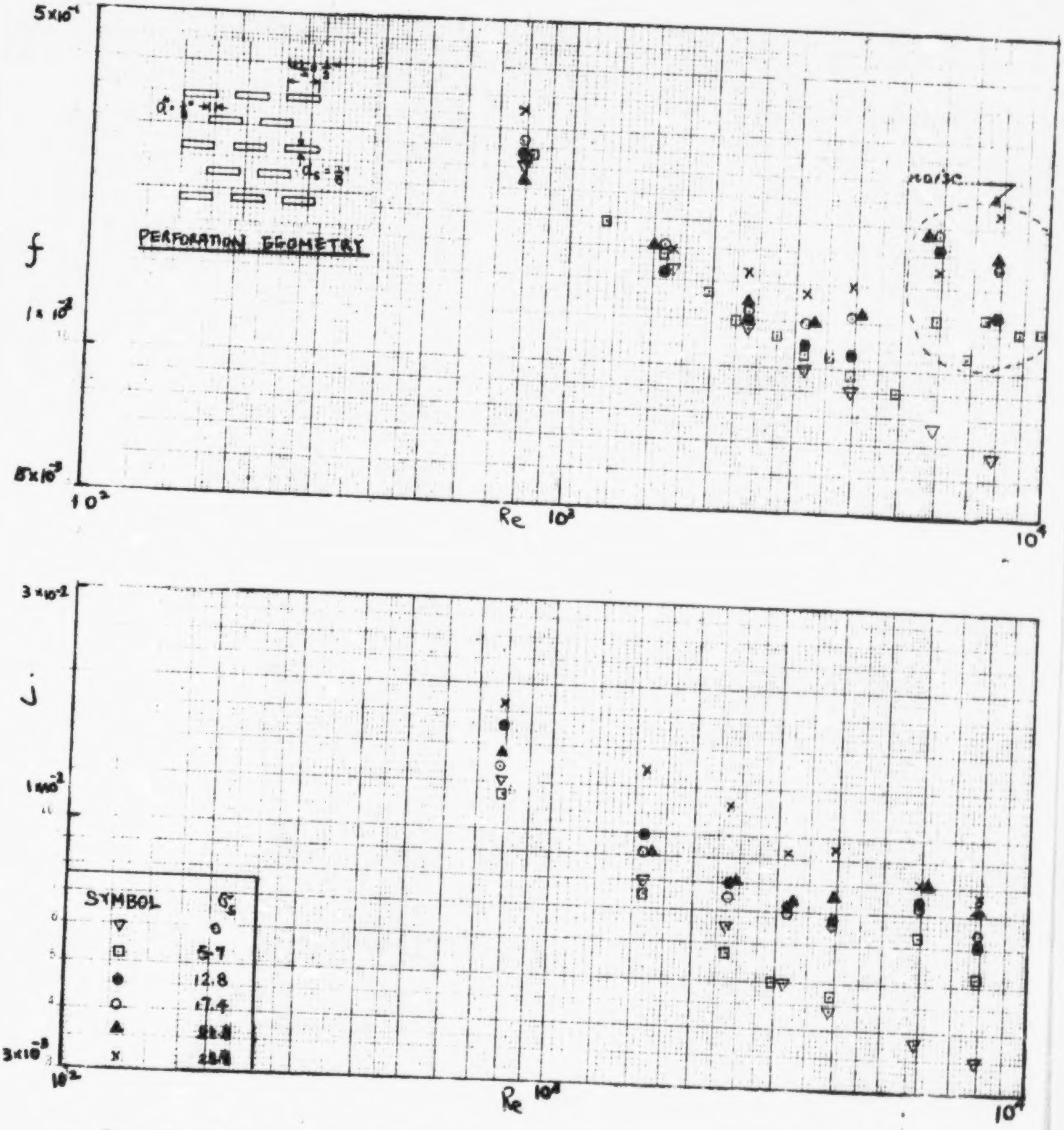

Fig. 10a. f and j versus Re, for t/b=0.141, 1/2" x 1/8" slots in overlap arrangement.

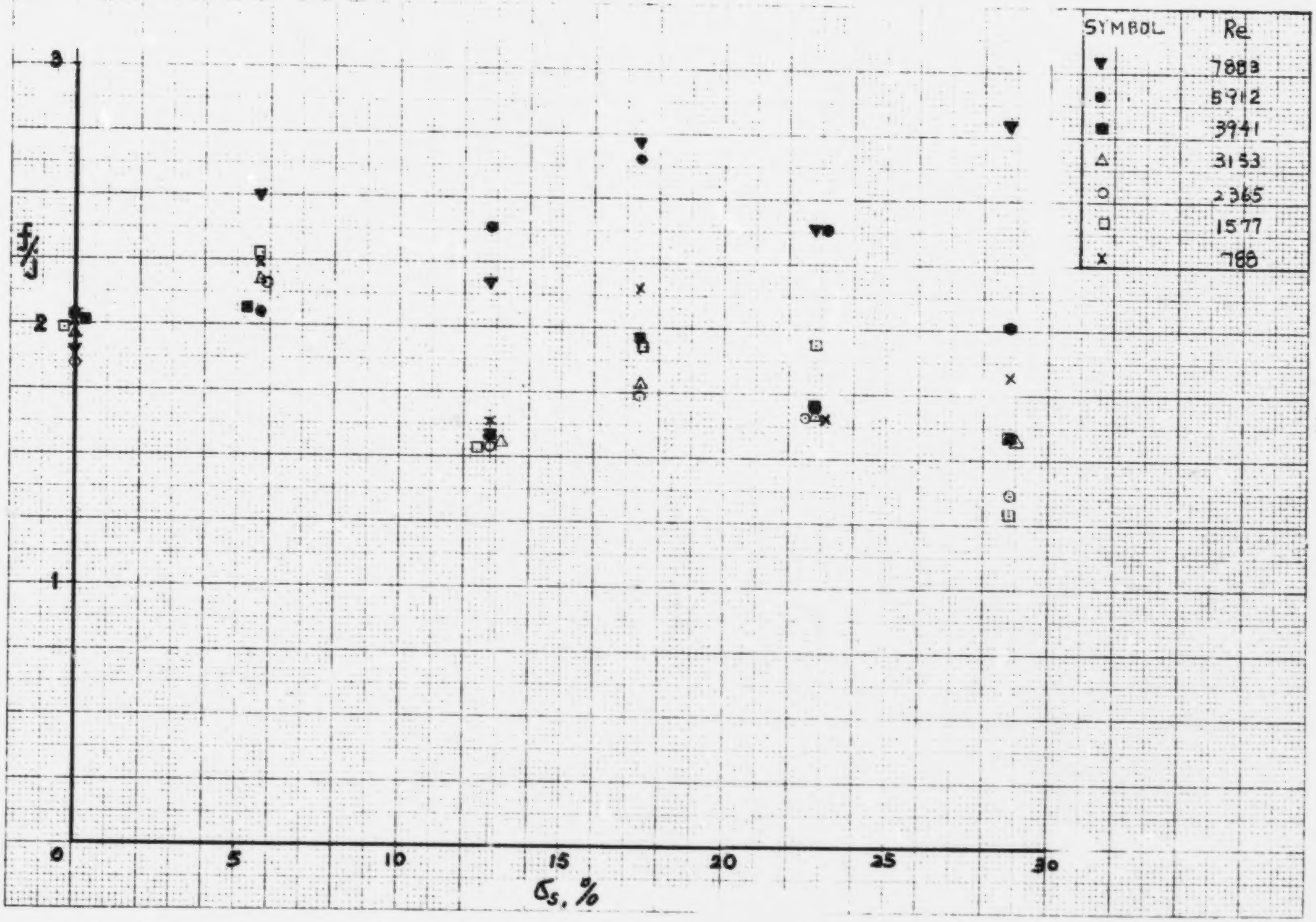

Fig. 10b f/J versus σ_s for t/b=0.141 1/2" x 1/8" slots in overlap arrangement.

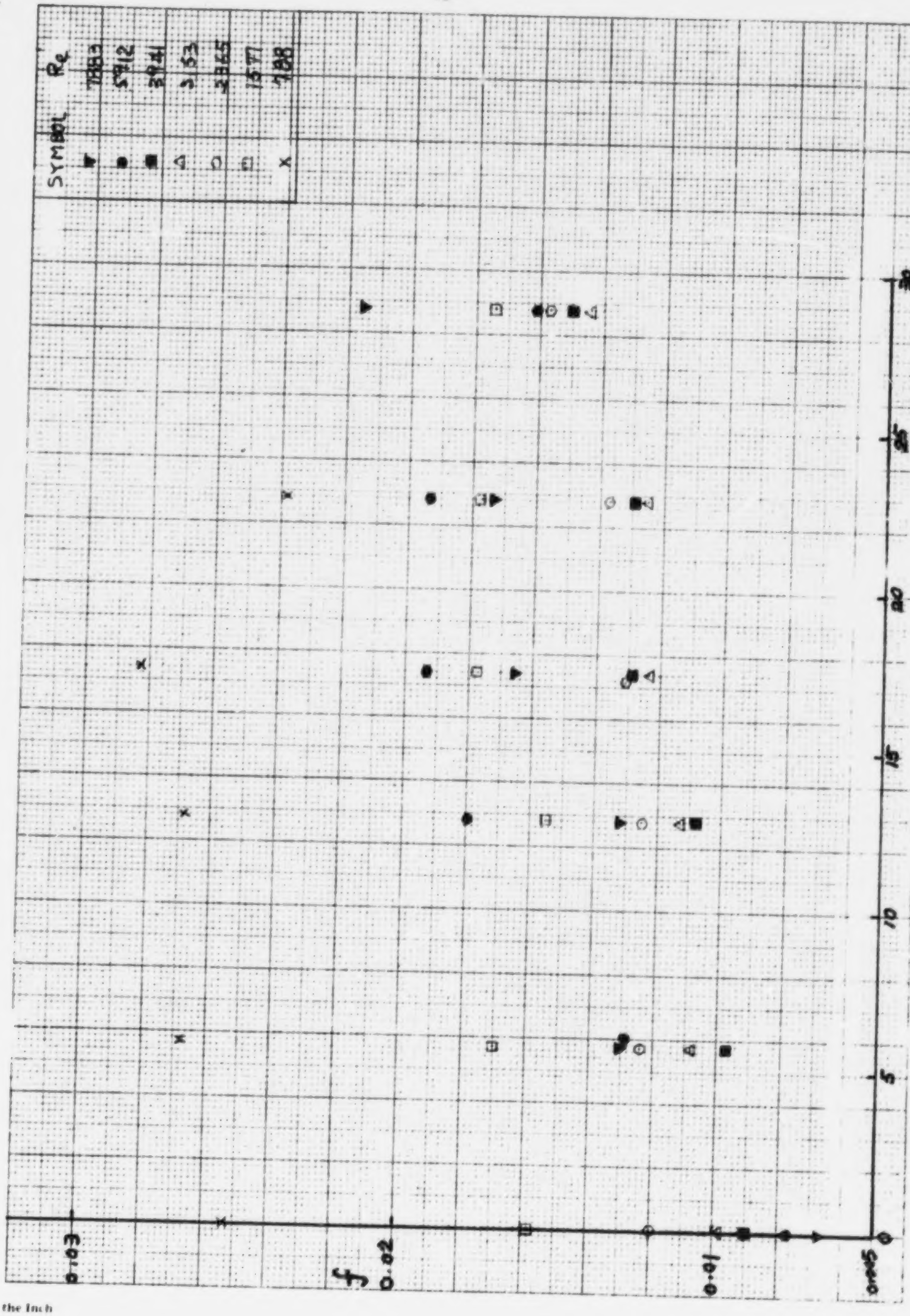

Fig. 10c. f versus δ_s, for t/b=0.141, 1/2" x 1/8" slots in overlap arrangement.

20 Squares to the Inch

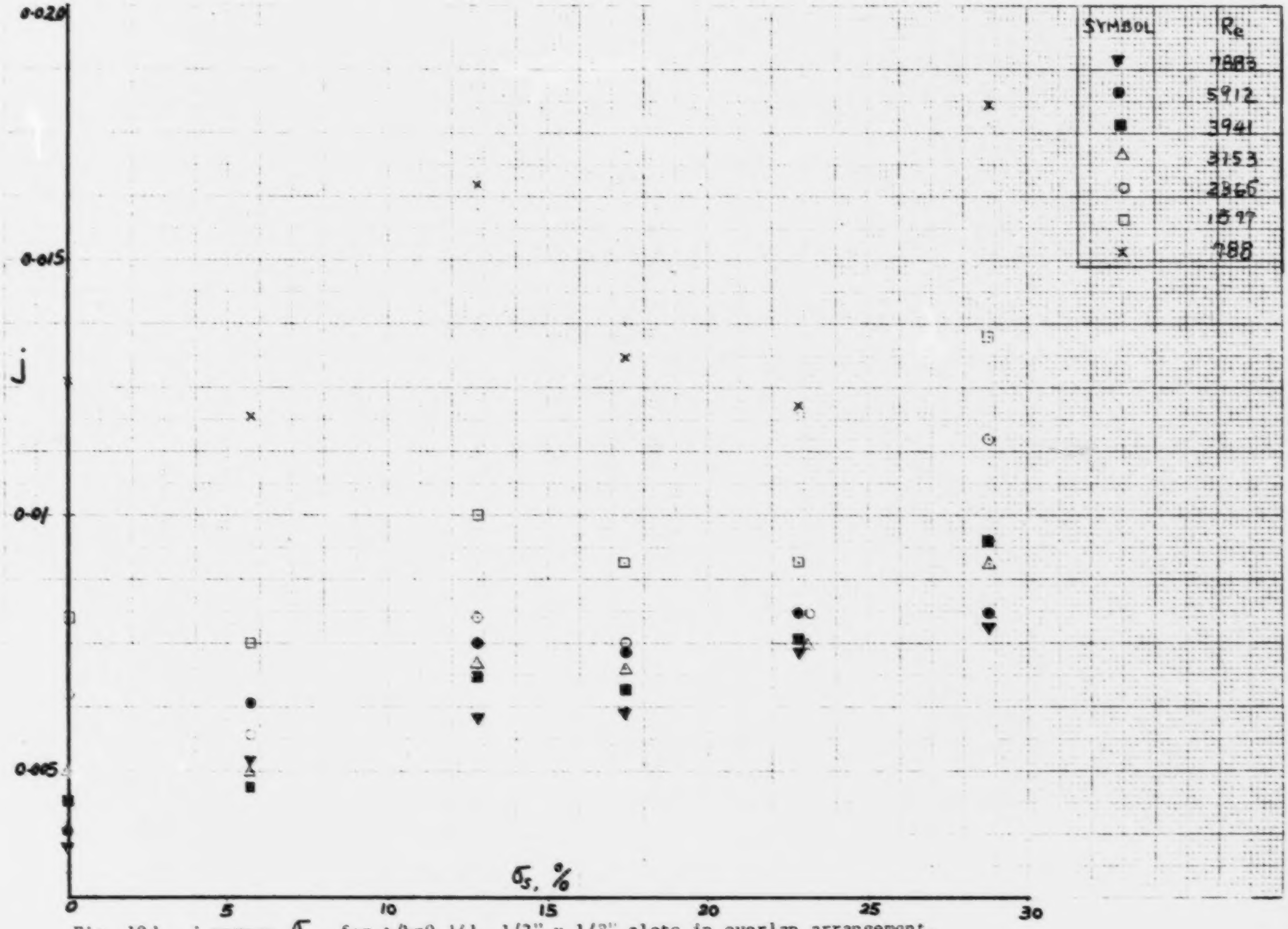

Fig. 10d. j versus σ_s, for t/b=0.141, 1/2" x 1/3" slots in overlap arrangement.

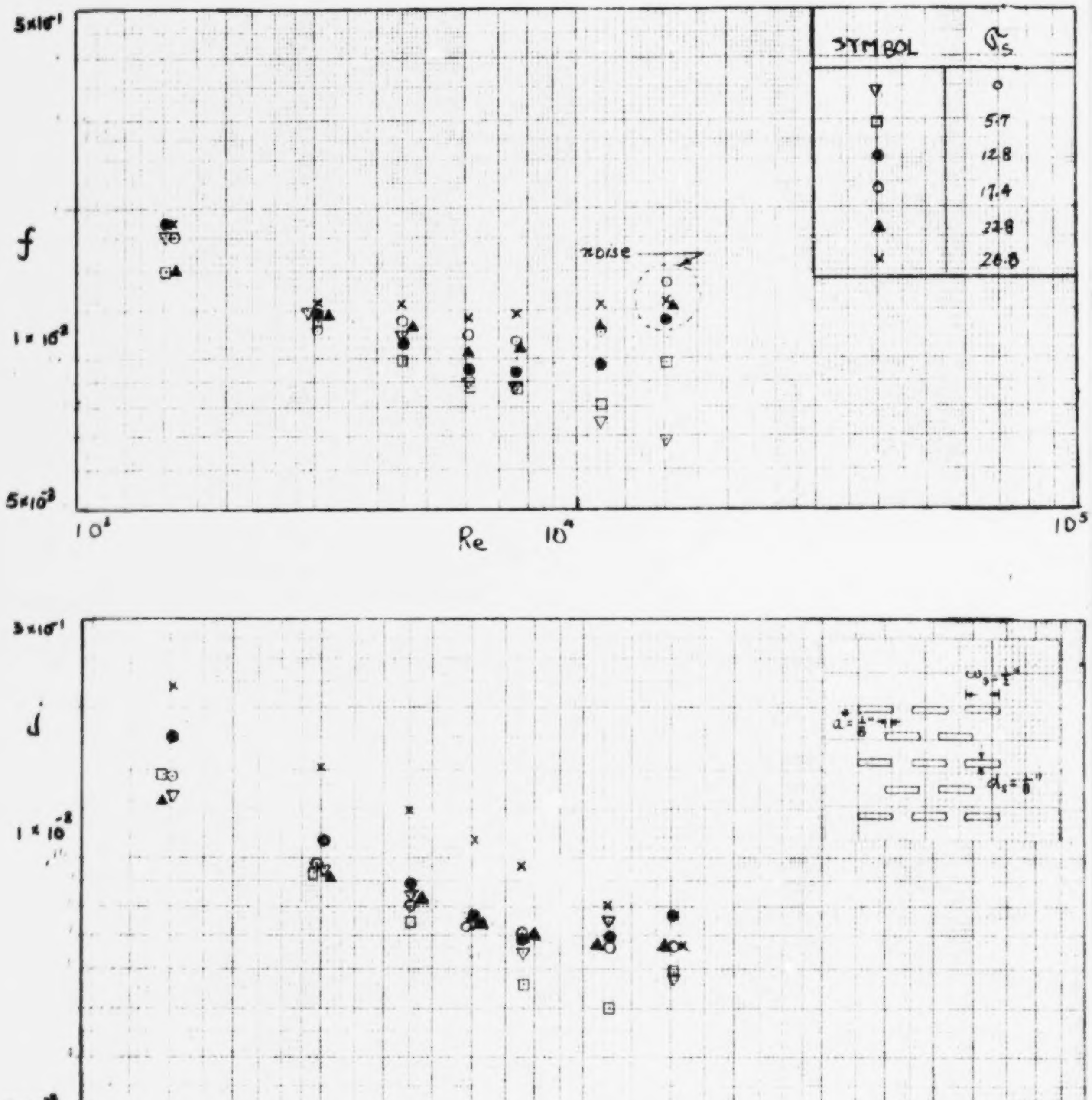

Fig. 11a. f and j versus Re, for t/b=0.0665, 1/2" x 1/8" slots in overlap arrangement

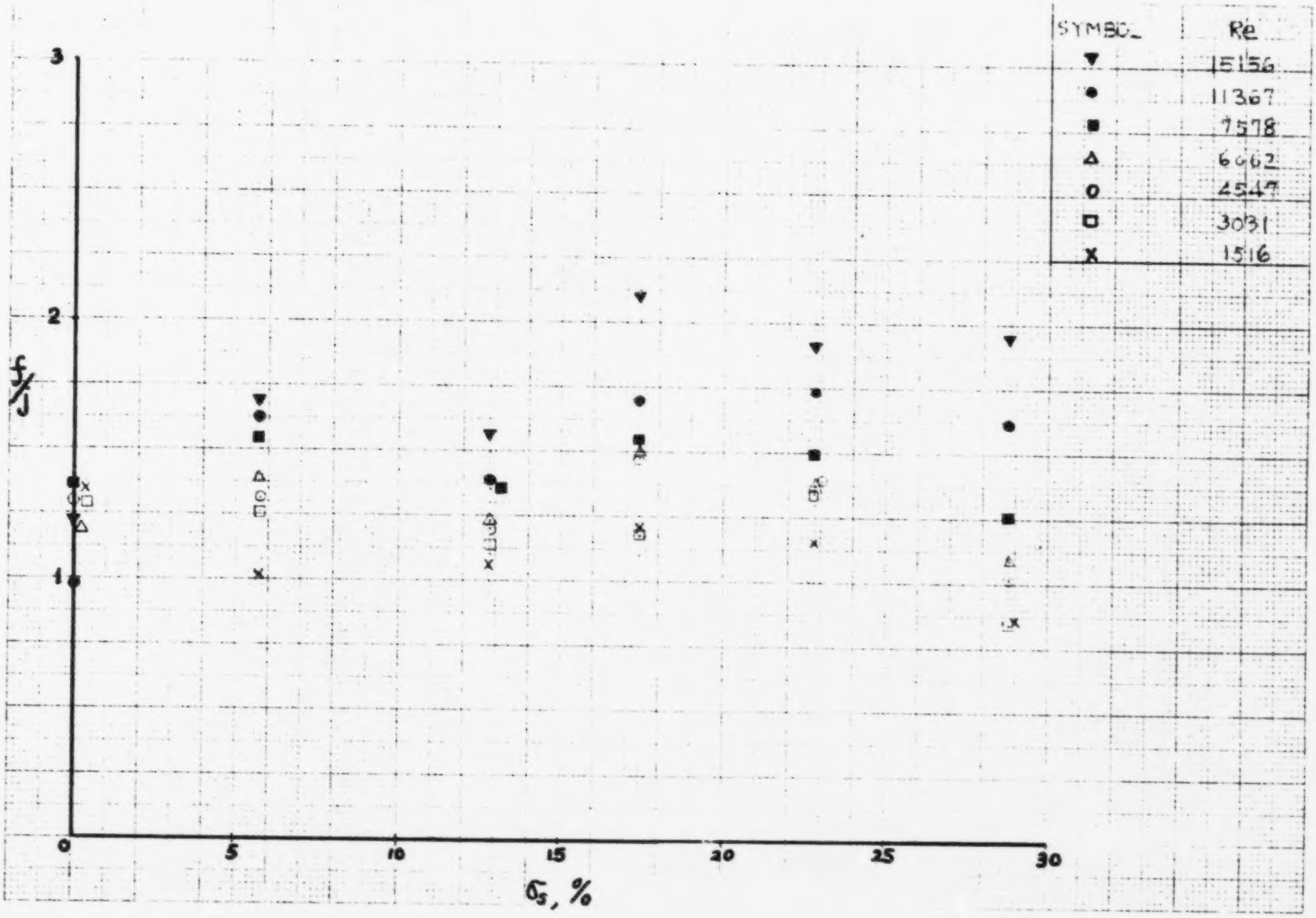

Fig. 11b. f/j versus σ_s, for t/b=0.0665, 1/2" x 1/8" slots in overlap arrangement

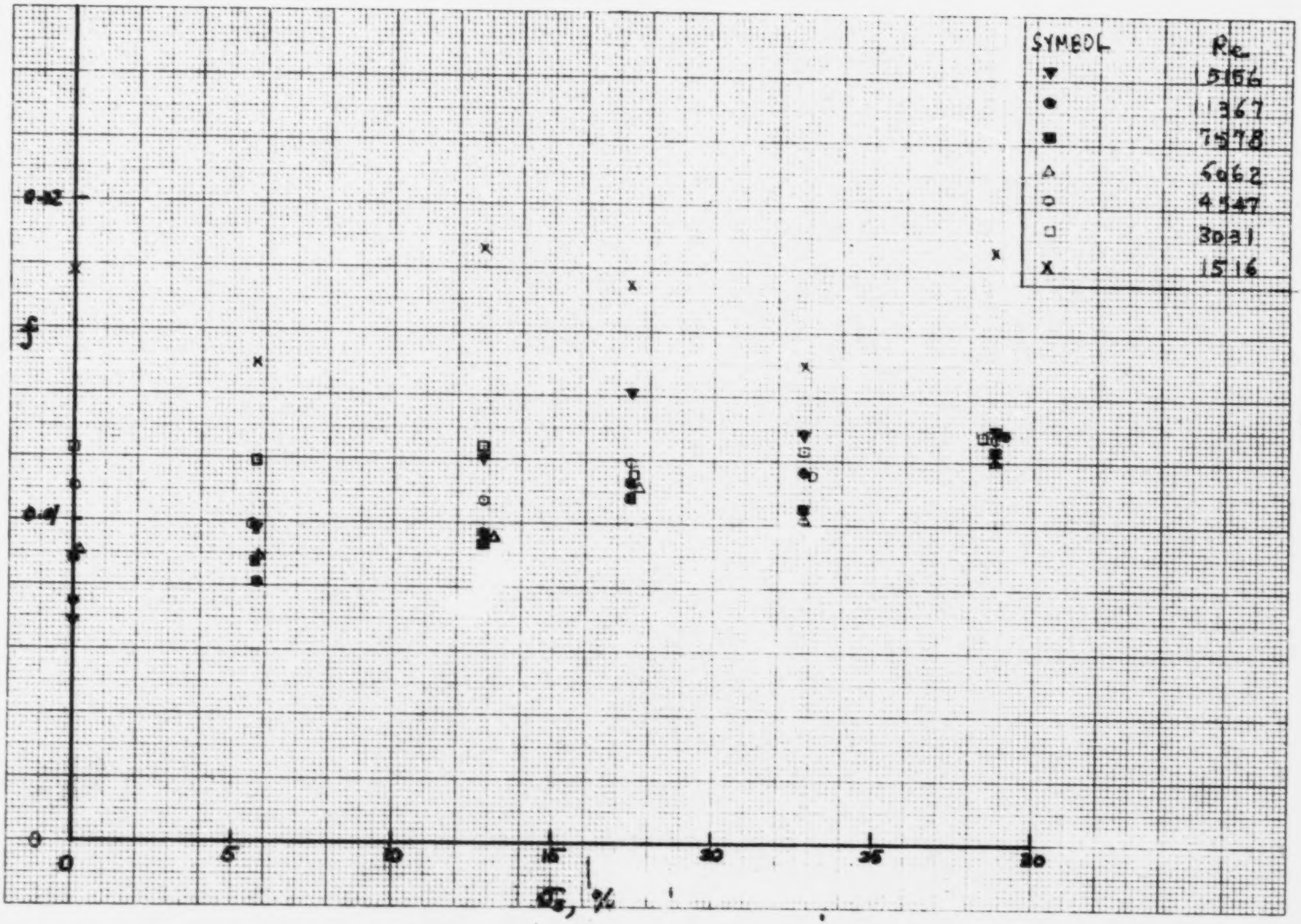

Fig. 11c. f versus σ_s, for t/b=0.0665, 1/2" x 1/8" slots in overlap arrangement.

20 Squares to the Inch

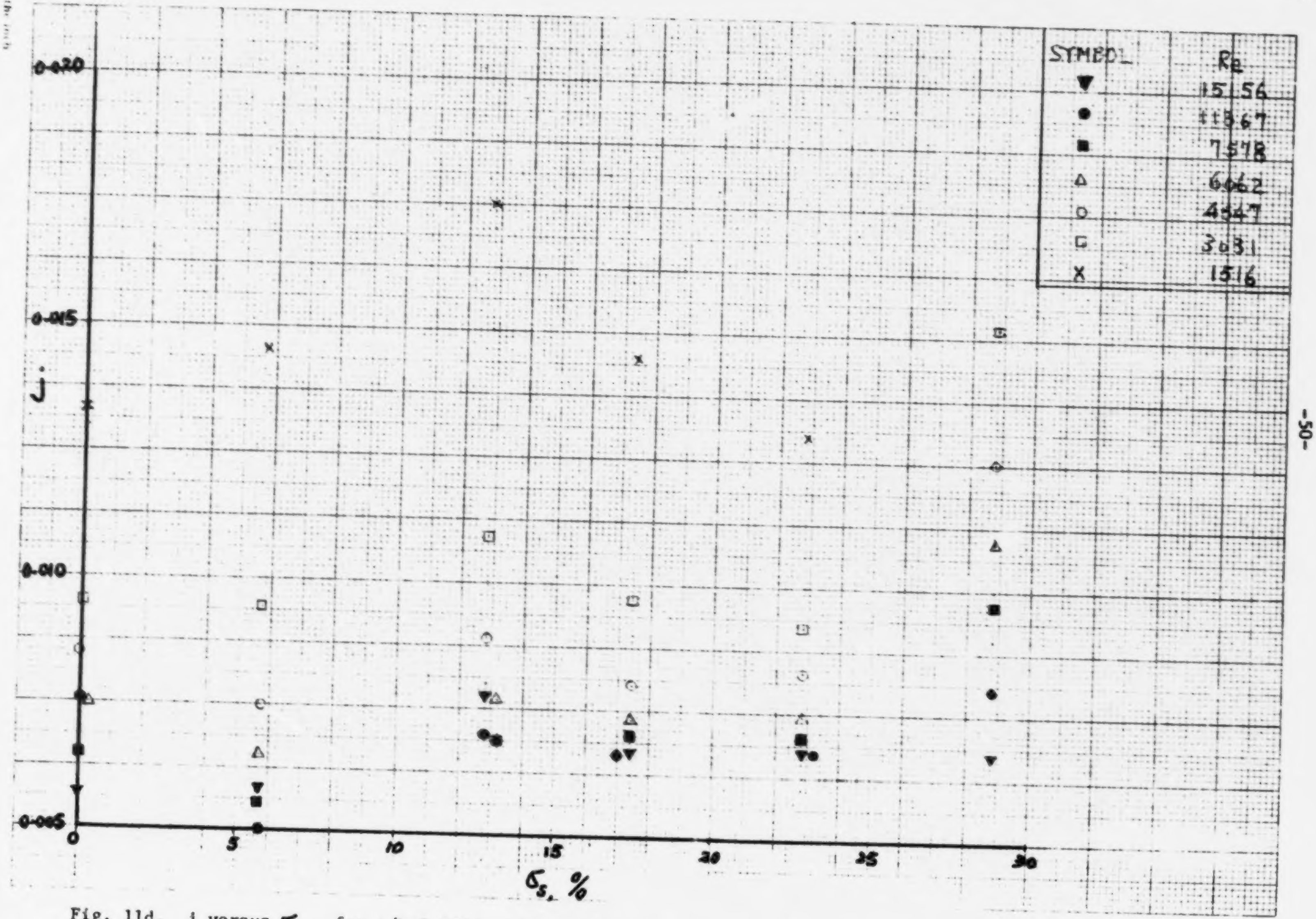

Fig. 11d. j versus σ_s, for t/b=0.0665, 1/2" x 1/8" slots in overlap arrangement.

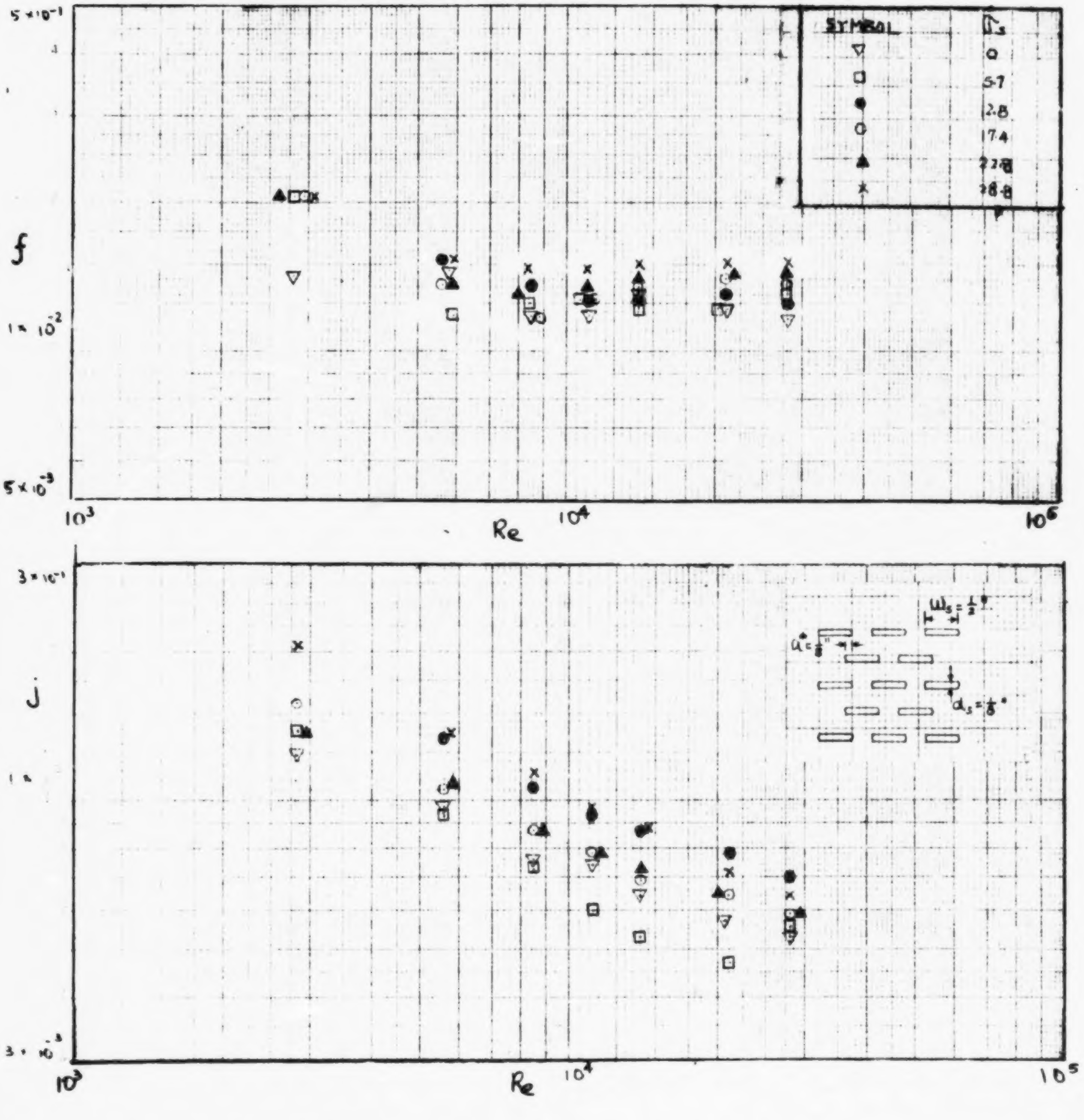

Fig. 12a. f and j versus Re, for t/b=0.0321, 1/2" x 1/8" slots in overlap arrangement.

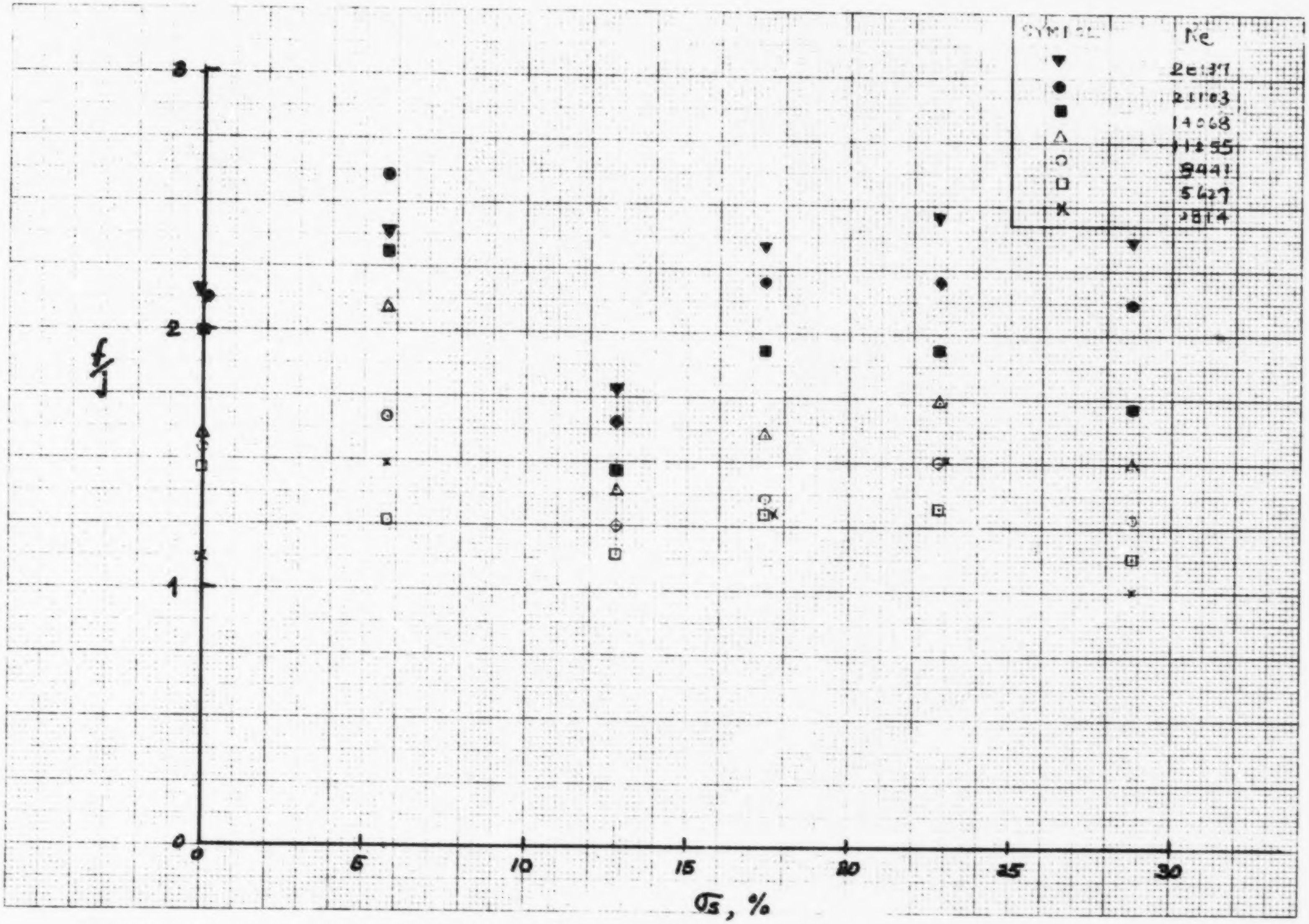

Fig. 12b. f/j versus σ_s, for t/b=0.0321, 1/2" x 1/8" slots in overlap arrangement.

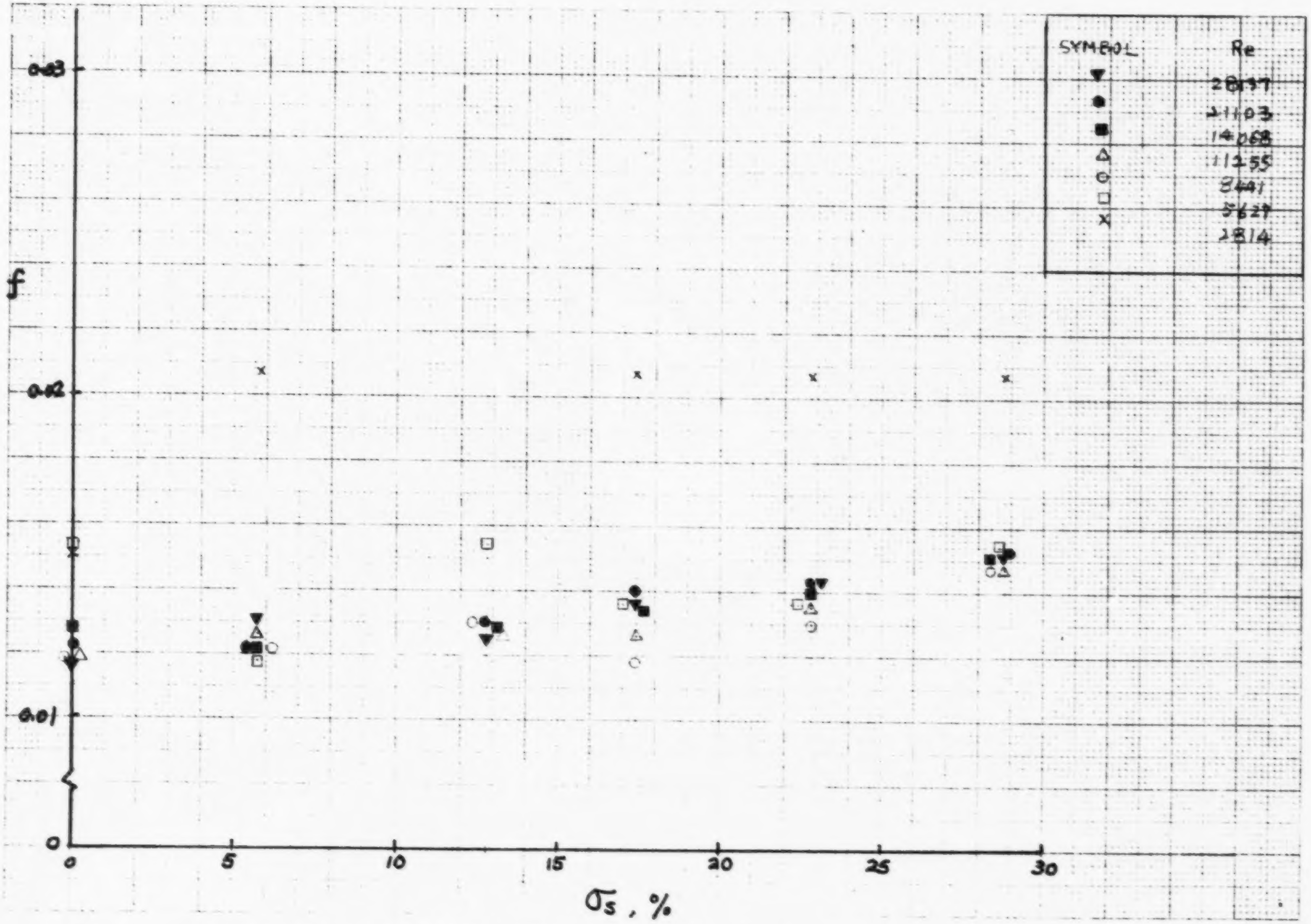

Fig. 12c. f versus σ_s, for t/b=0.0321, 1/2" x 1/8" slots in overlap arrangement.

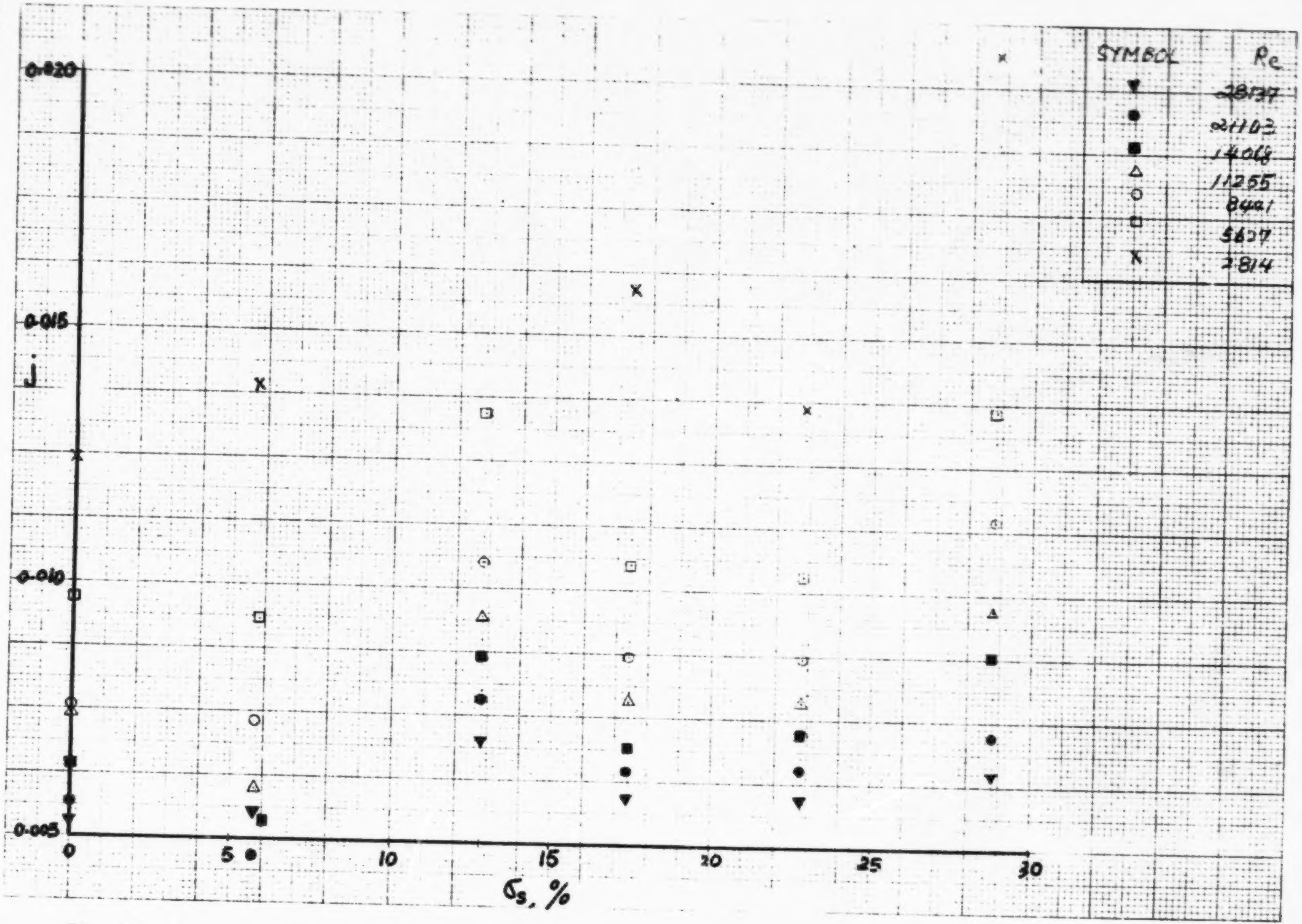

Fig. 12d. j versu σ_s, for t/b=0.0321, 1/2" x 1/8" slots in overlap arrangement.

20 Squares to the Inch

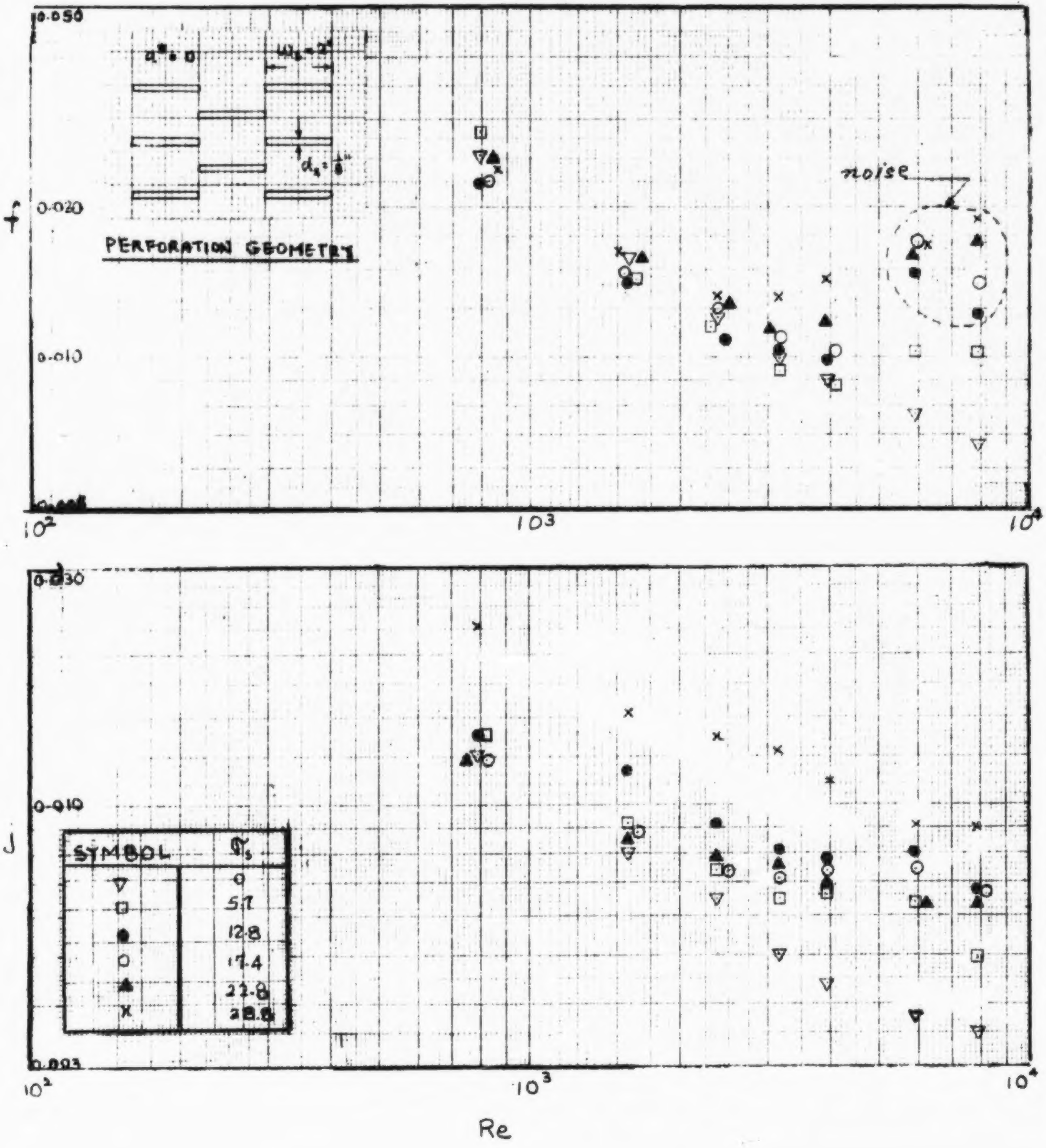

Fig. 13a. f and j versus Re, for t/b=0.141, 2" x 1/8" in in-line arrangement

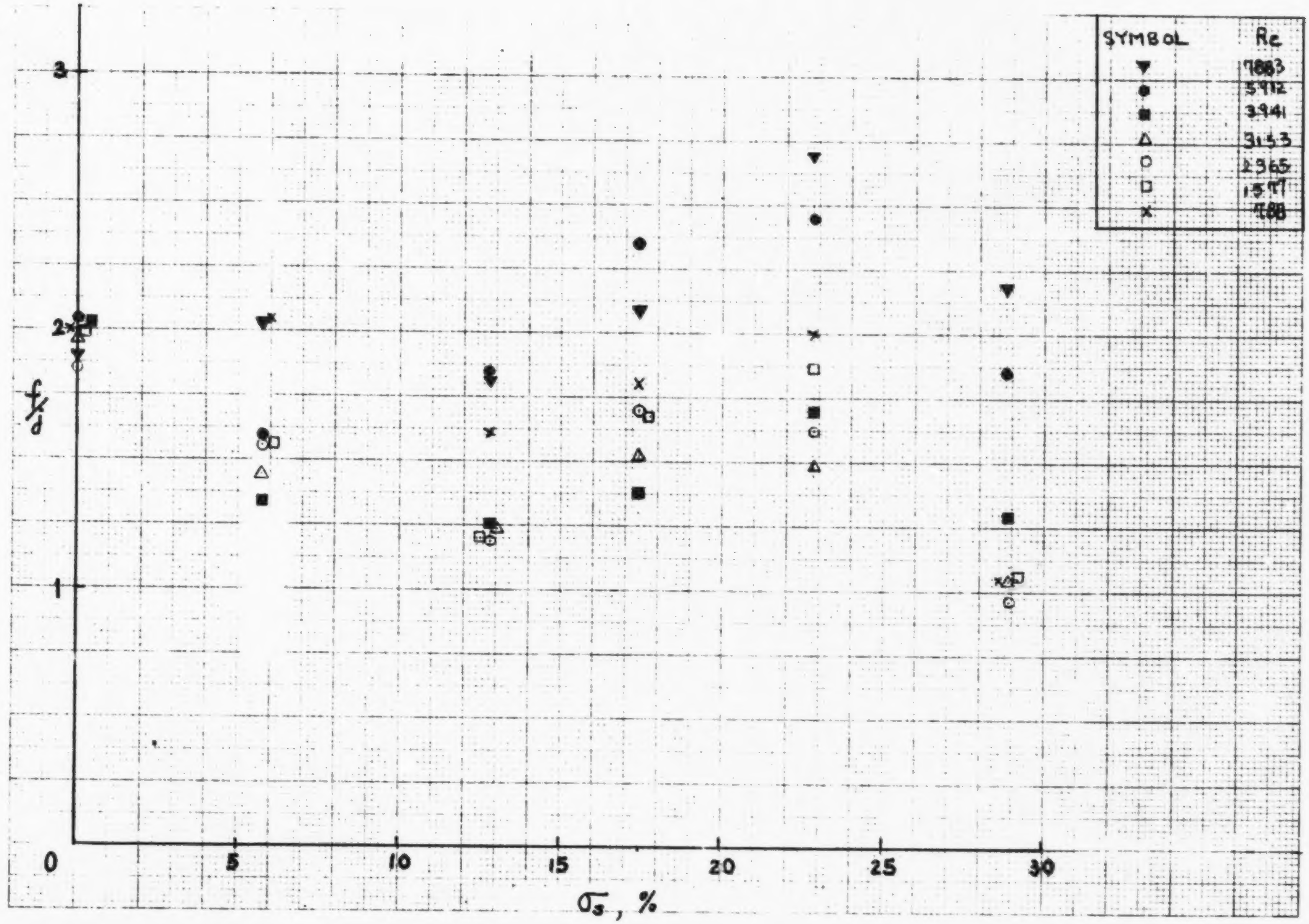

Fig. 13b. f/j versus σ_s, for t/b=0.141, 2" x 1/8" slots in in-line arrangement.

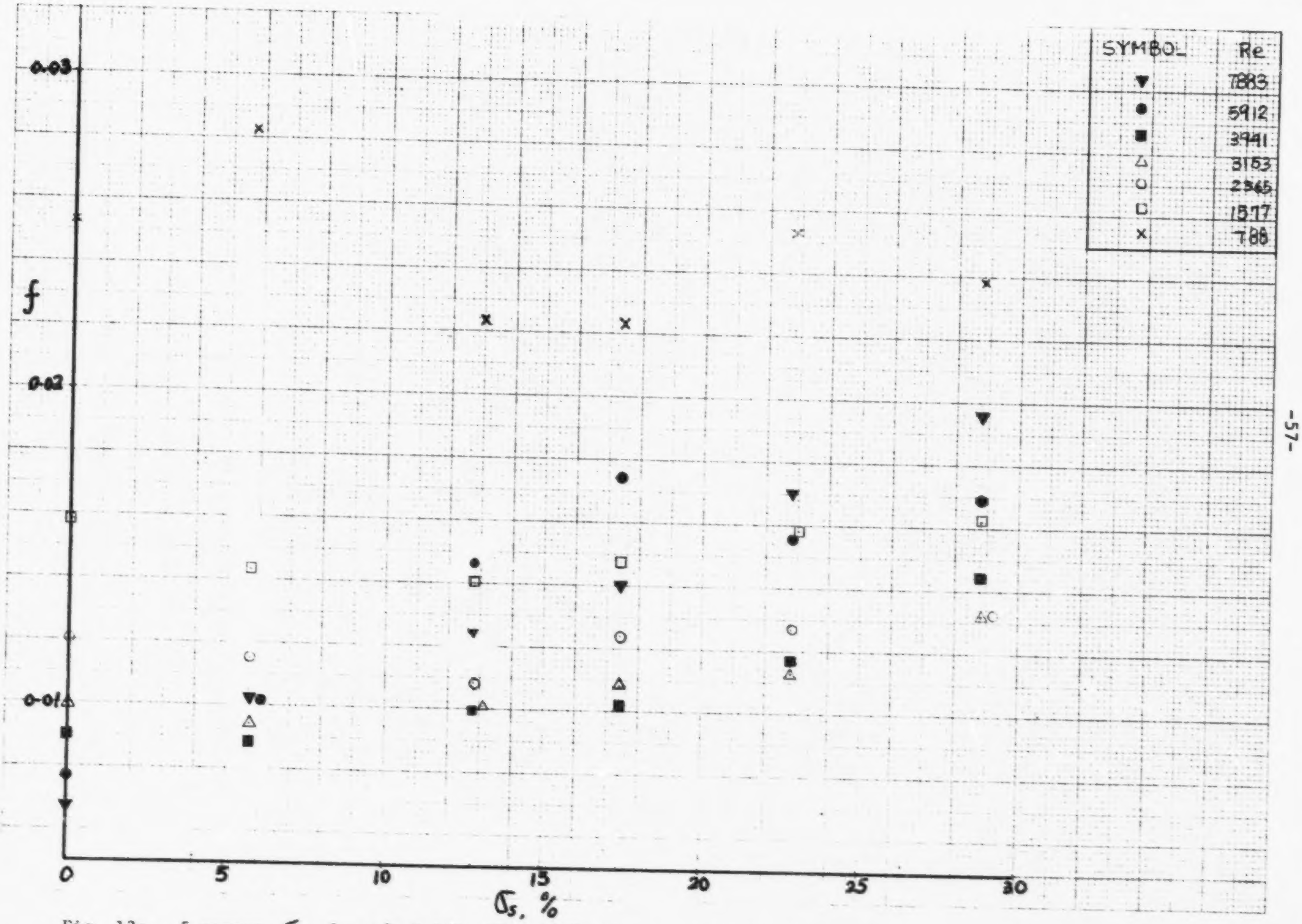

Fig. 13c. f versus σ_s, for t/b=0.141, 2" x 1/8" slots in in-line arrangement.

20 Squares to the Inch

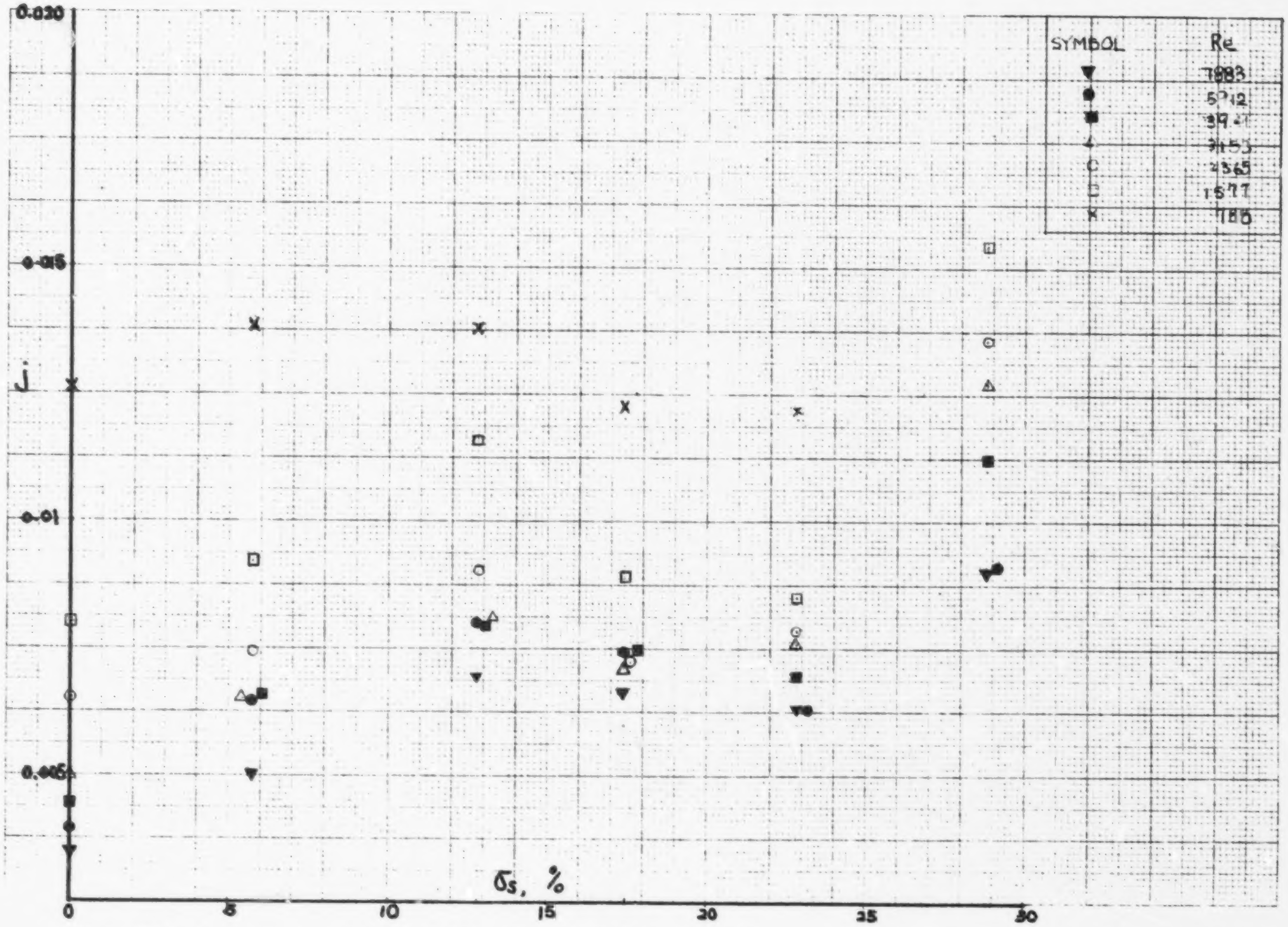

Fig. 13d. j versus σ s, for t/b=0.141, 2" x 1/8" slots in in-line arrangement.

20 Squares to the Inch

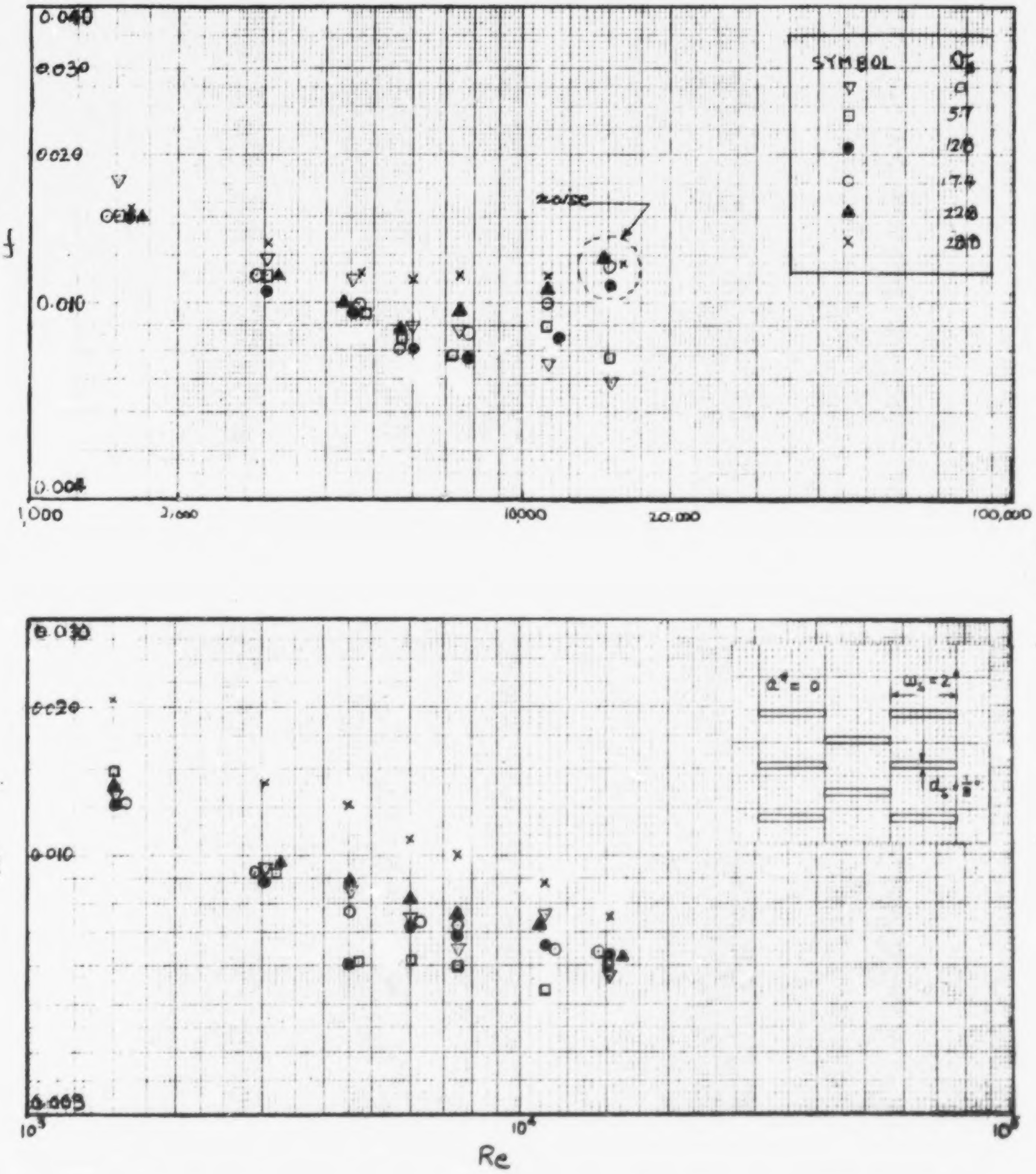

Fig. 14a. f and j versus Re, for t/b=0.0665, 2" x 1/8" slots in in-line arrangement.

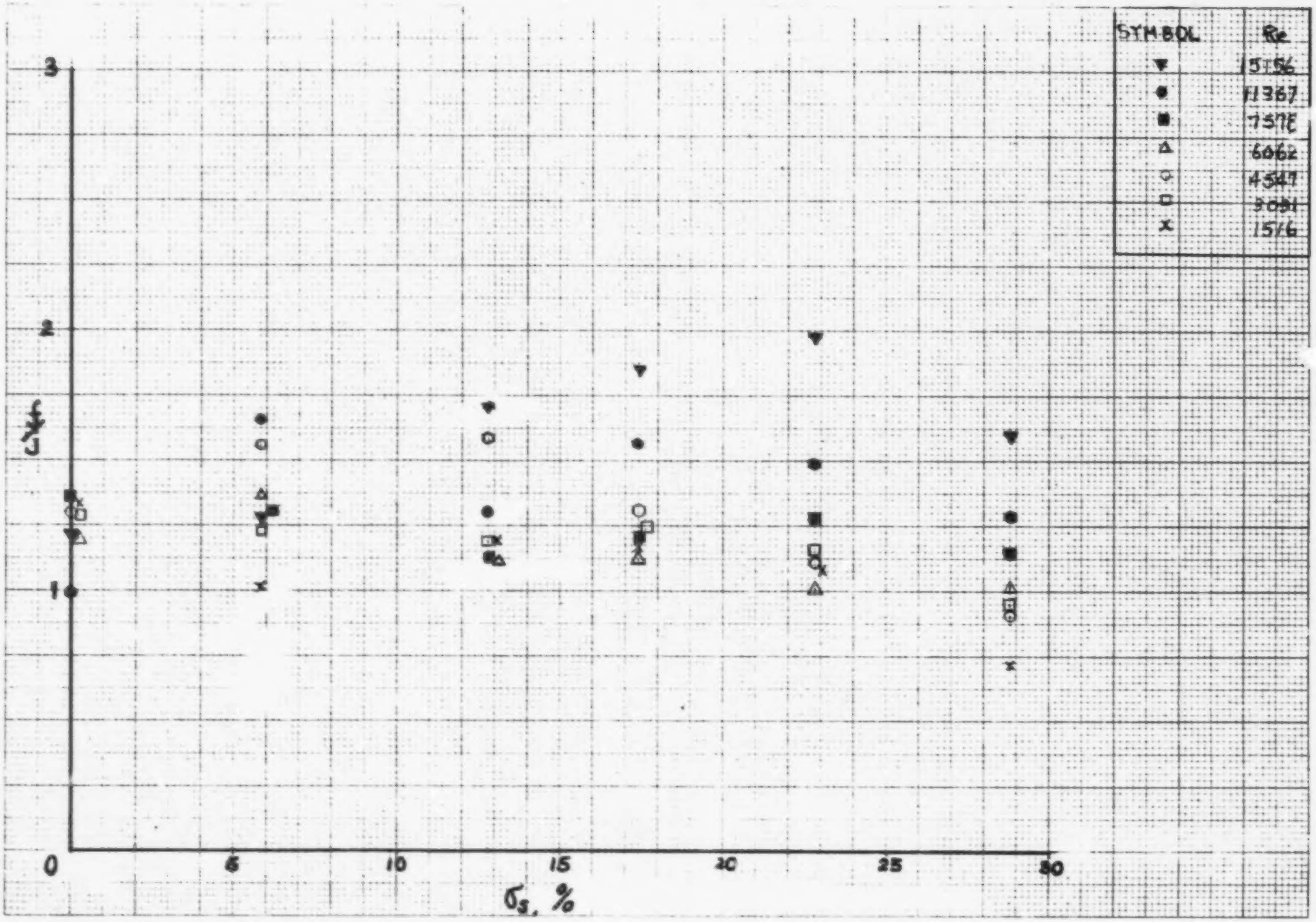

Fig. 14b. f/j versus σ_s, for t/b=0.0665, 2" x 1/8" slots in in-line arrangement.

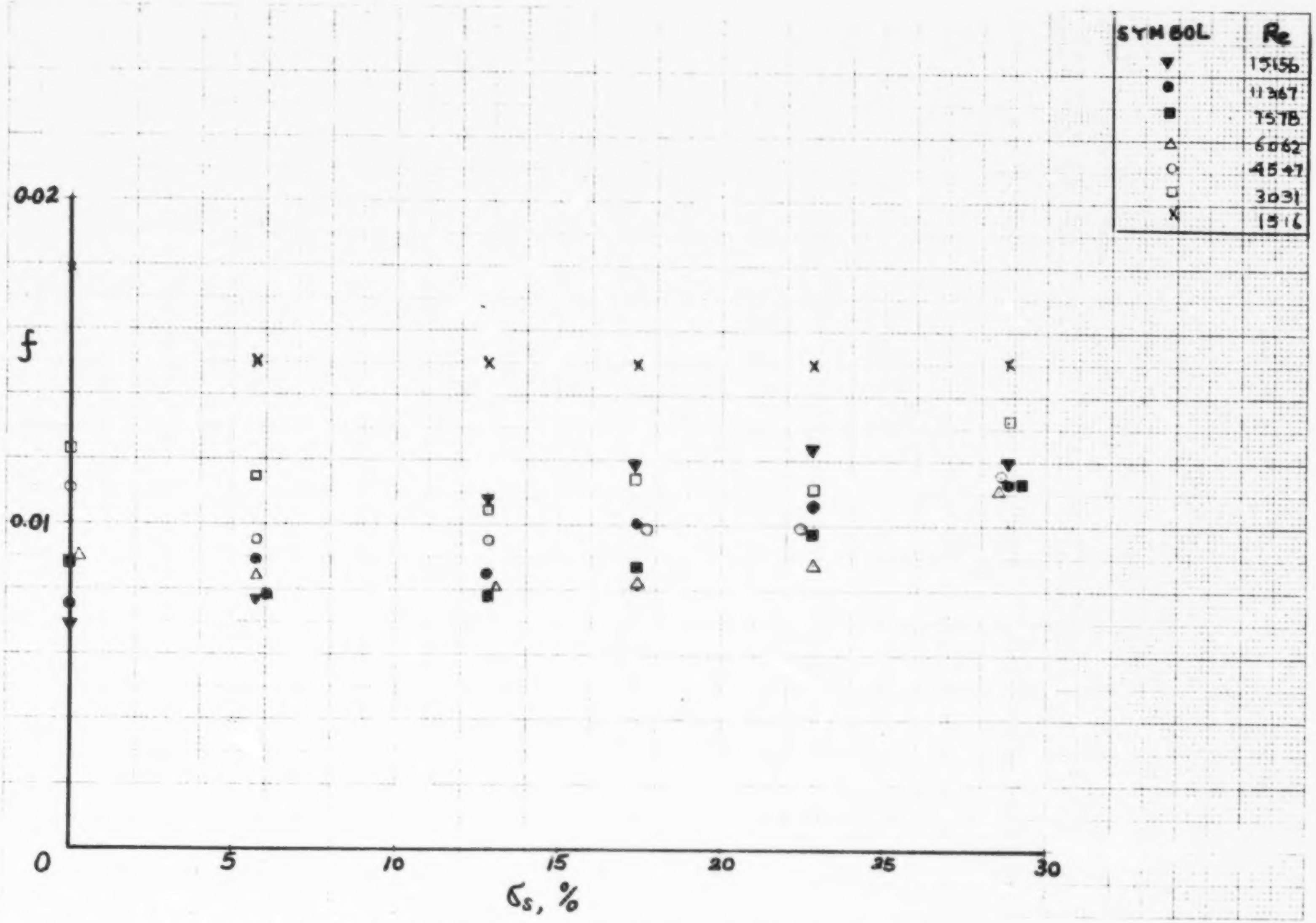

Fig. 14c. f versus σ_s, for t/b=0.0665, 2" x 1/8" slots in in-line arrangement.

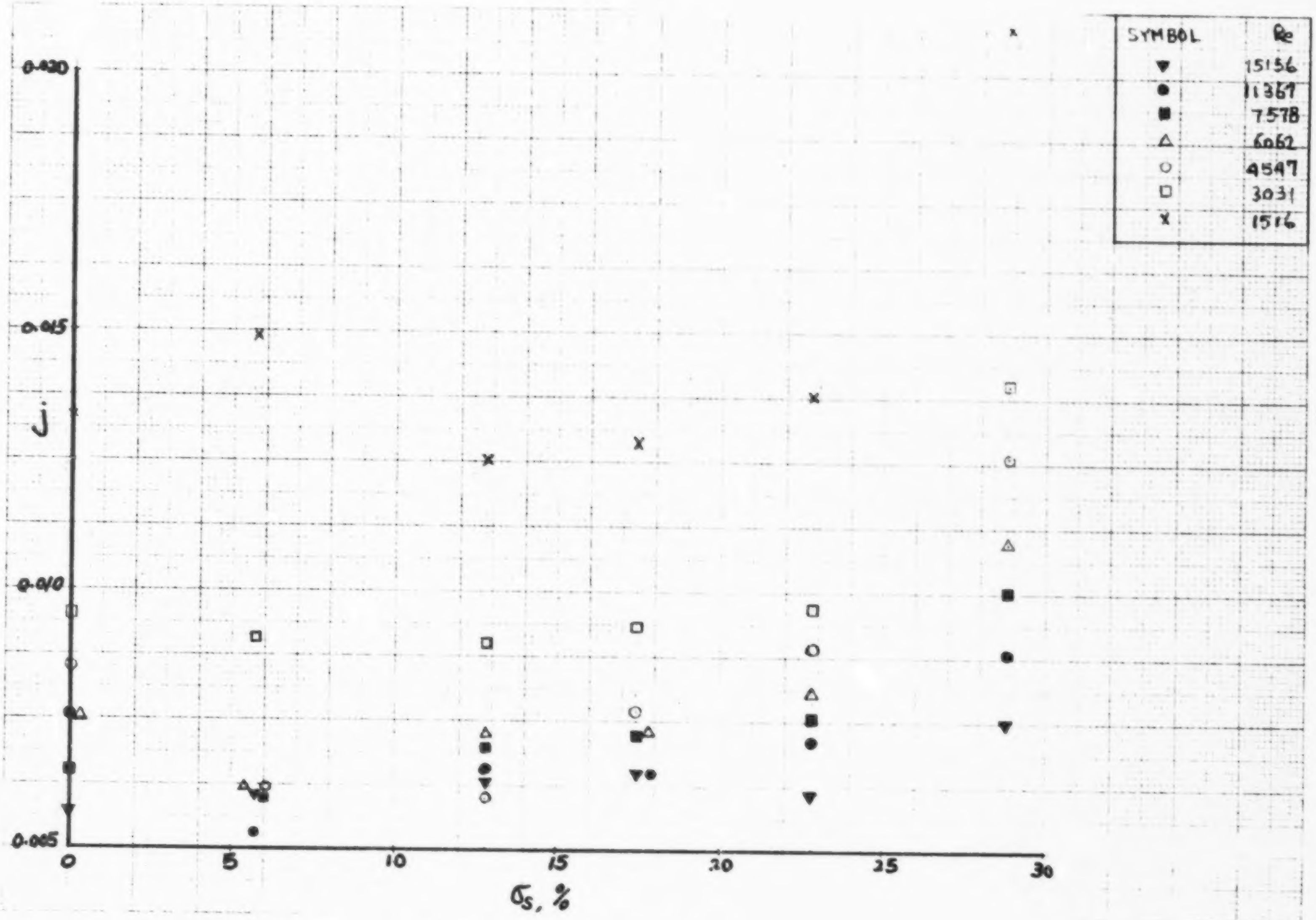

Fig. 14d. j versus σ_s, for t/b=0.0665, 2" x 1/8" slots in in-line arrangement.

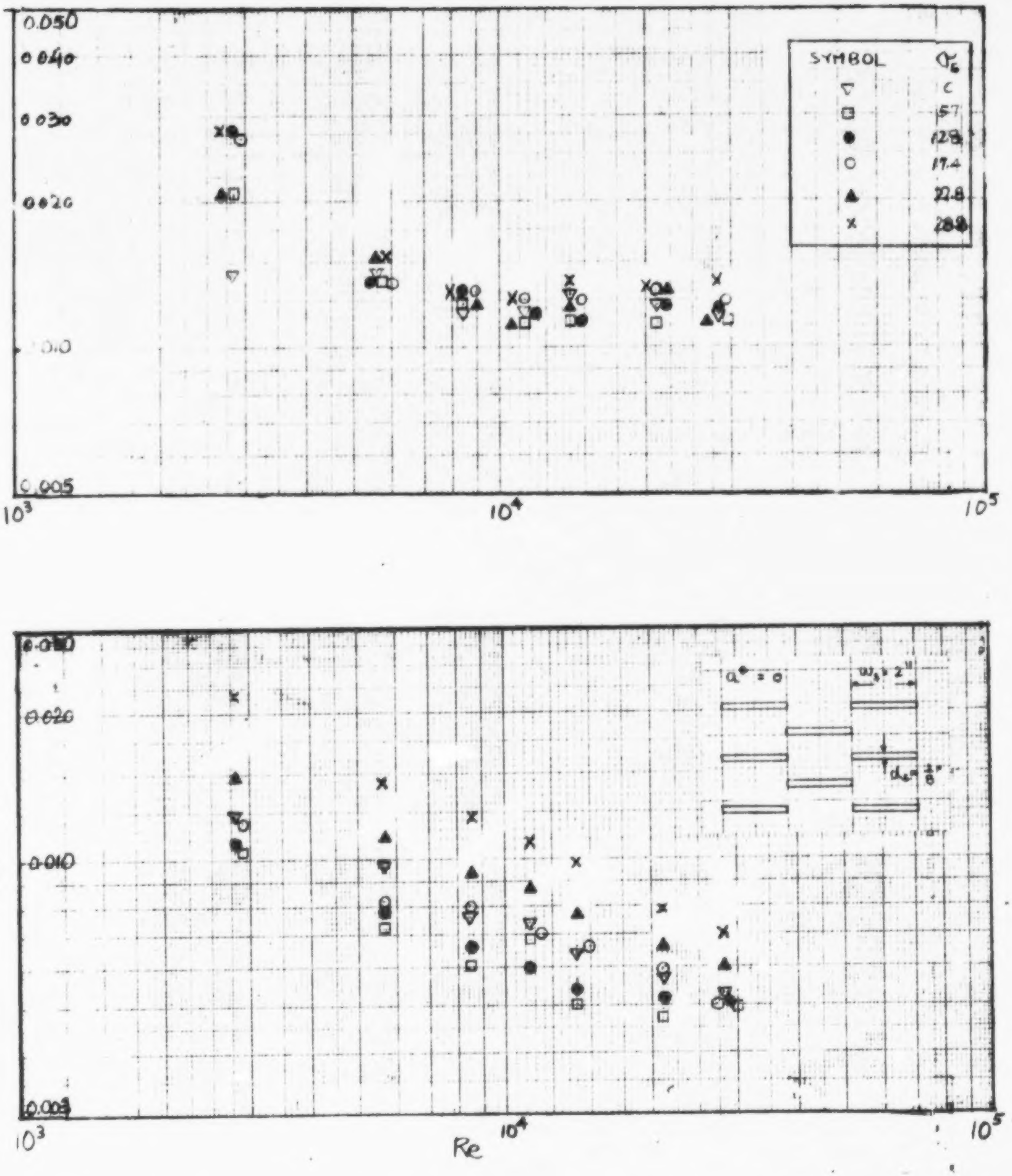

Fig. 15a. f and j versus Re, for t/b=0.0321, 2" x 1/8" slots in in-line arrangement.

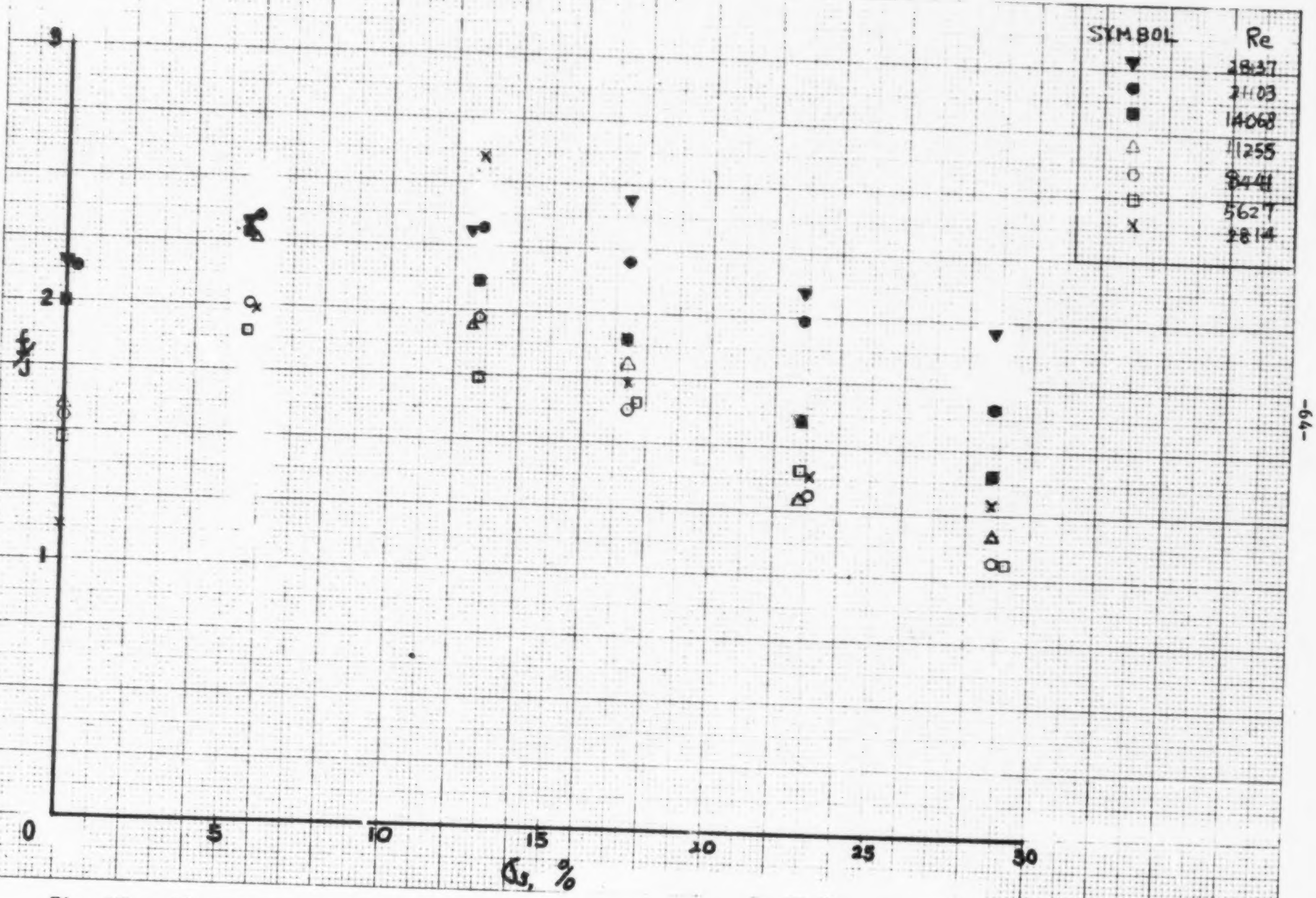

Fig. 15b. f/j versus σ_s, for t/b=0.0321, 2" x 1/8" slots in in-line arrangement.

20 Squares to the Inch

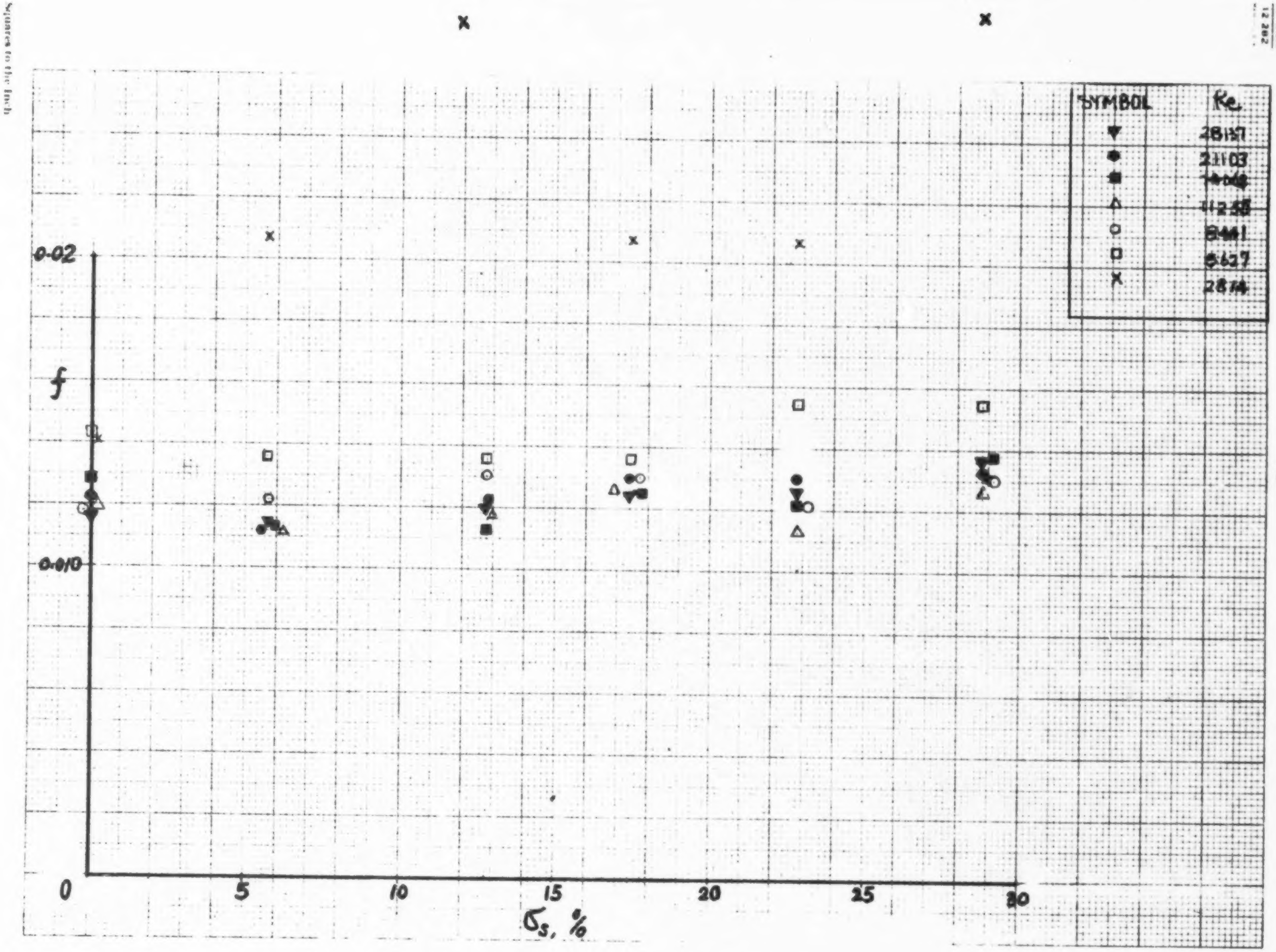

Fig. 15c. f versus σ_s, for t/b=0.0321, 2" x 1/8" slots in in-line arrangement

20 Squares to the Inch

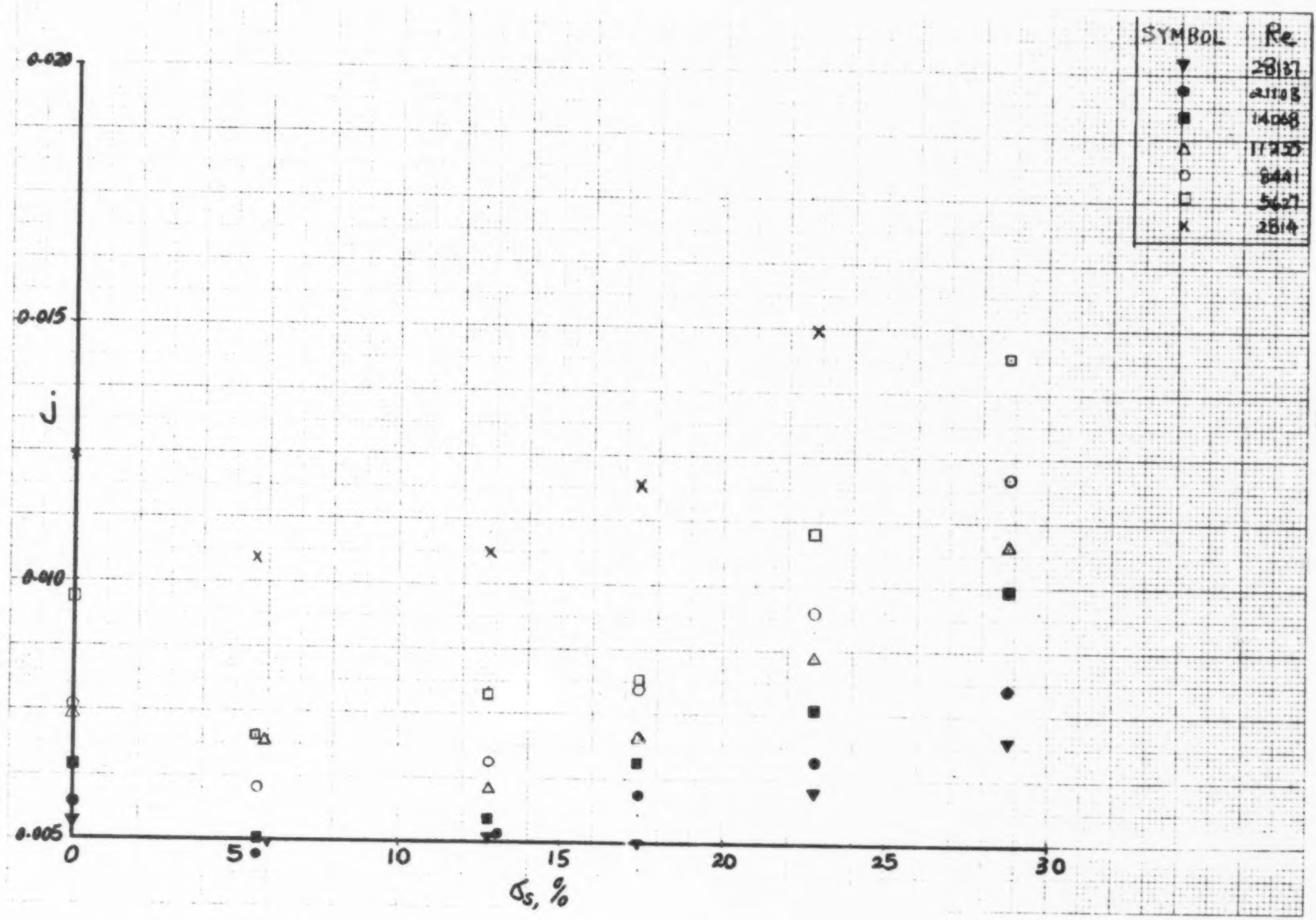

Fig. 15d. j versus σ_s, for t/b=0.0321, 2" x 1/8" slots in in-line arrangement.

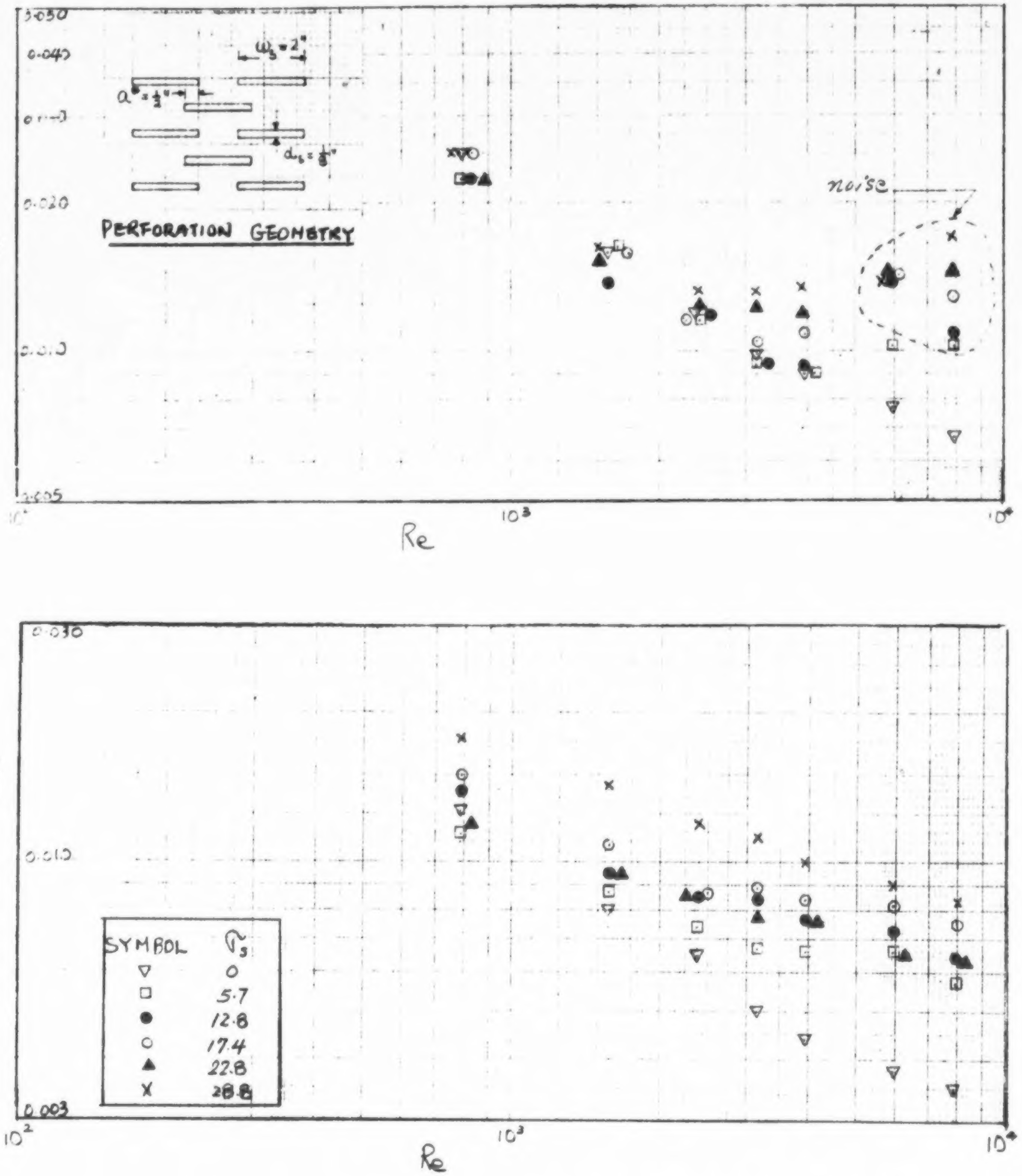

Fig. 16a. f and j versus Re, vor t/b=0.141, 2" x 1/8" slots in overlap arrangement.

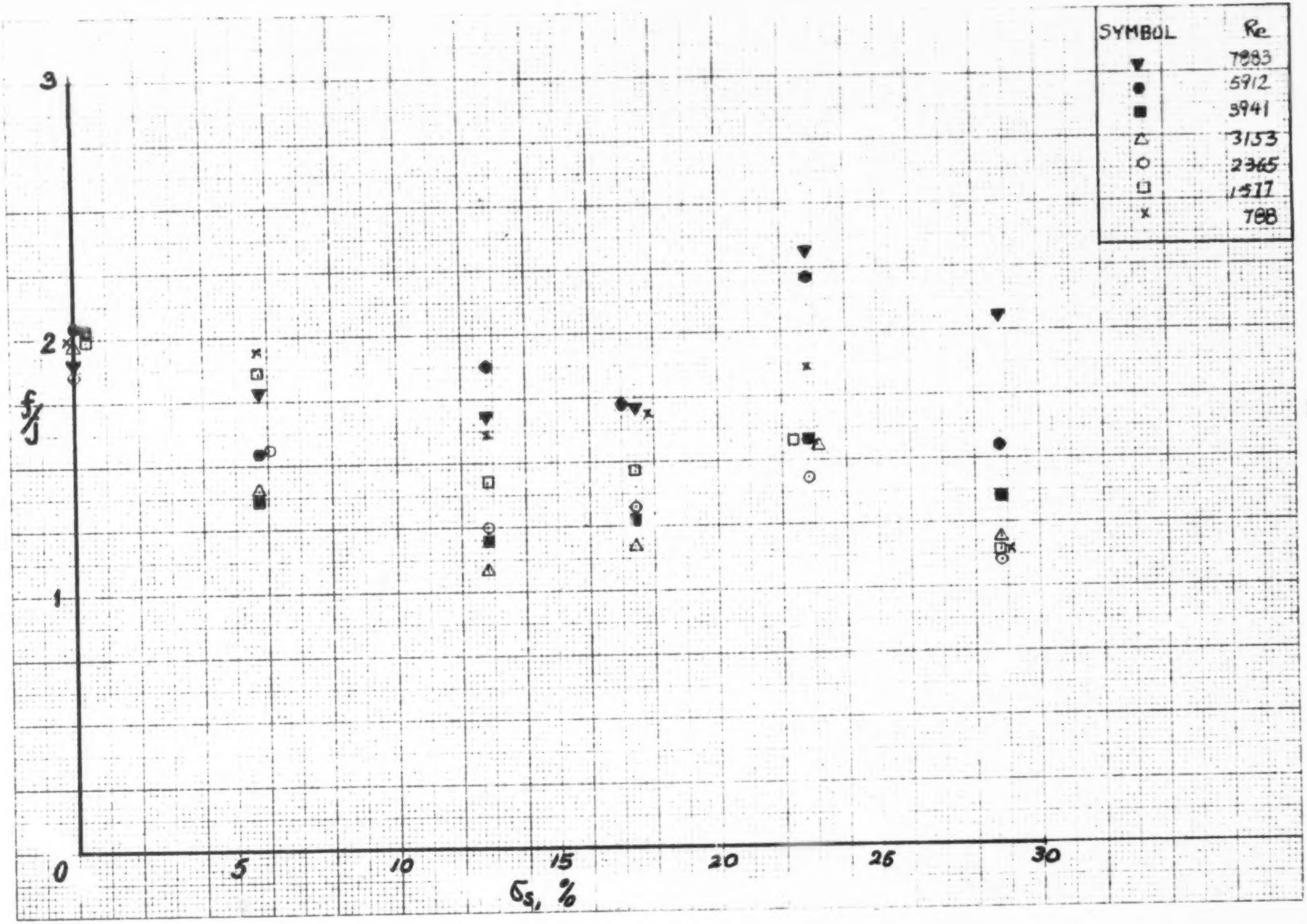

Fig. 16b. f/j versus σ_s, for t/b=0.141, 2" x 1/8" slots in overlap arrangement.

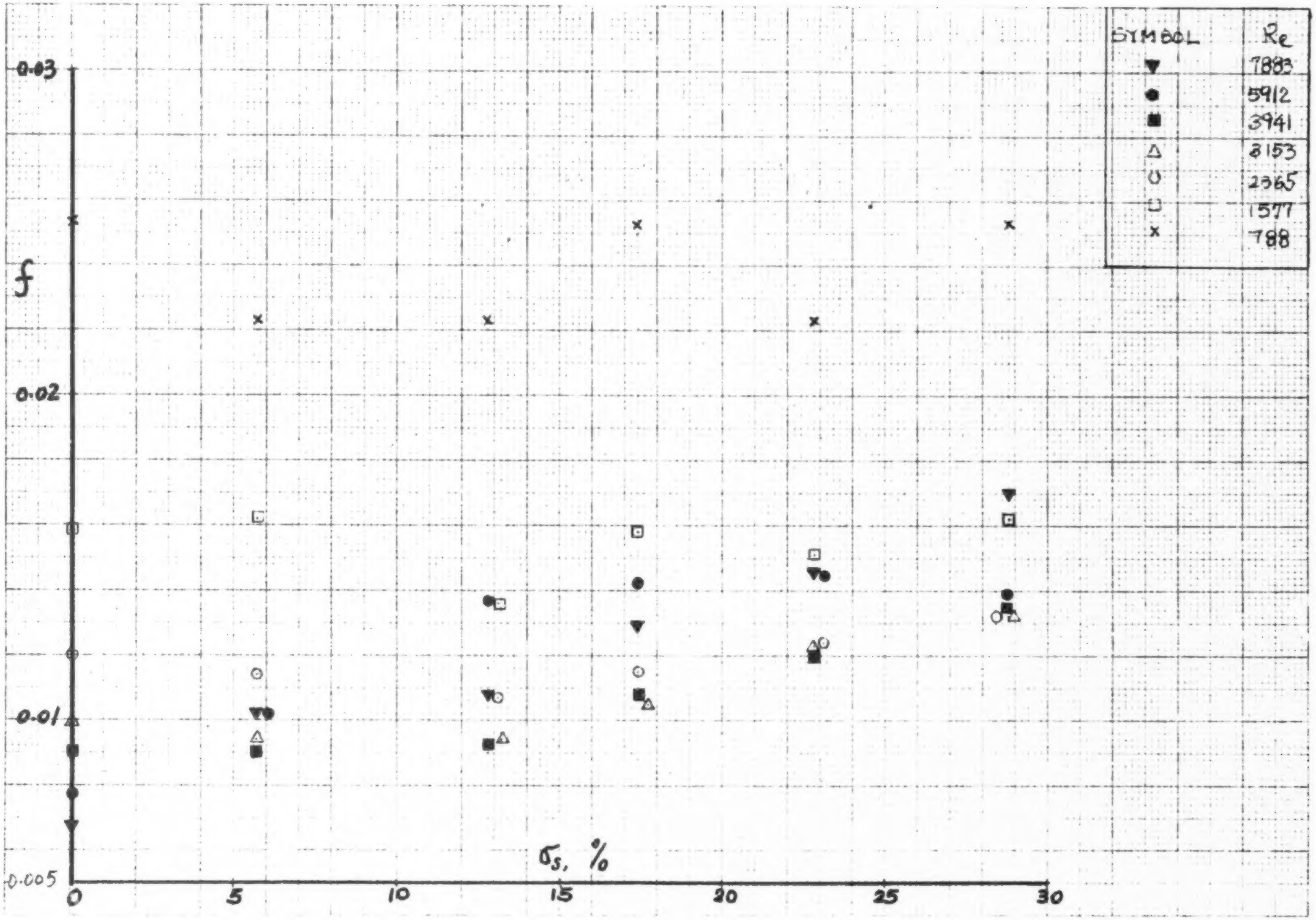

Fig. 16c. f versus σ_s, for t/b=0.141, 2" x 1/8" slots in overlap arrangement.

20 Squares to the inch

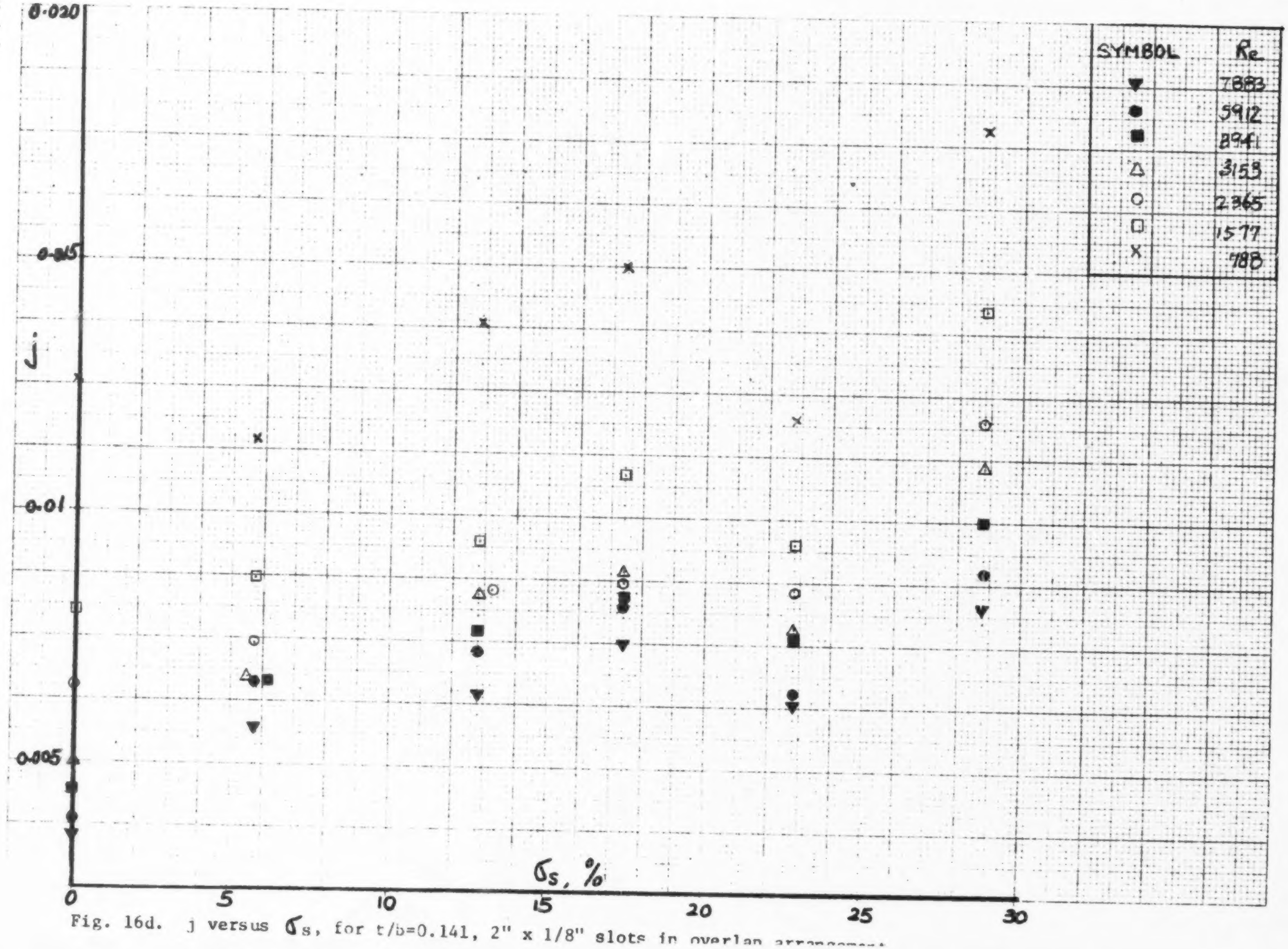

Fig. 16d. j versus σs, for t/b=0.141, 2" x 1/8" slots in overlap arrangement

20 Squares to the inch

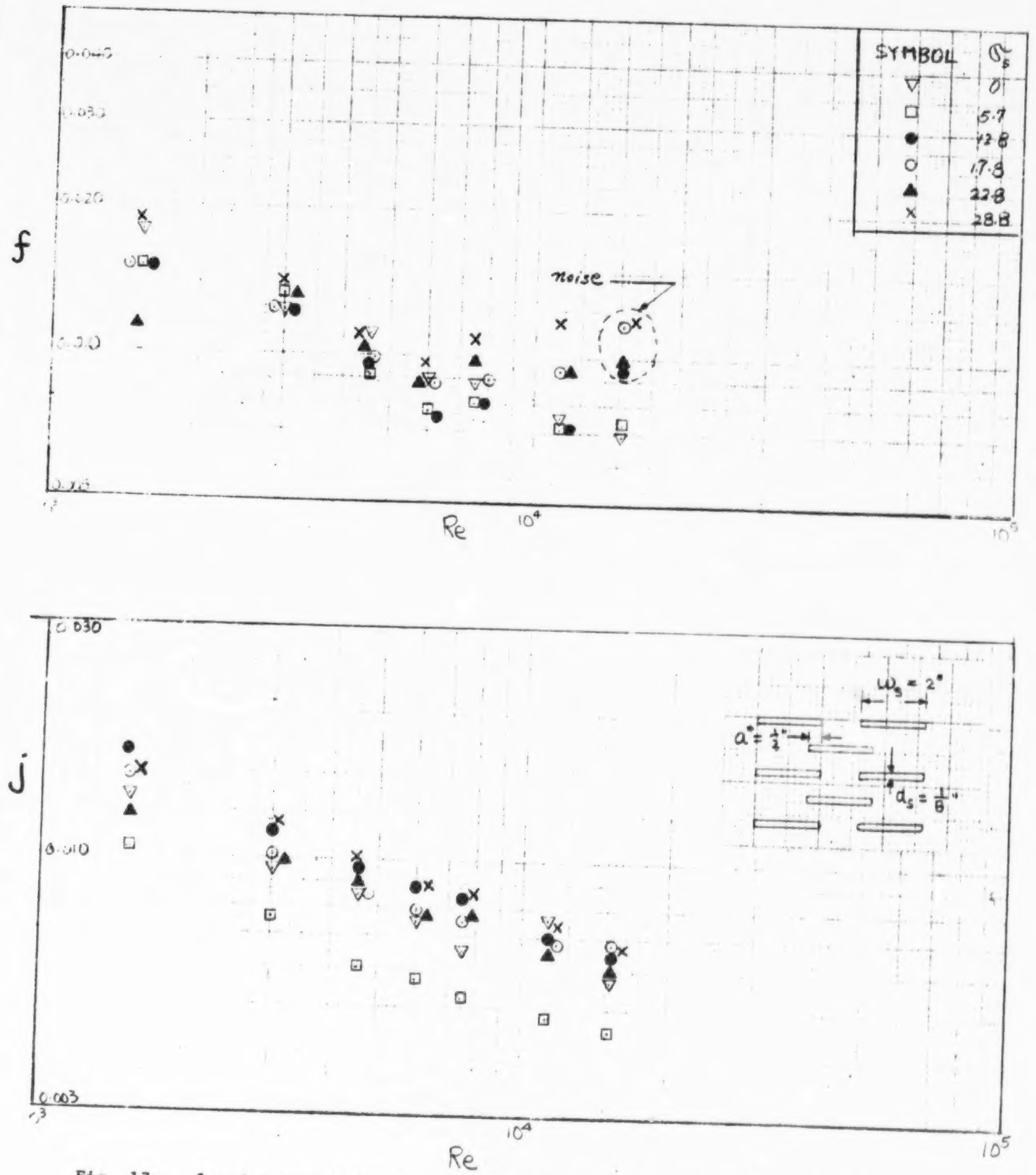

Fig. 17a. f and j versus Re, for t/b=0.0665, 2" x 1.8" slots in overlap arrangement.

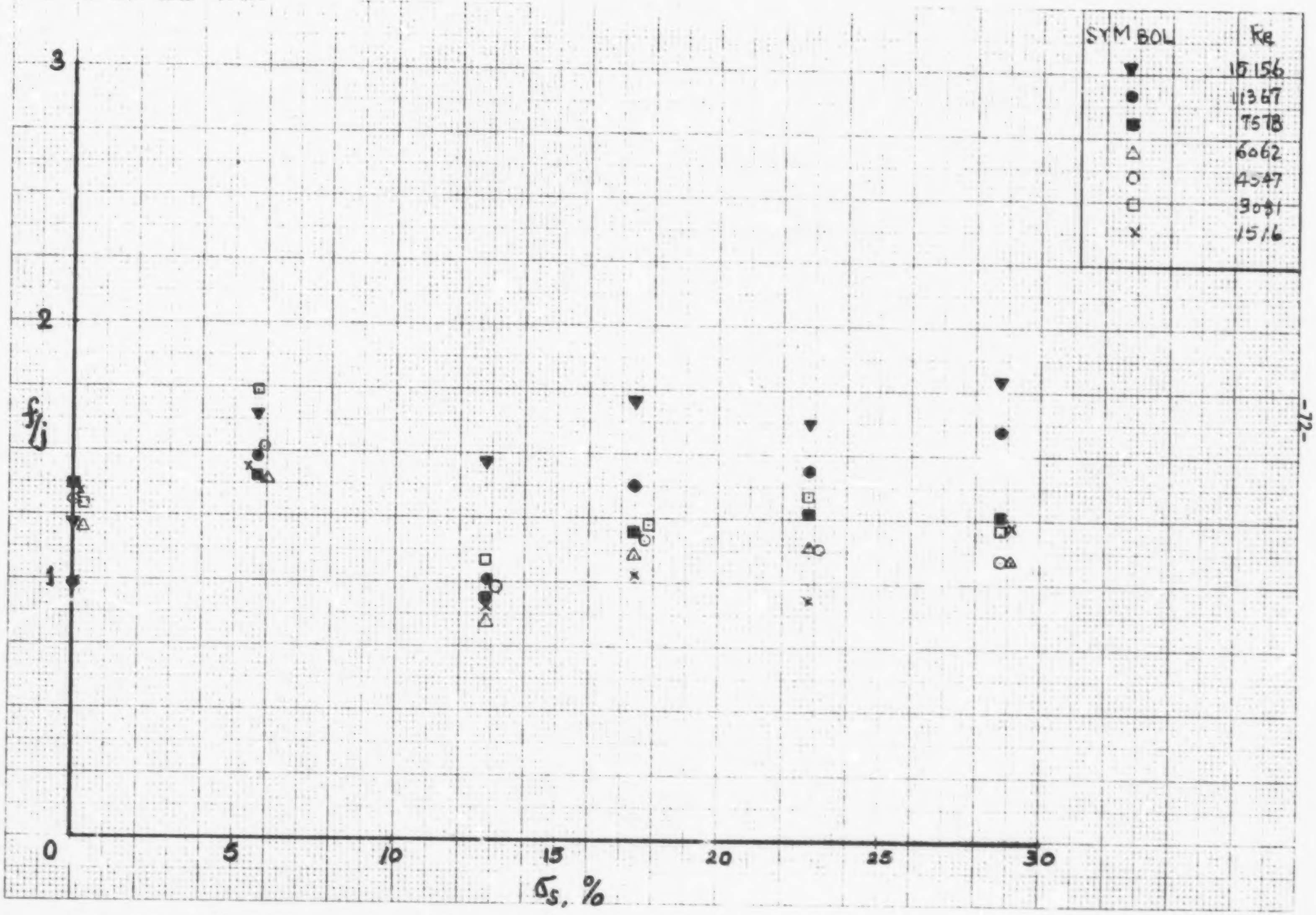

Fig. 17b. f/j versus σ_s, for t/b=0.0665, 2" x 1/8" slots in overlap arrangement.

20 Squares to the Inch

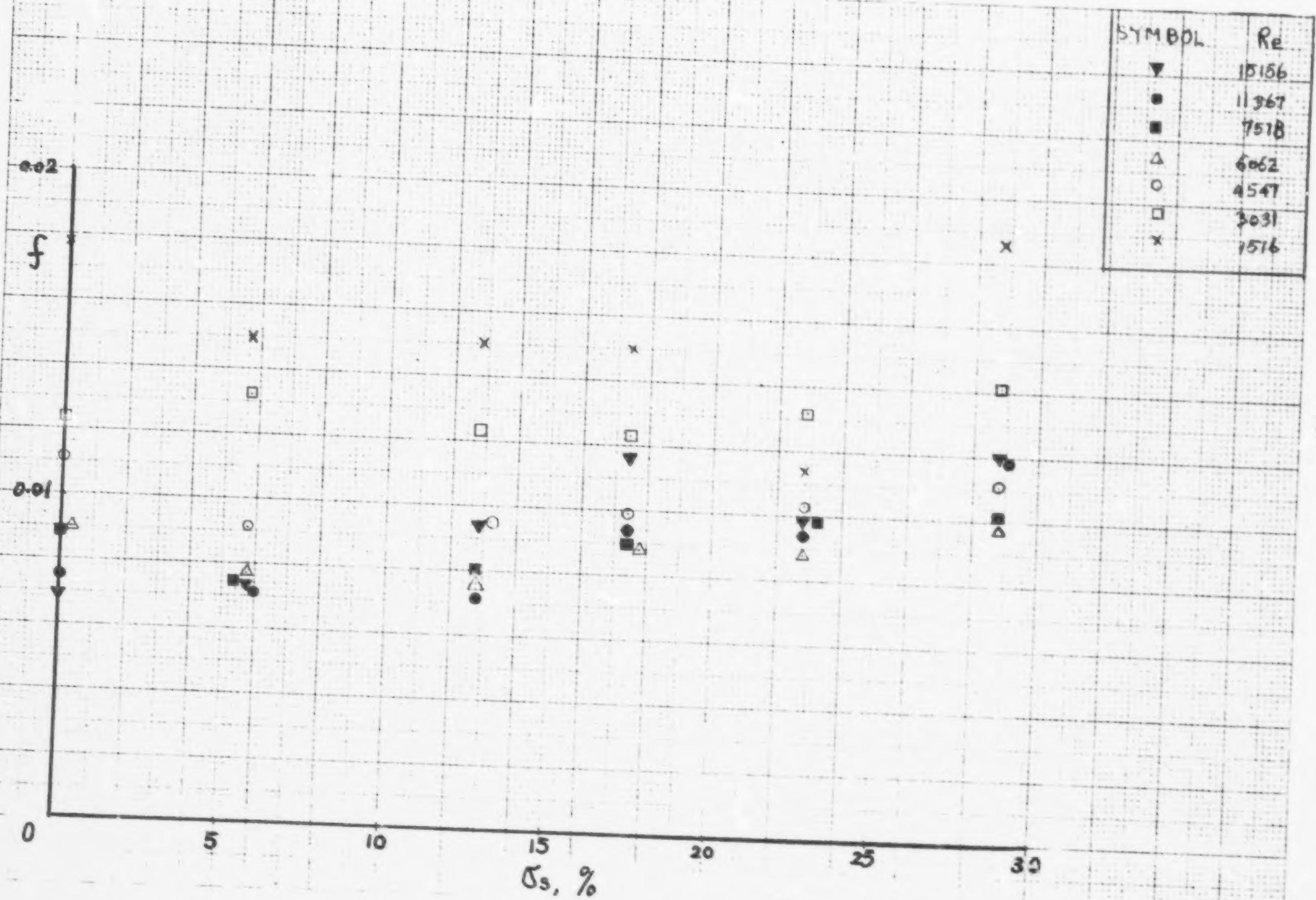

Fig. 17c. f versus σ_s, for t/b=0.0665, 2" x 1/8" slots in overlap arrangement.

20 Squares to the Inch

20 Squares to the Inch

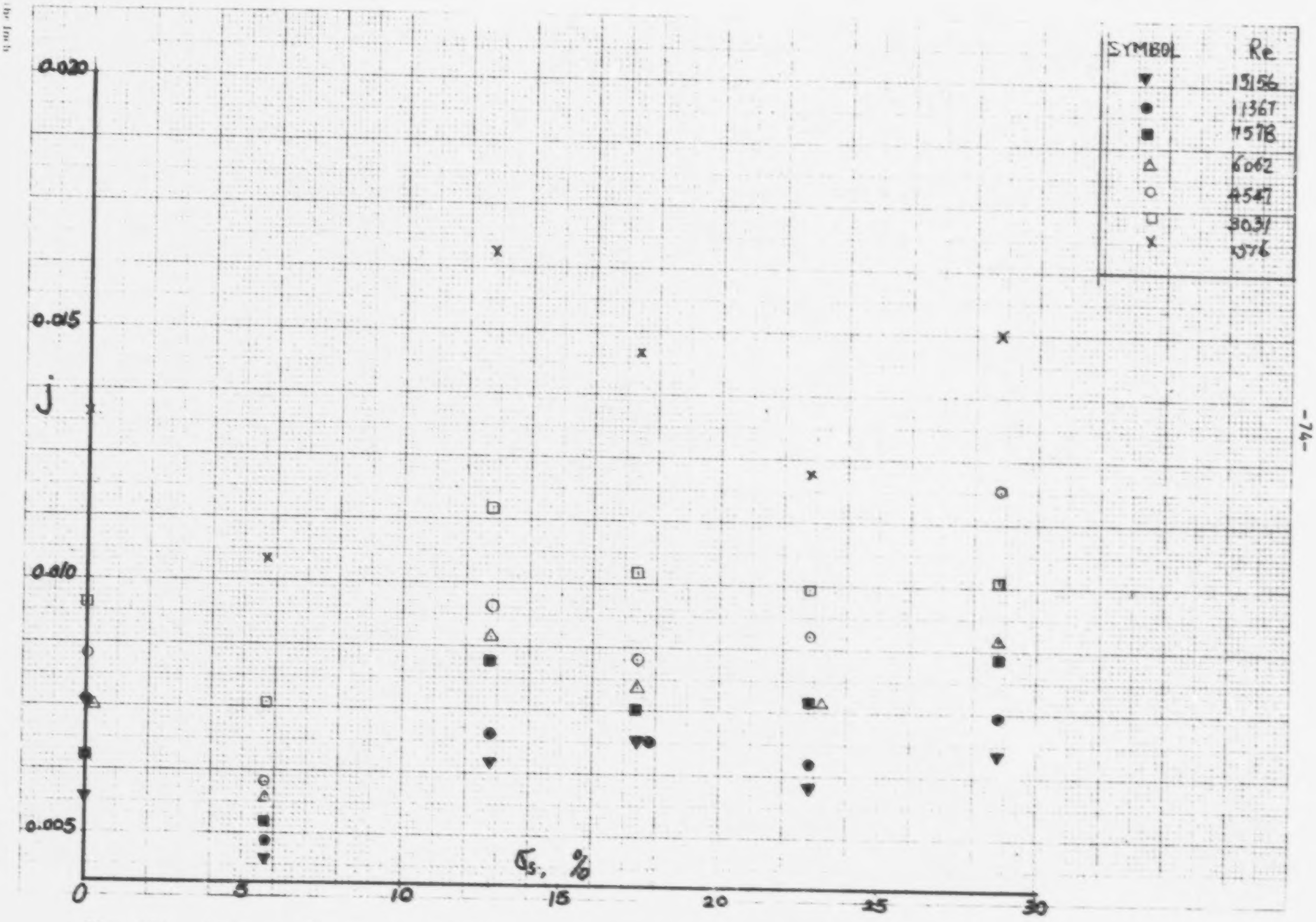

Fig. 17d. j versus σ_s, for t/b=0.0665, 2" x 1/8" slots in overlap arrangement.

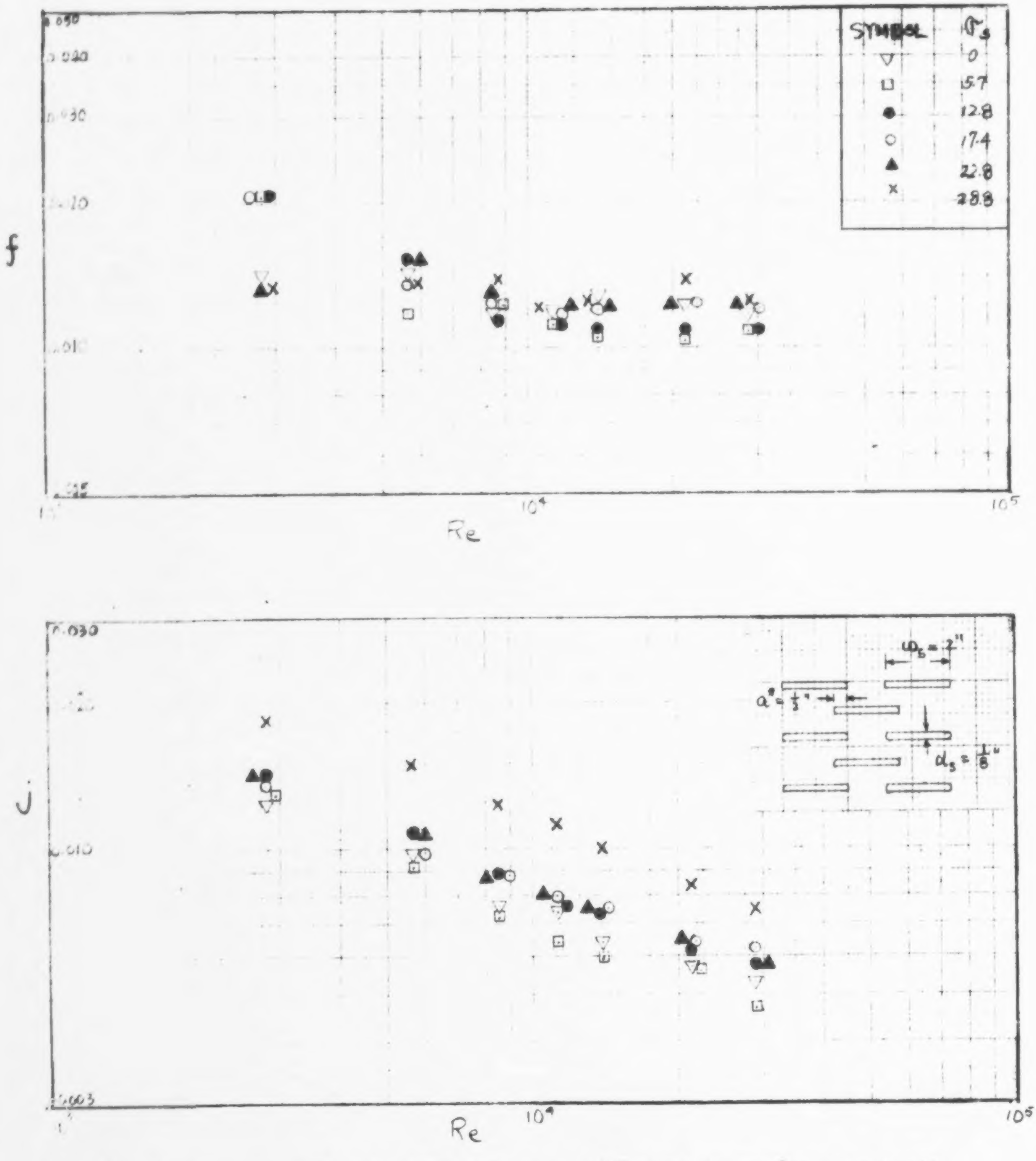

Fig. 13a. f and j versus Re, for t/b=0.0321, 2" x 1/8" slots in overlap arrangement.

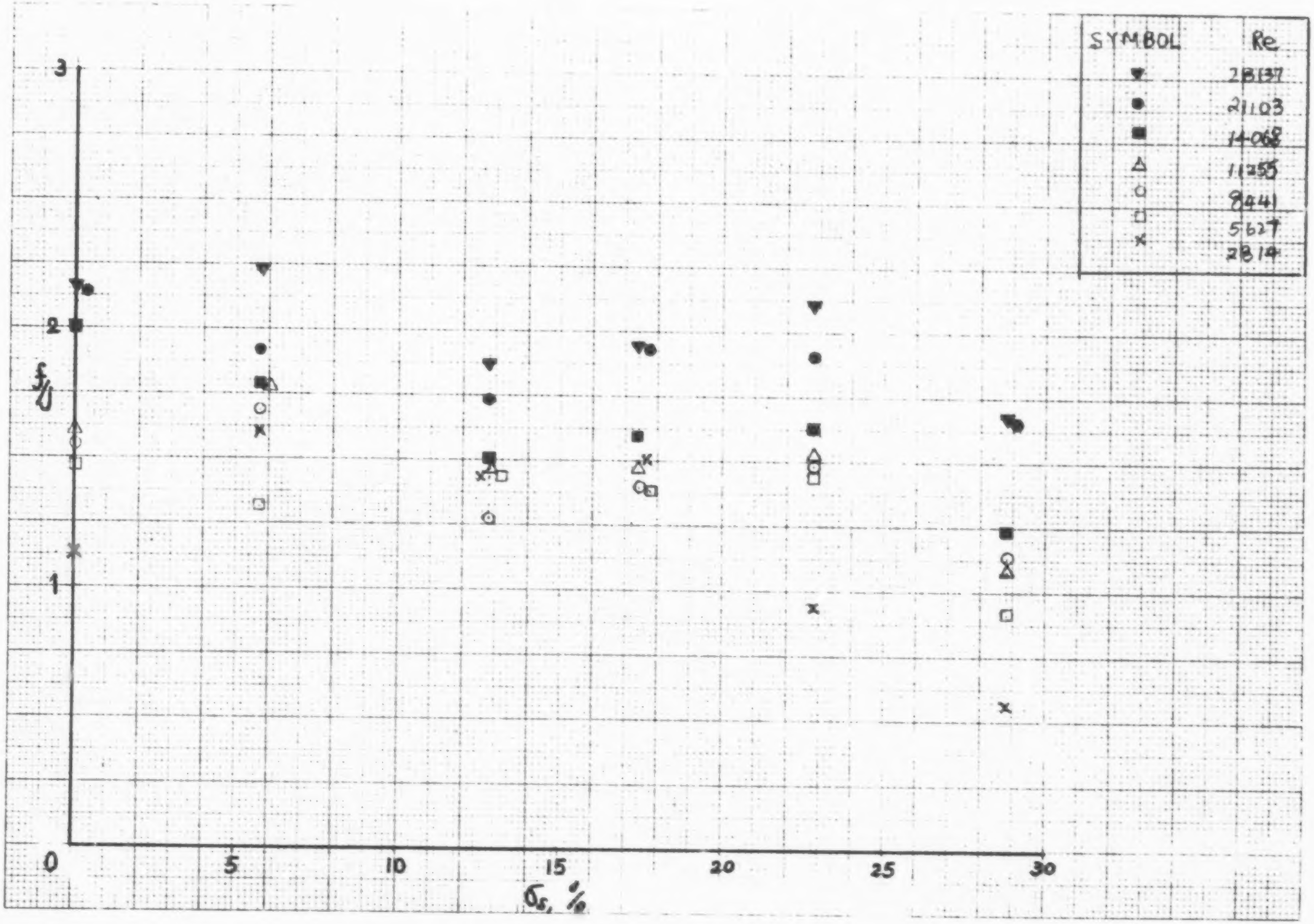

Fig. 18b. f/j versus σ_s, for t/b=0.0321, 2" x 1/8" slots in overlap arrangement.

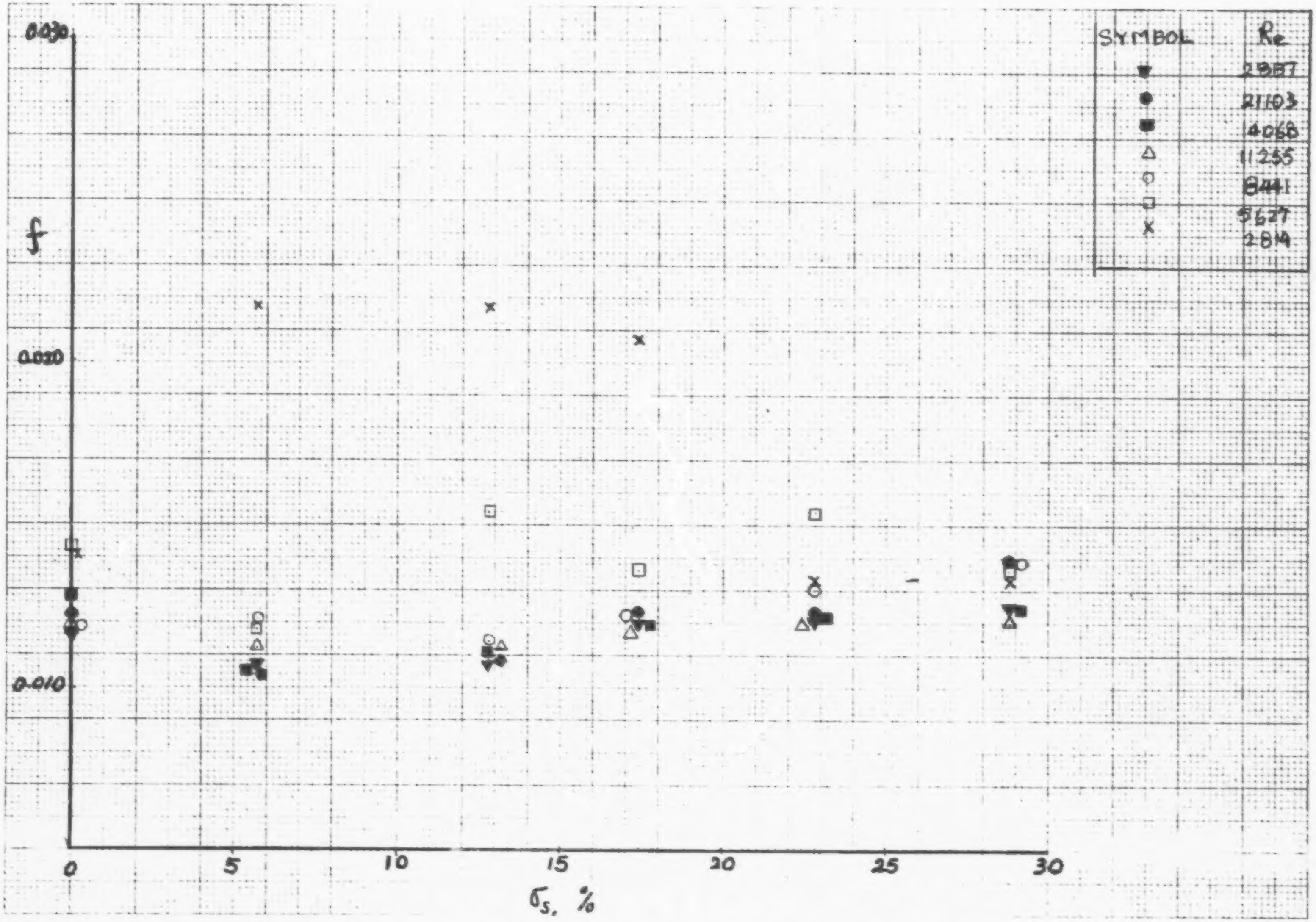

Fig. 18c. f versus σ_s, for t/b=0.0321, 2" x 1/8" slots in overlap arrangement.

20 Squares to the Inch

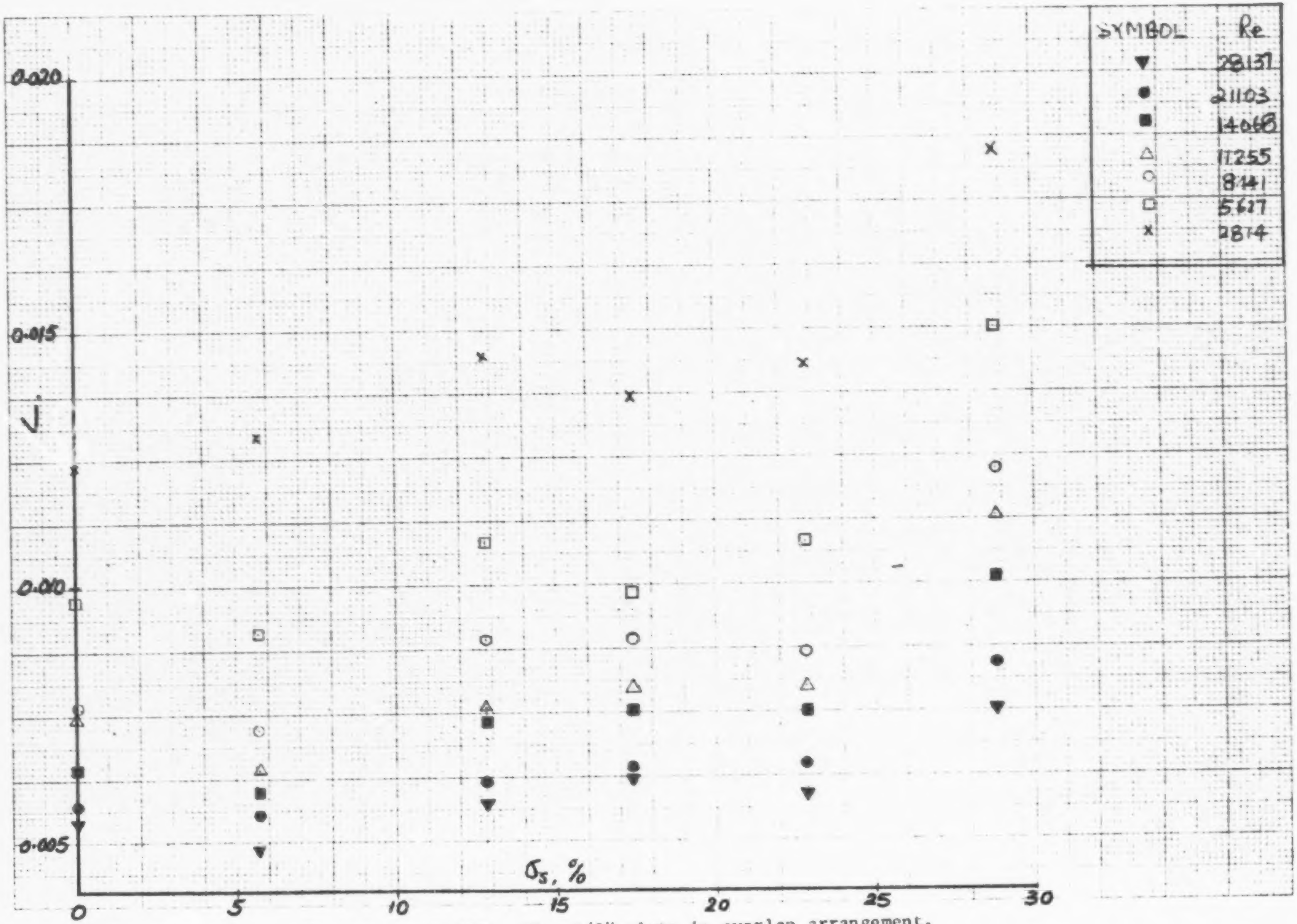

Fig. 13d. j versus σ_s, for t/b=0.0321, 2" x 1/8" slots in overlap arrangement.

20 Squares to the Inch

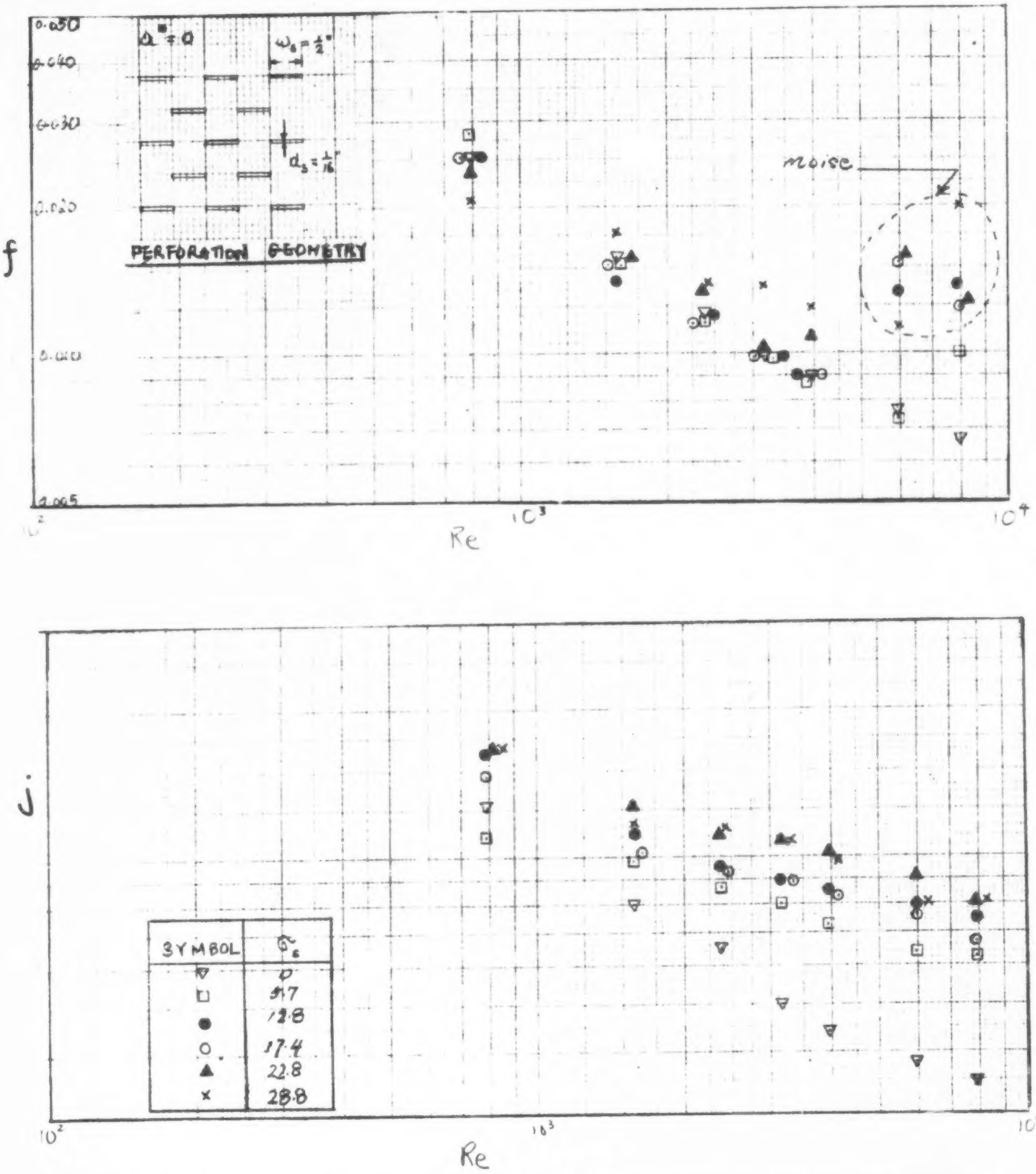

Fig. 19a. f and j versus Re, for t/b=0.141, 1/2" x 1/16" slots in in-line arrangement.

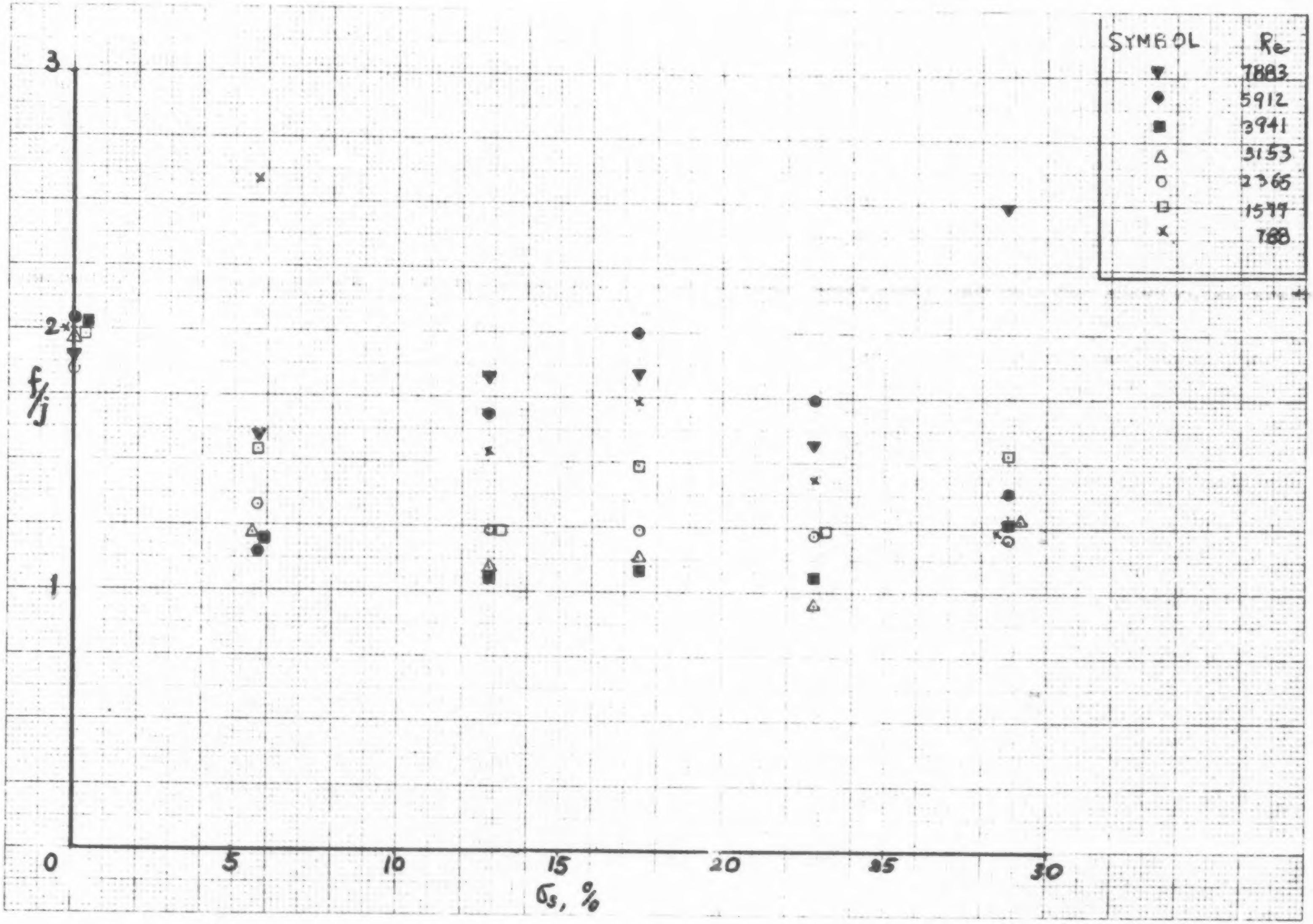

Fig. 19b. f/j versus σ_s, for t/b=0.141, 1/2" x 1/16" slots in in-line arrangement.

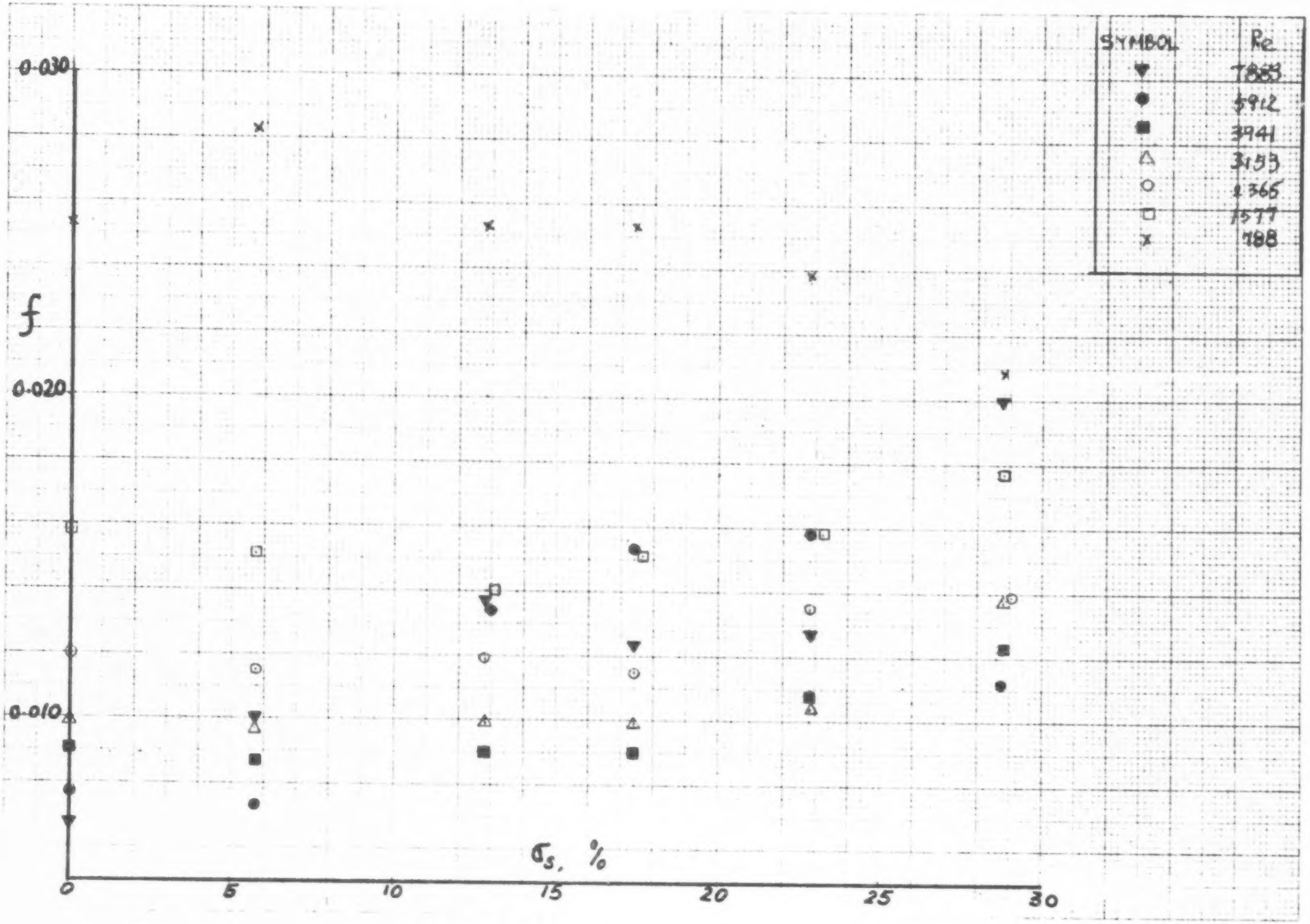

Fig. 19c. f versus σ_s, for t/b=0.141, 1/2" x 1/16" slots in in-line arrangement.

20 Squares to the Inch

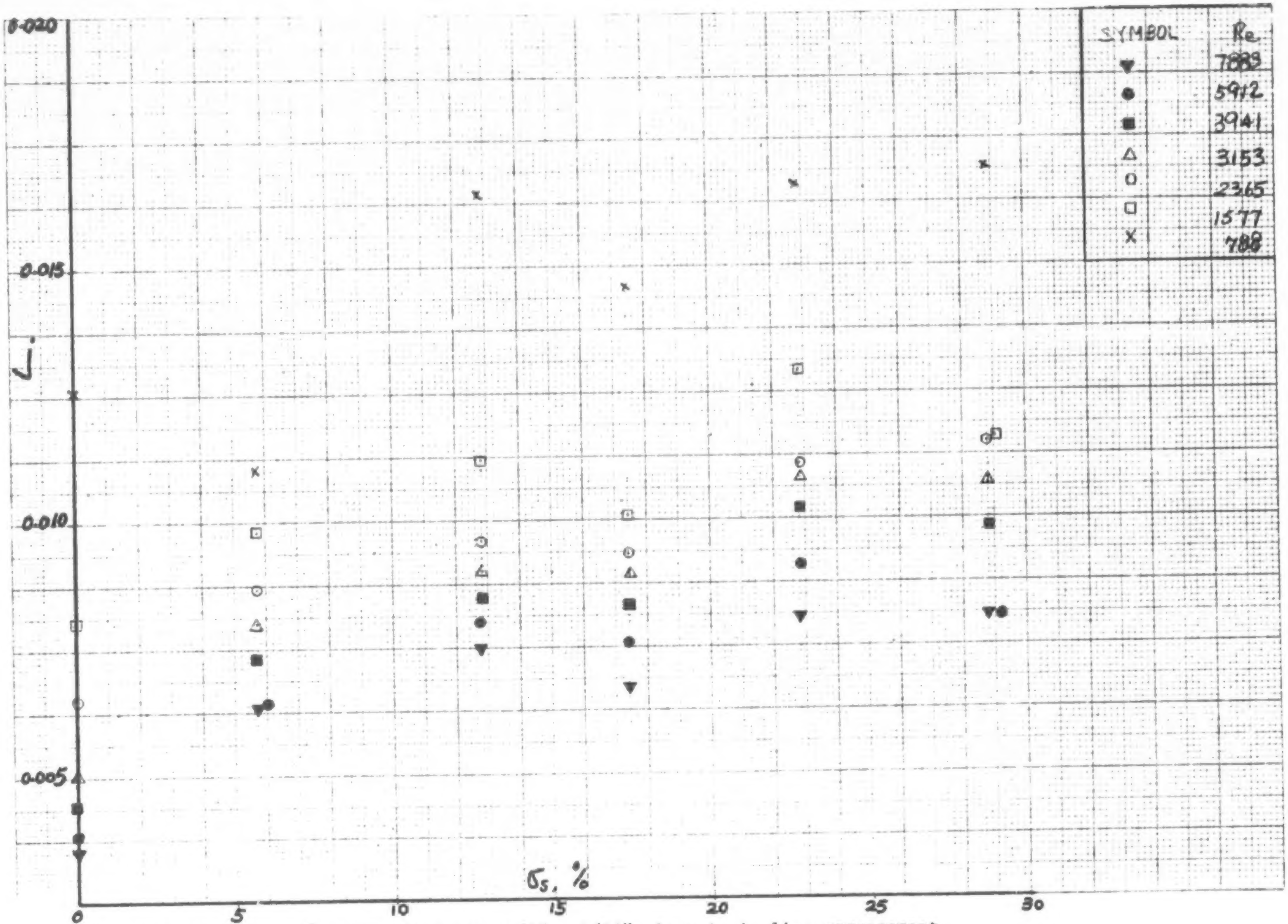

Fig. 19d. j versus σ_s, for t/b=0.141, 1/2" x 1/16" slots in in-line arrangement.

20 Squares to the Inch

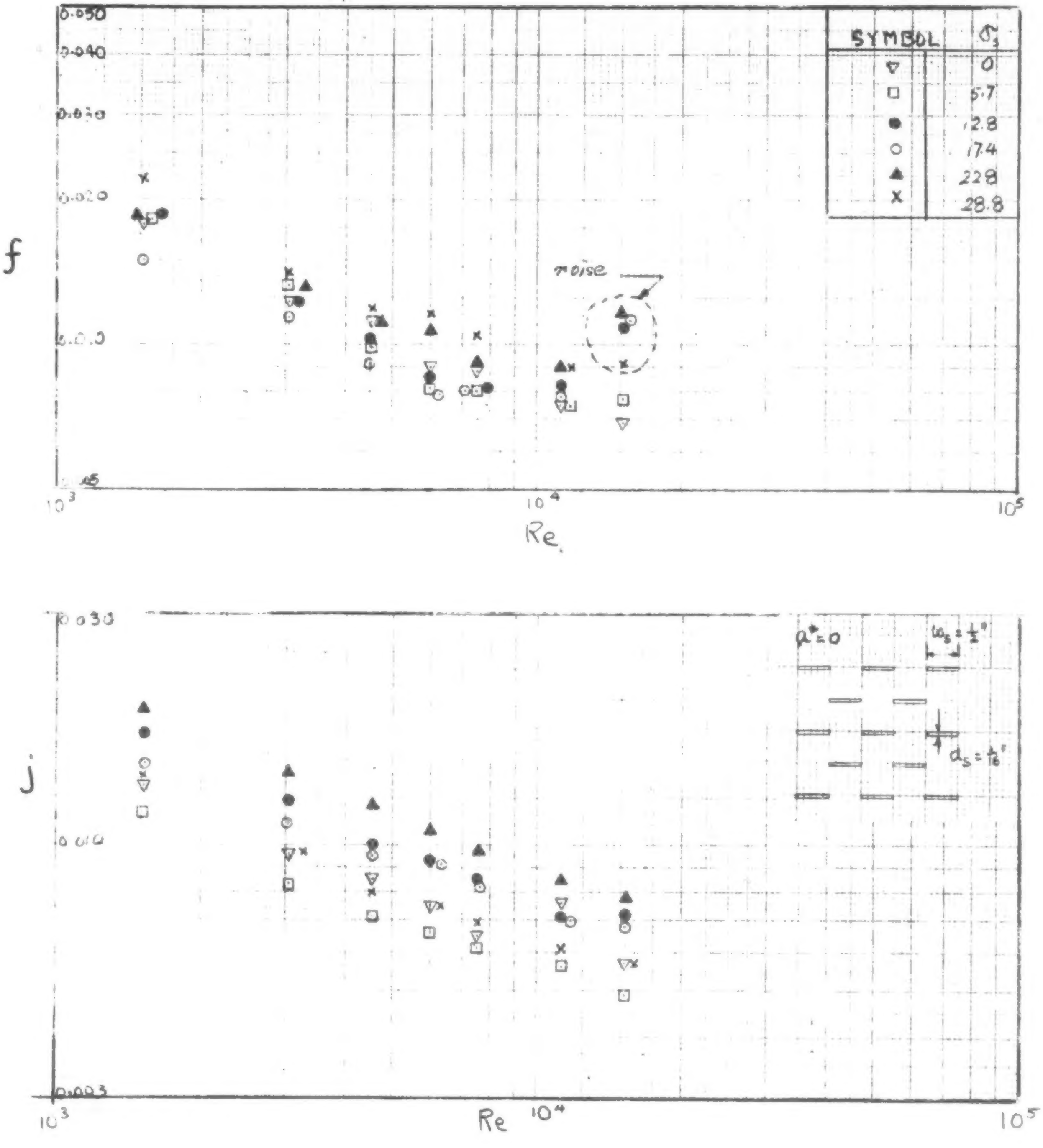

Fig. 20a. f and j versus Re, for t/b=0.0665, 1/2" x 1/16" slots in in-line arrangement.

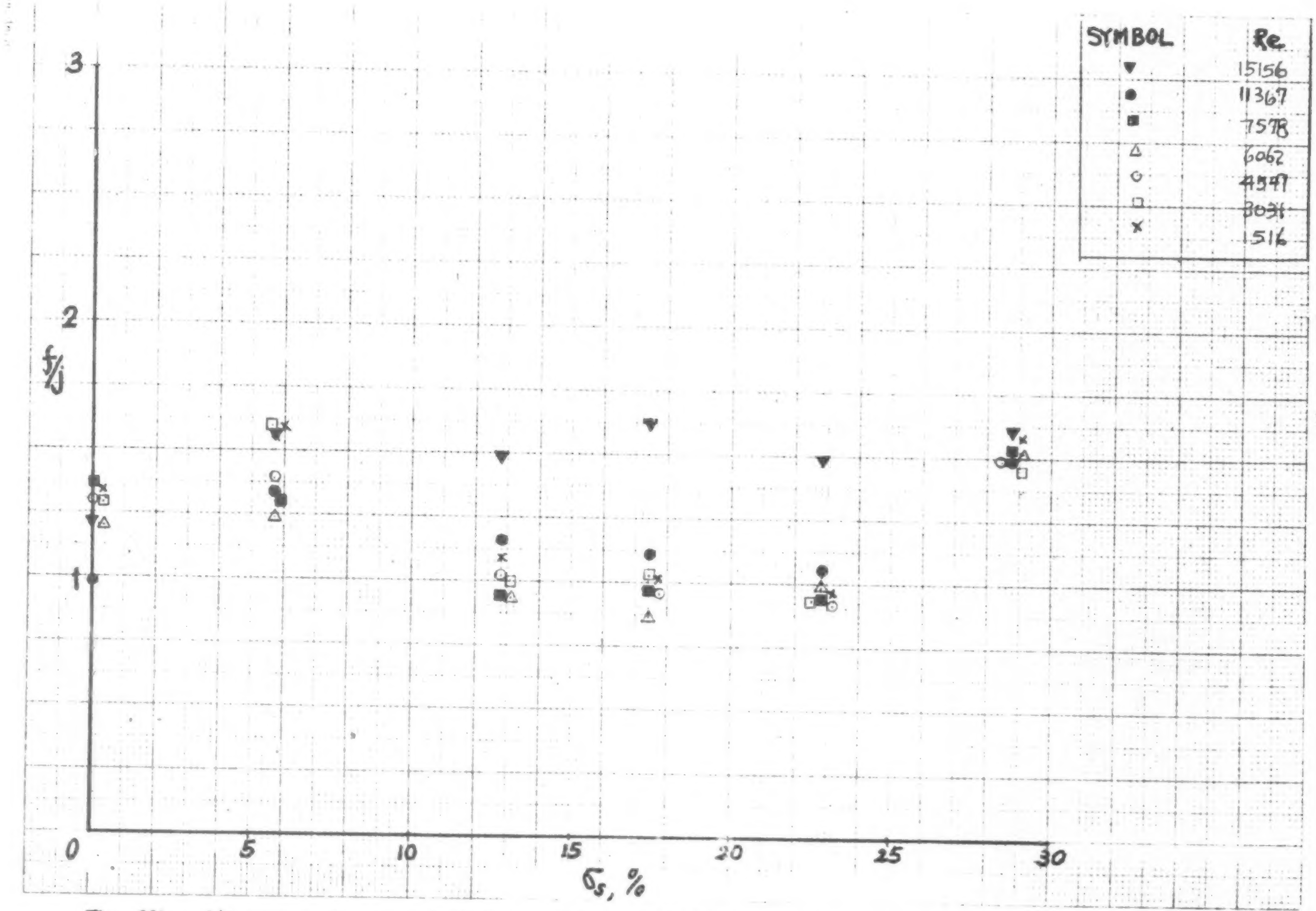

Fig. 20b. f/j versus σ_s, for t/b=0.0665, 1/2" x 1/16" slots in in-line arrangement.

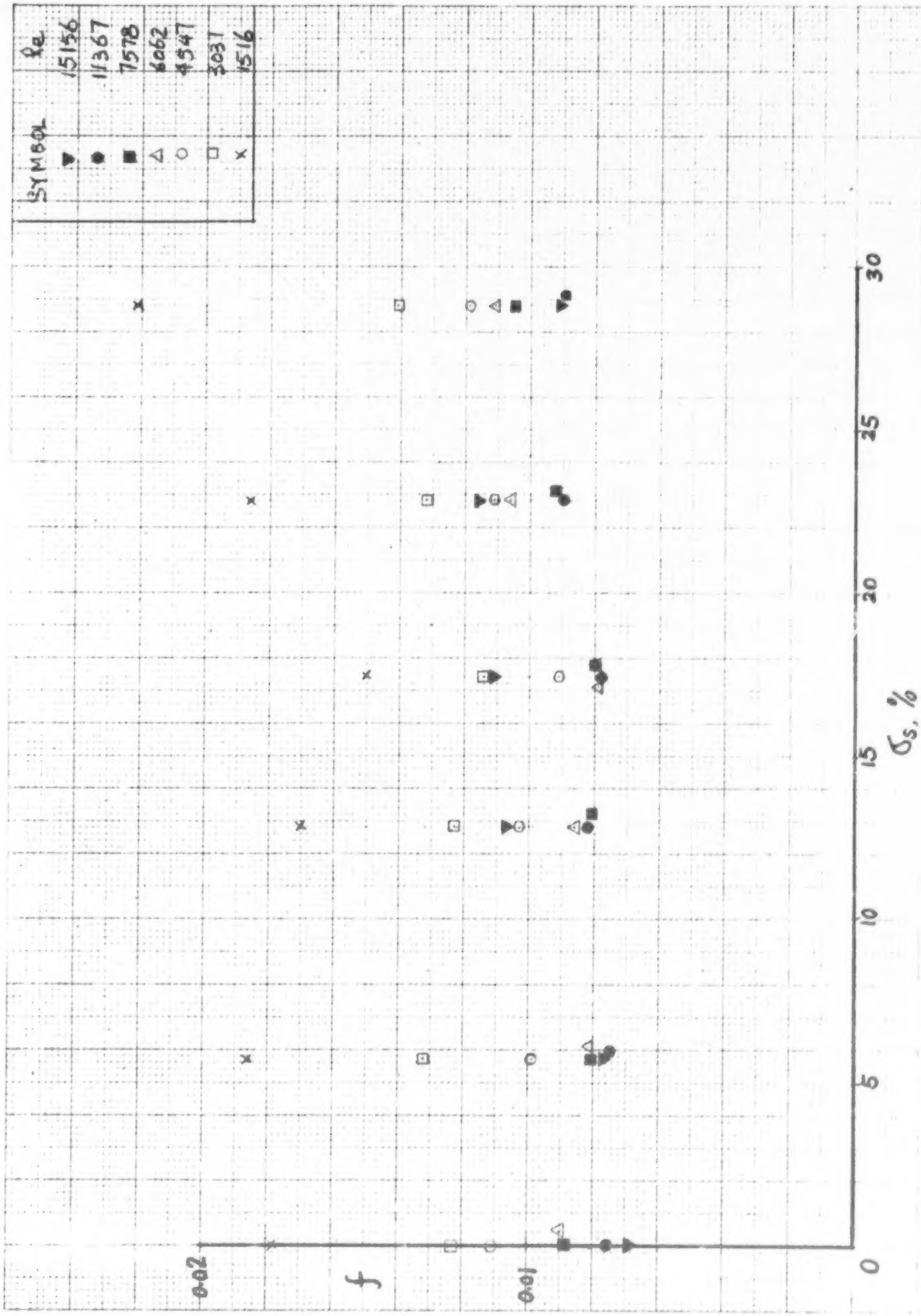

Fig. 20c. f versus σ_s, for t/p=0.0665, 1/2" x 1/16" slots in in-line arrangement.

20 Squares to the Inch

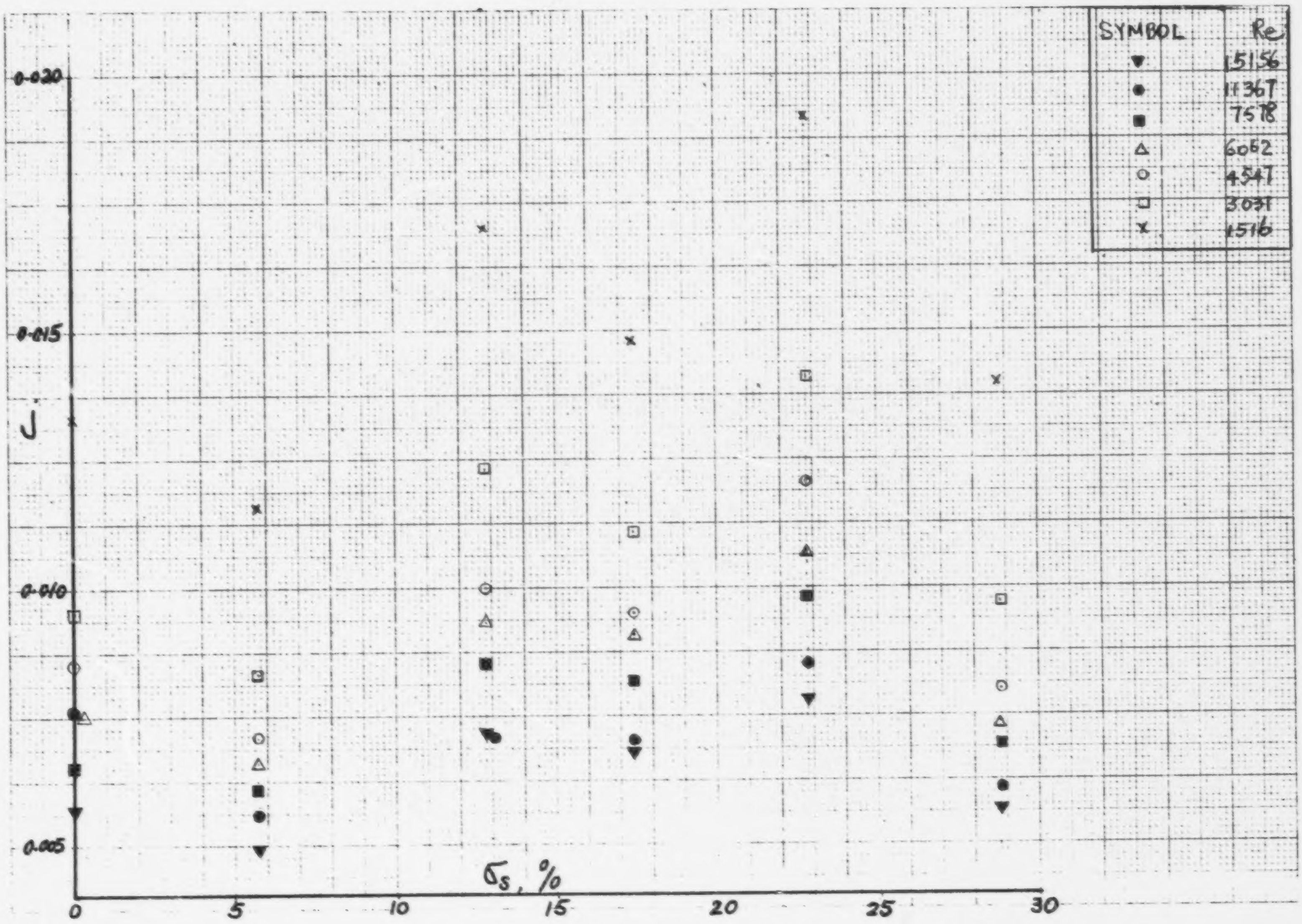

Fig. 20d. j versus σ_s, for t/b=0.0665, 1/2" x 1/16" slots in in-line arrangement.

20 Squares to the Inch

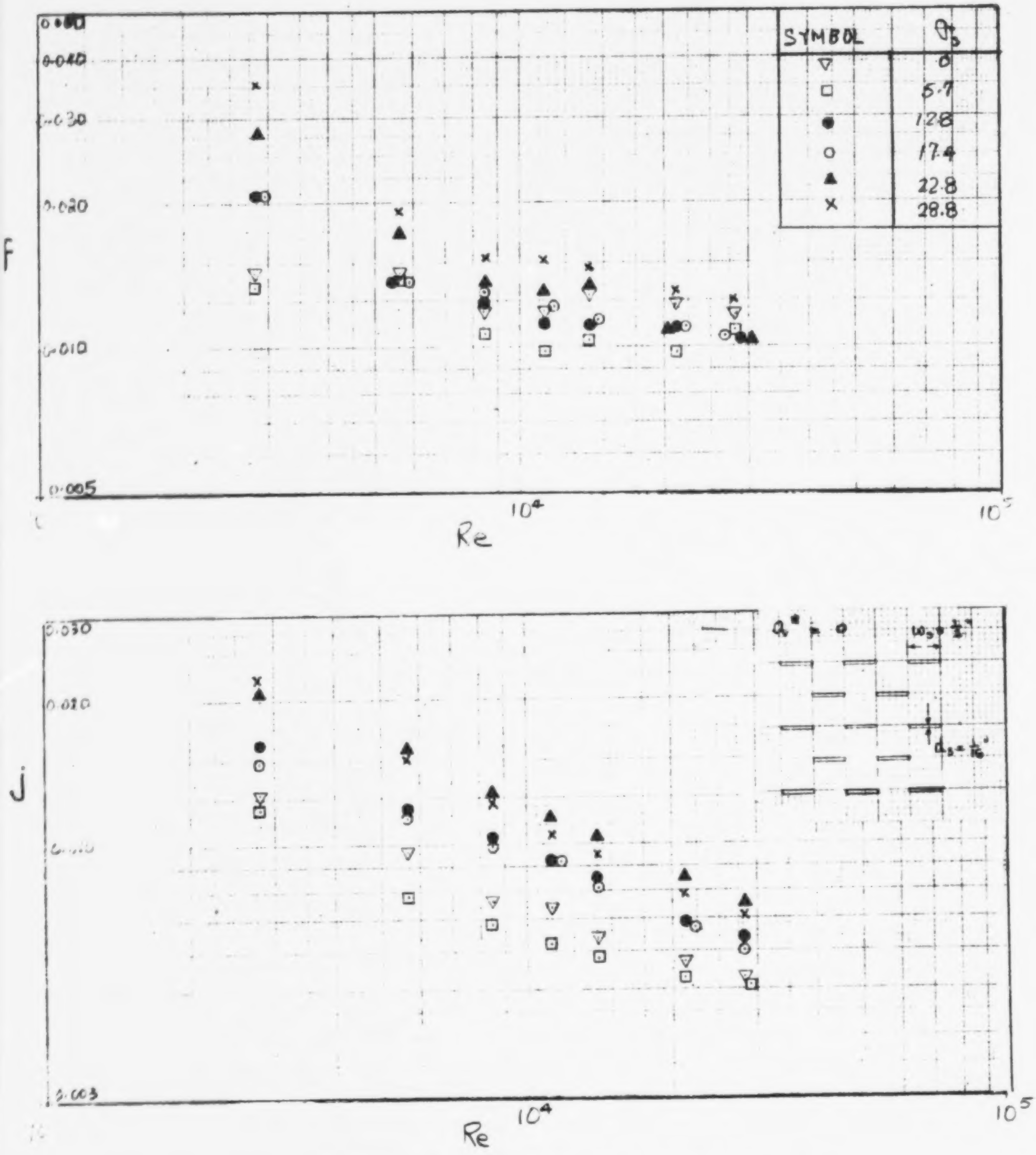

Fig. 21a. f and j versus Re, for t/b=0.0321, 1/2" x 1/16" slots in in-line arrangement.

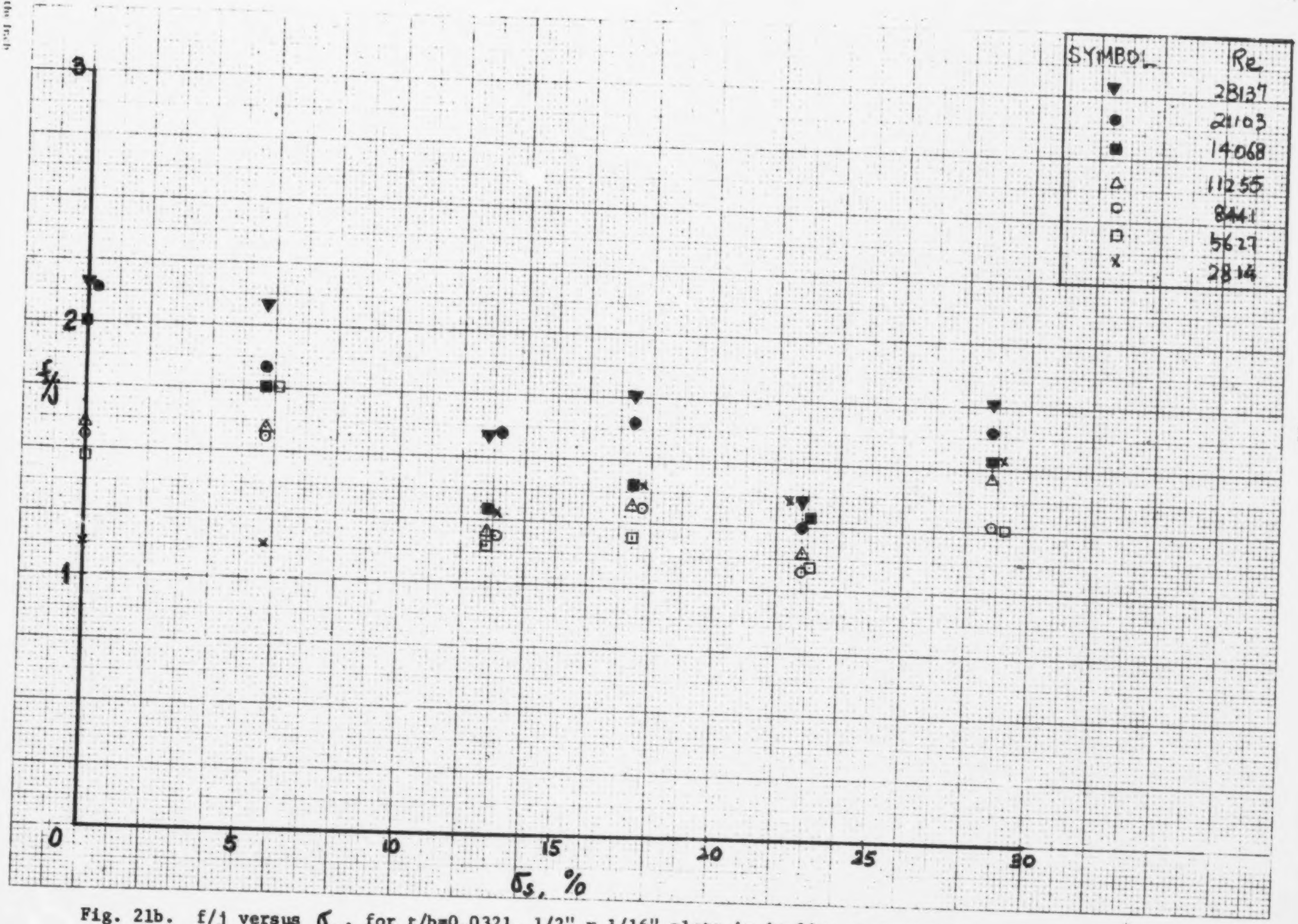

Fig. 21b. f/j versus σ_s, for t/b=0.0321, 1/2" x 1/16" slots in in-line arrangement.

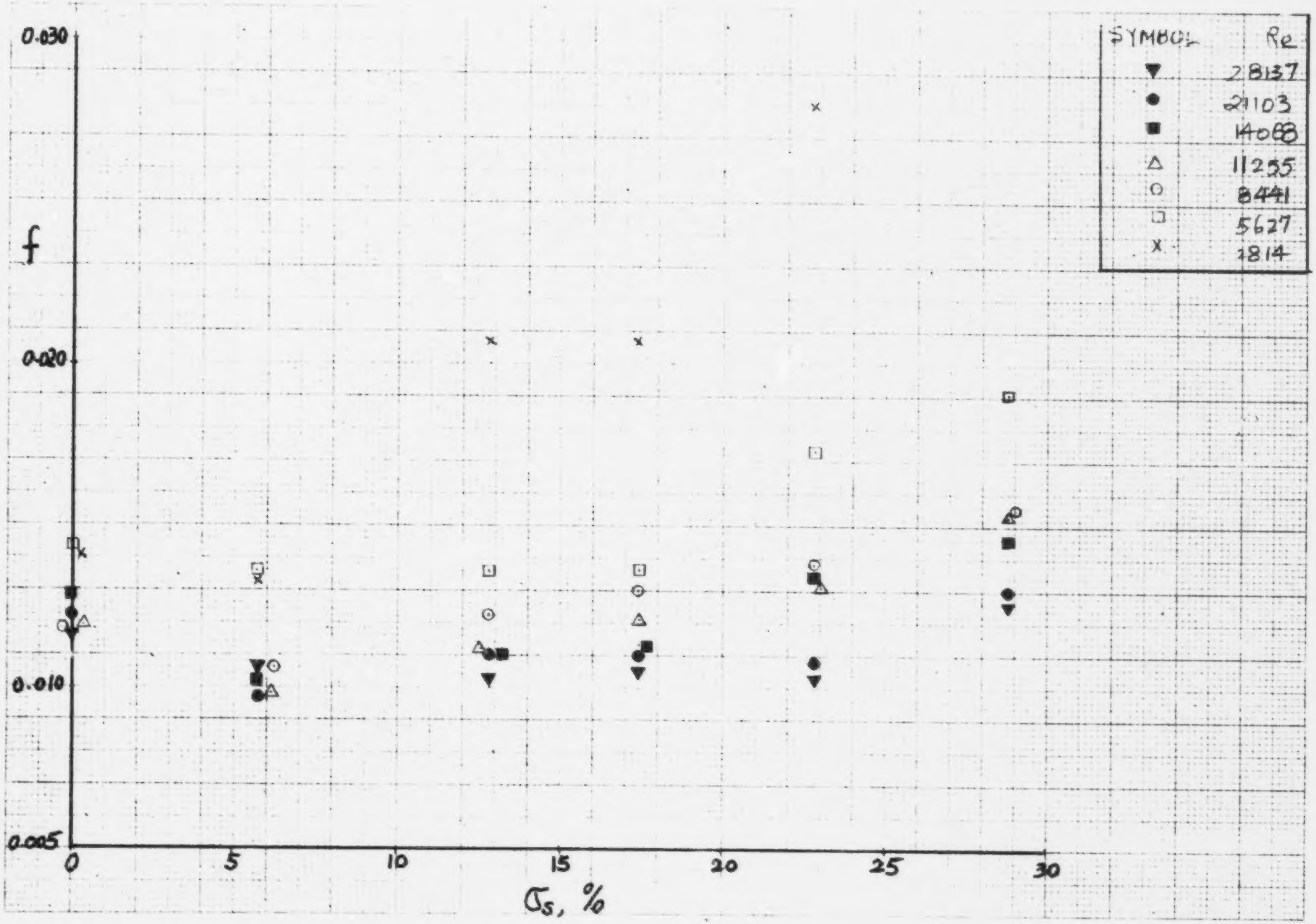

Fig. 21c. f versus σ_s, for t/b=0.0321, 1/2" x 1/16" slots in in-line arrangement.

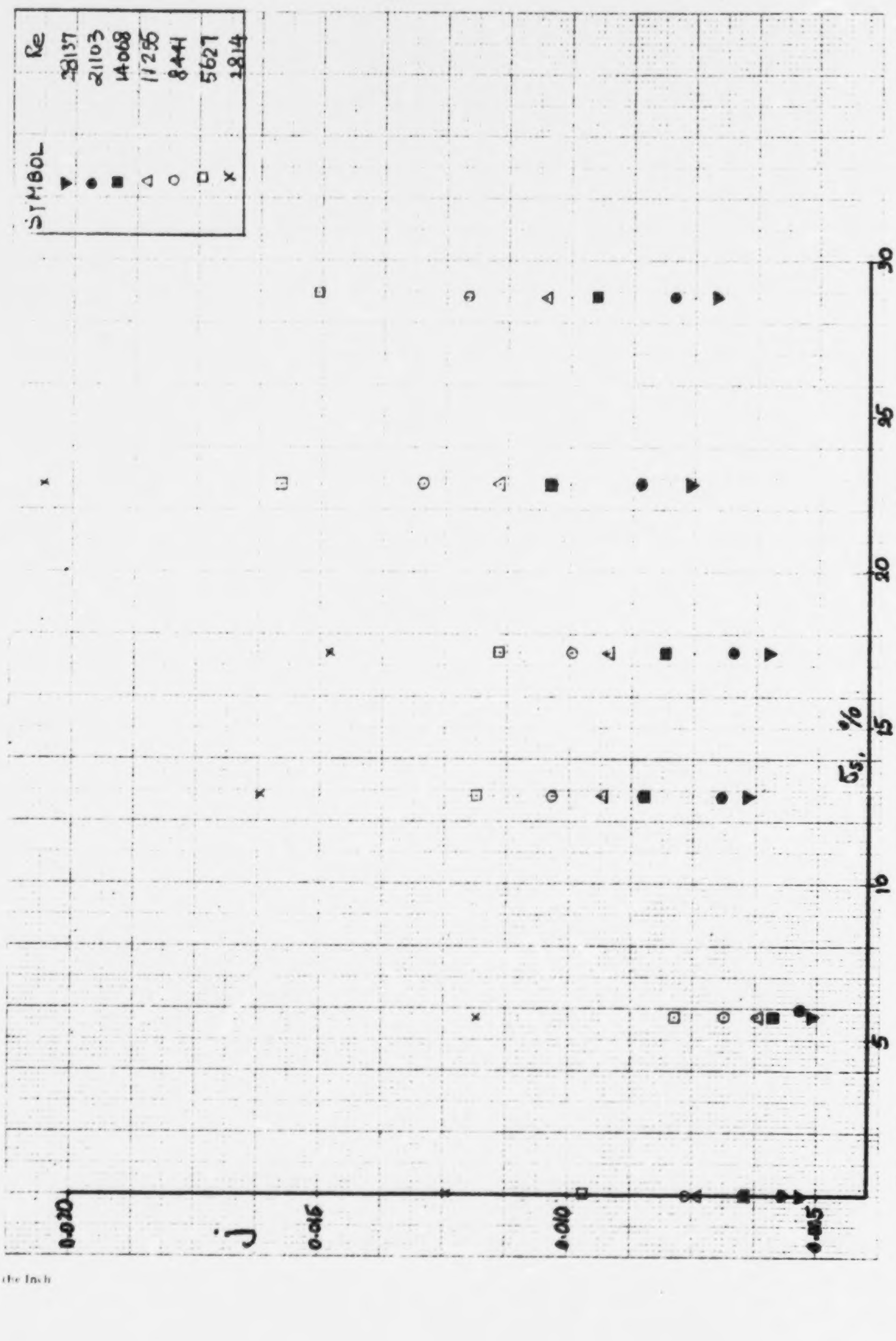

Fig. 21d. j versus σ_s, for t/b=0.0321, 1/2" x 1/16" slots in in-line arrangement.

20 Squares to the Inch

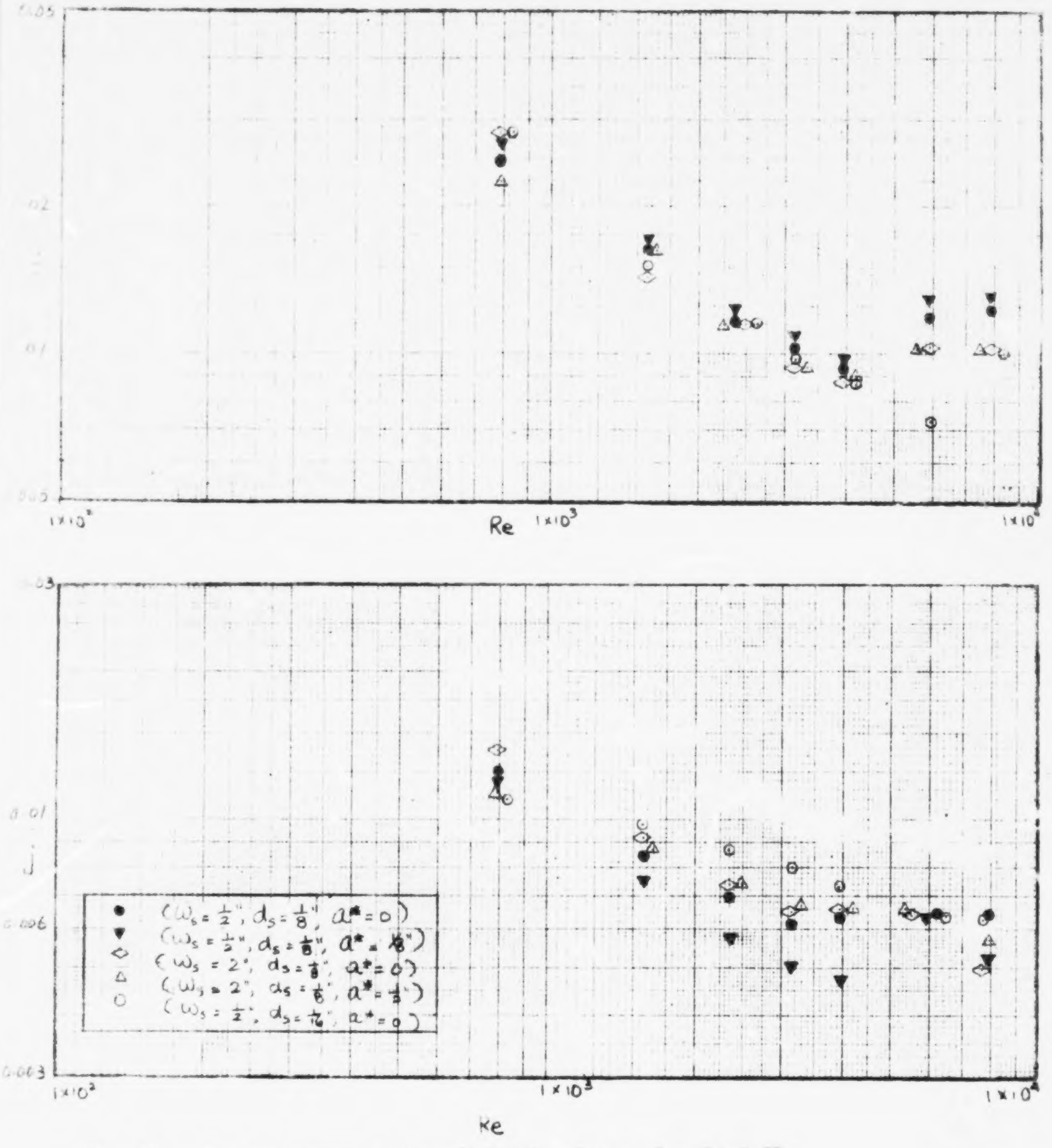

Fig. 22a. f and j versus Re for t/b=0.141, slots; for σ_s=5.7%.

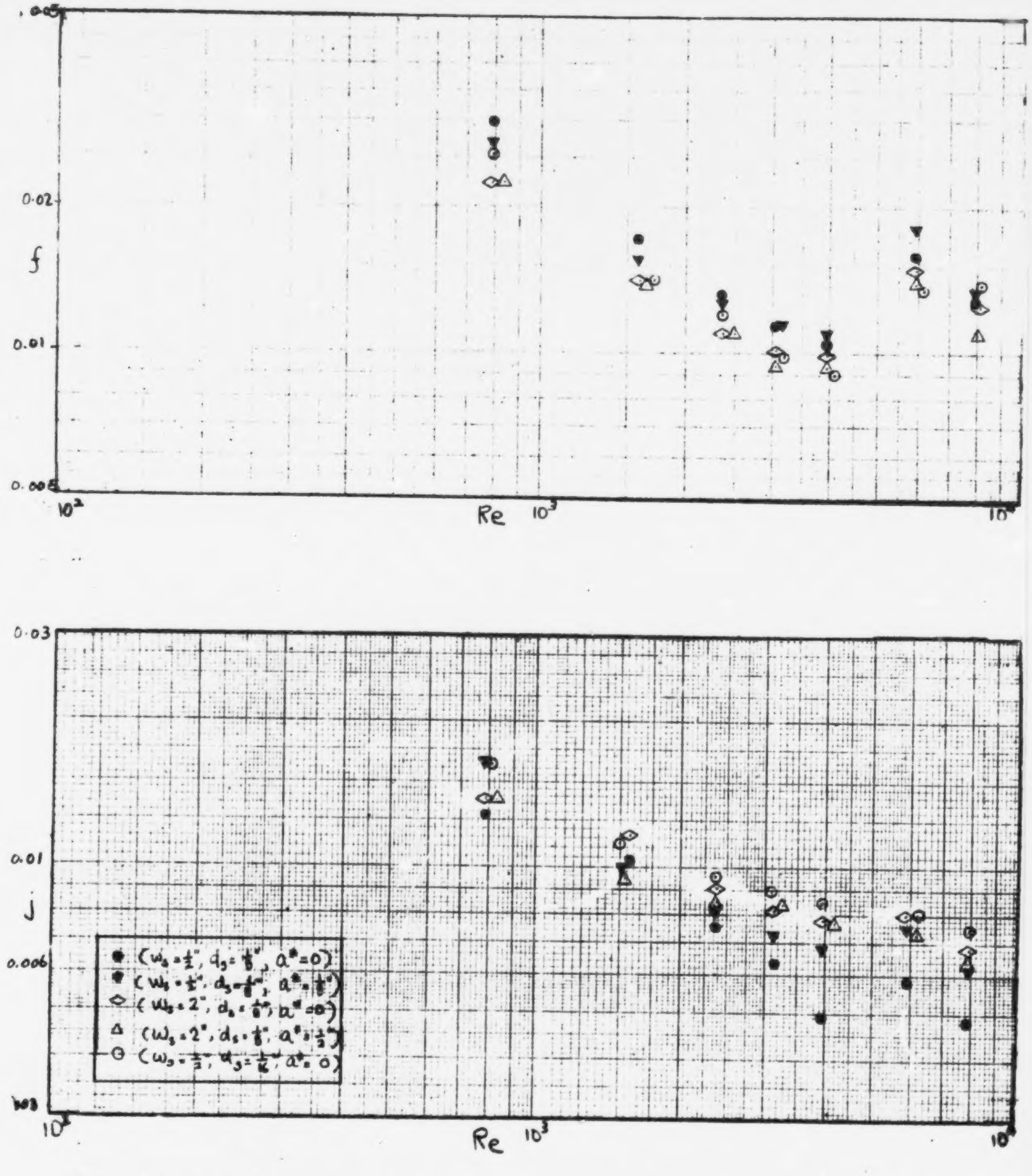

Fig. 22b. f and j versus Re for t/b=0.141, slots; for σ_s=12.8%.

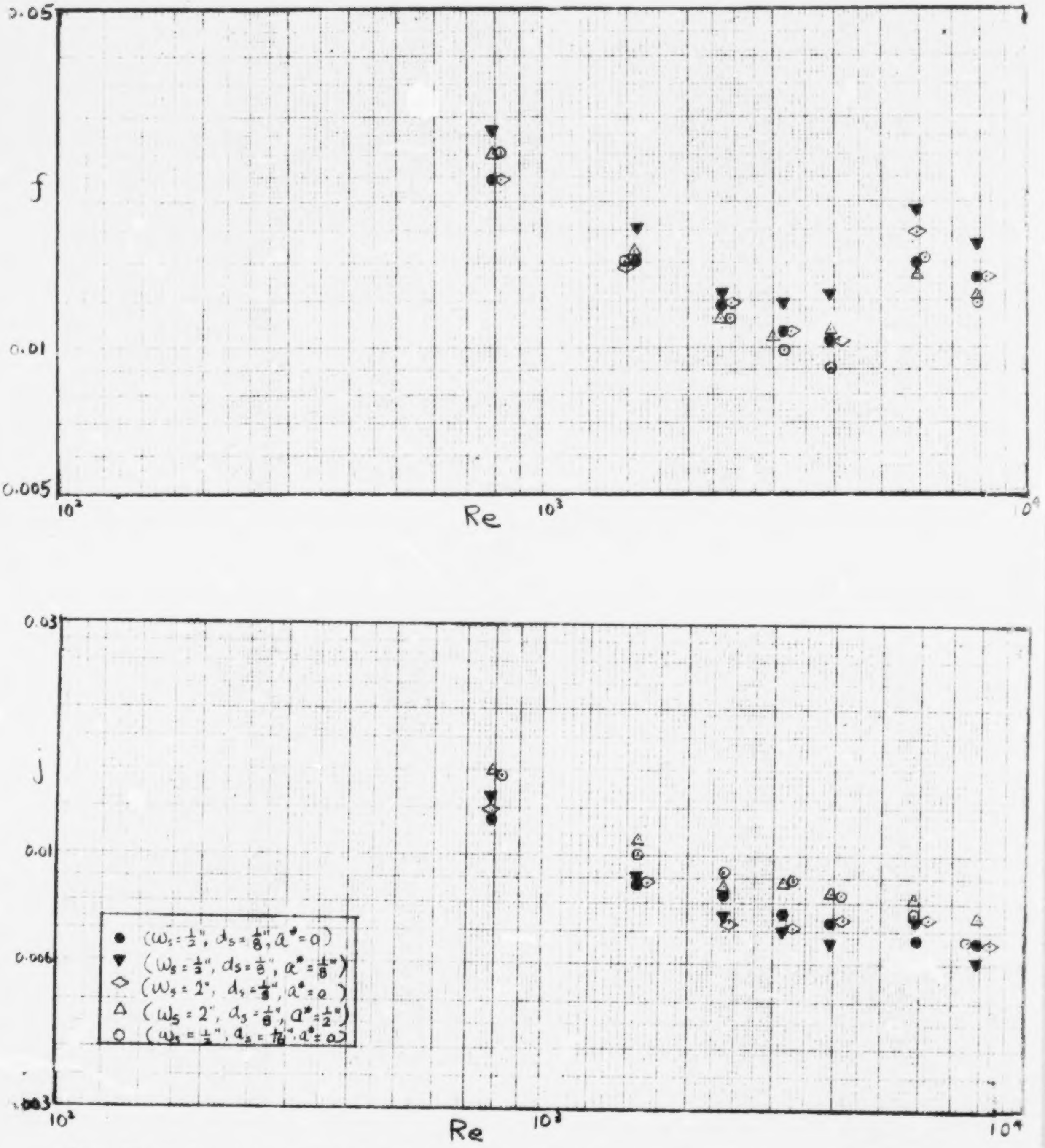

Fig. 22c. f and j versus Re for t/b=0.141, slots; for σ_s=17.4%.

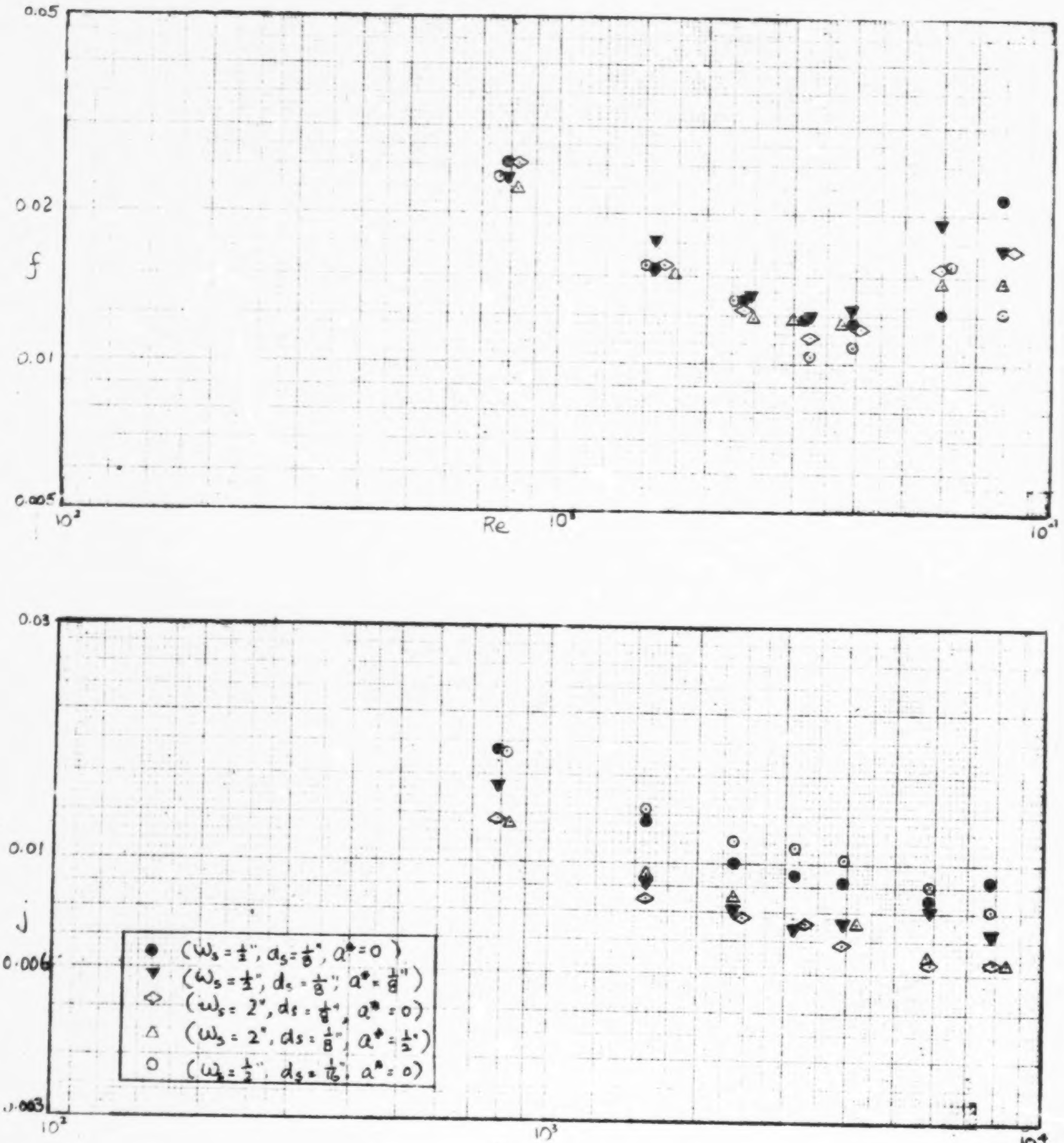

Fig. 22d. f and j versus Re for t/b=0.141, slots; for σ_s=22.8%.

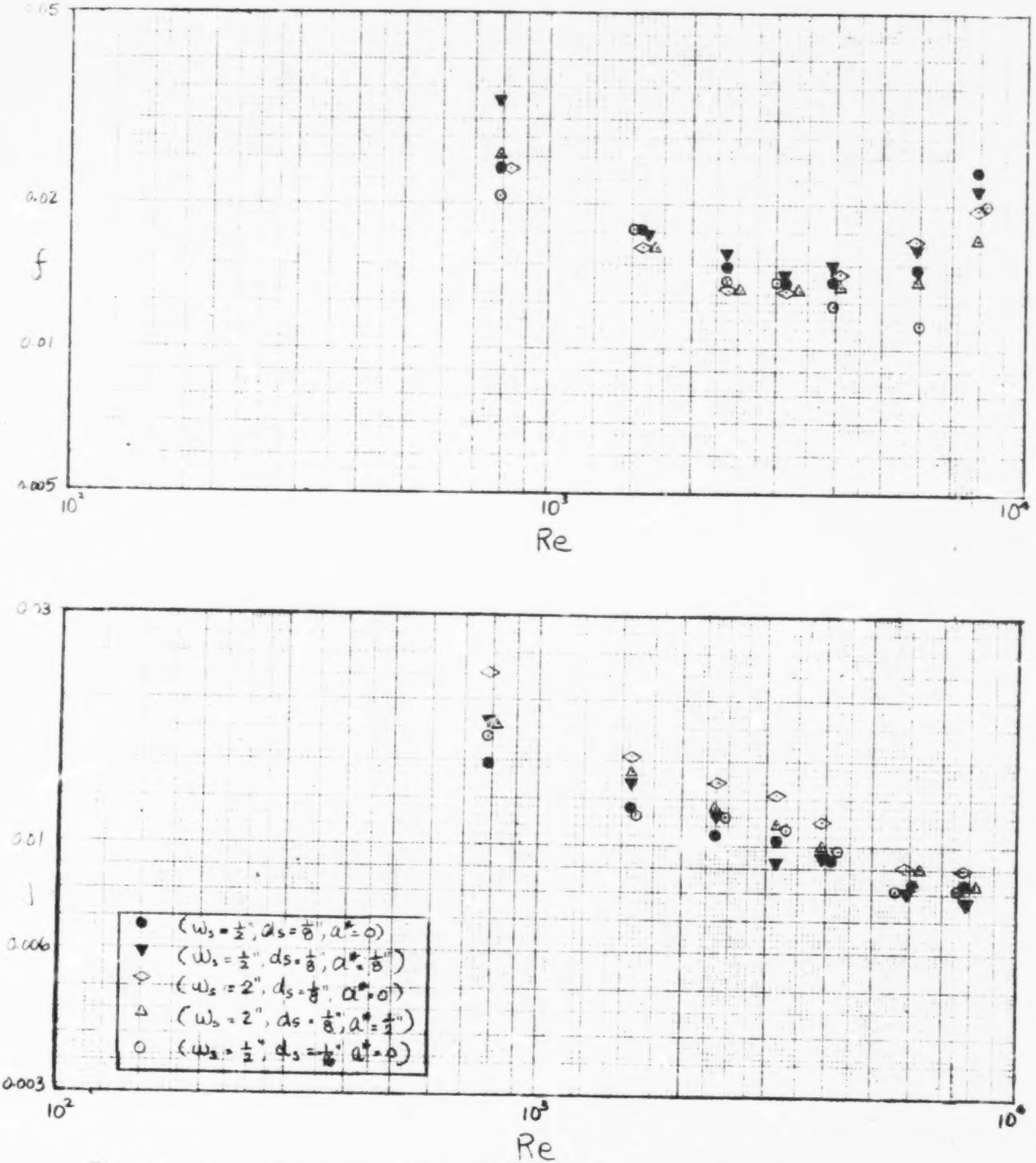

Fig. 22e. f and j versus Re for t/b=0.141 slots; for σ_s=28.8%.

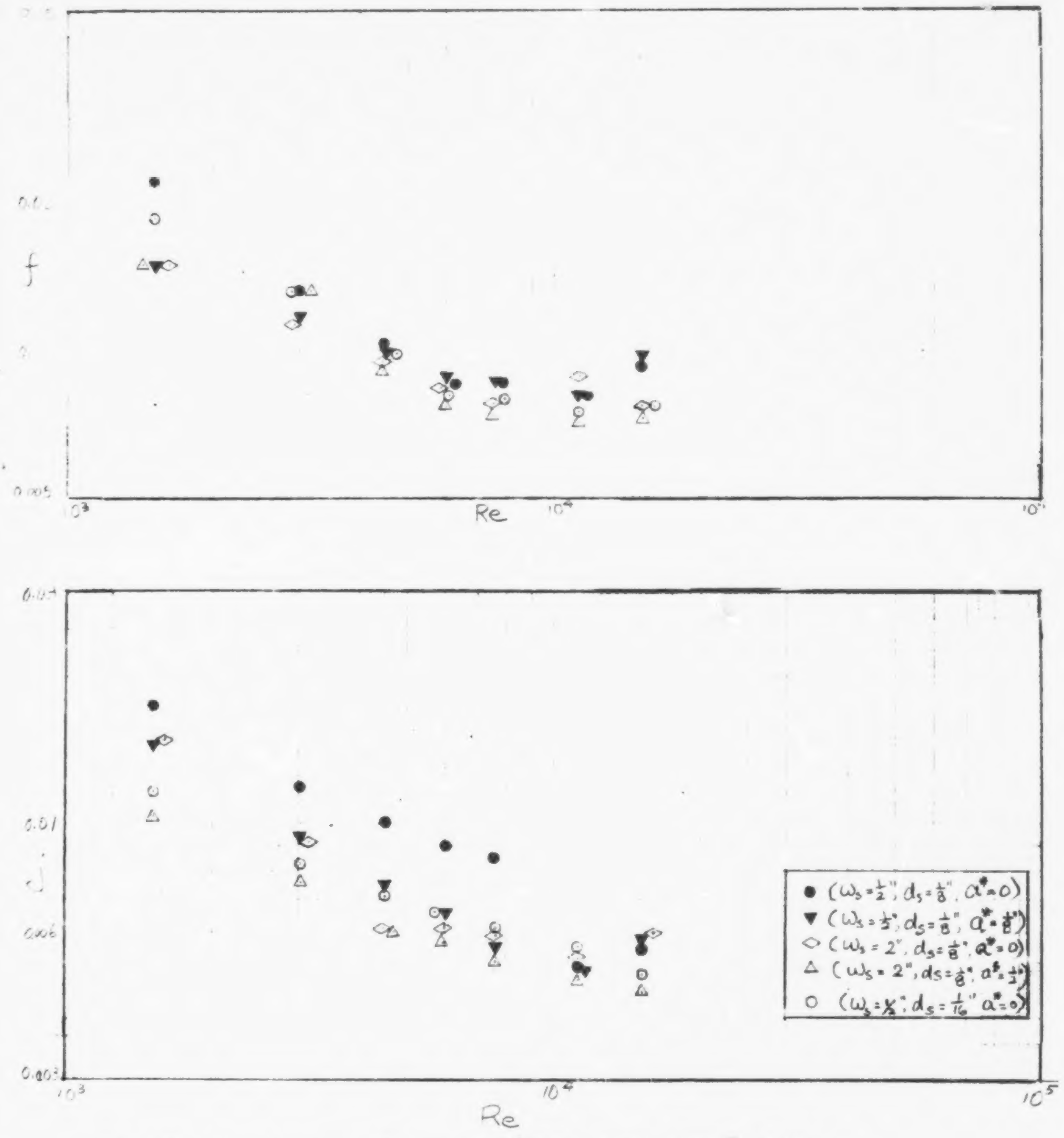

Fig. 23a. f and j versus Re for t/b=0.0665, slots; for δ_s=5.7%.

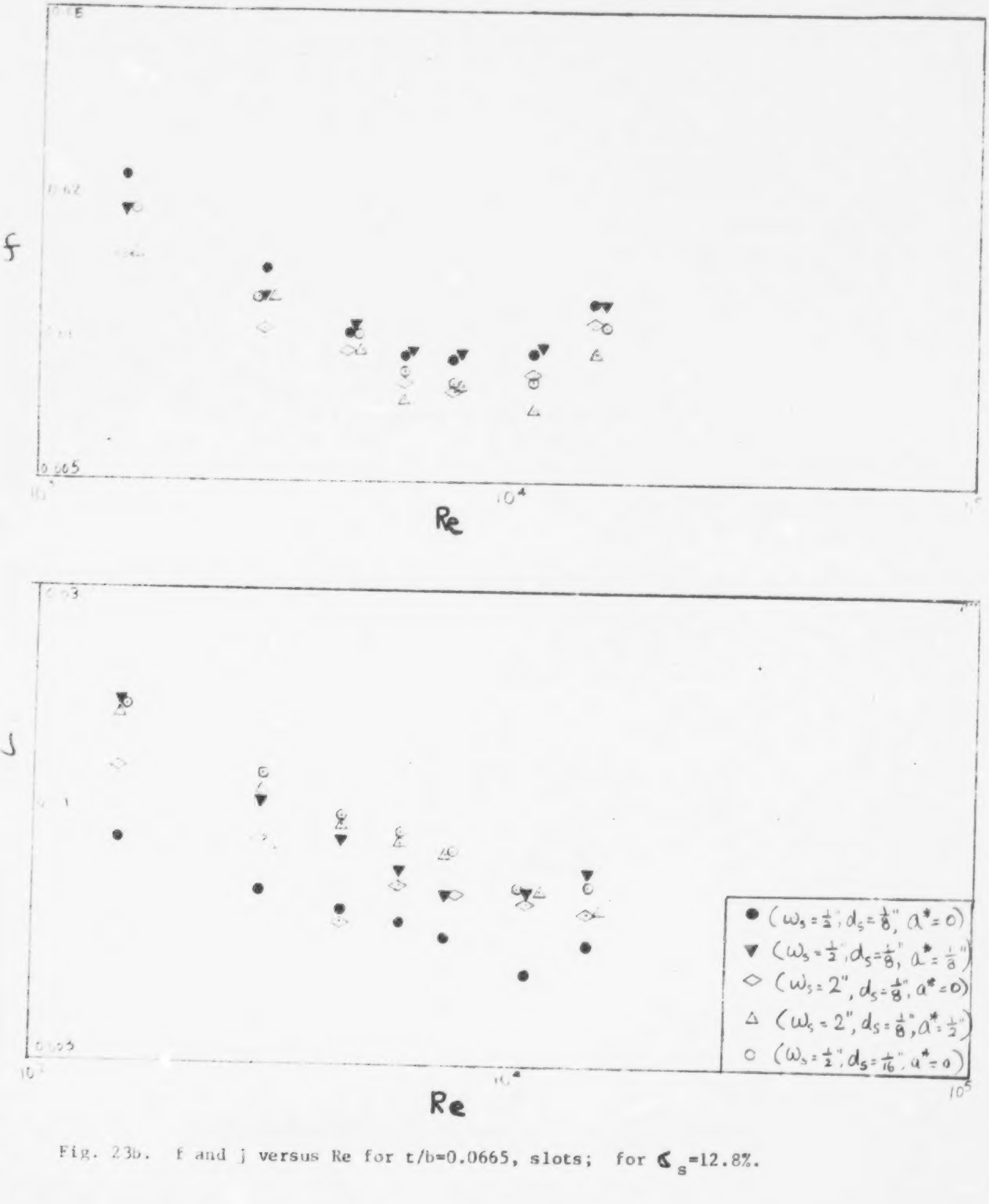

Fig. 23b. f and j versus Re for t/b=0.0665, slots; for σ_s=12.8%.

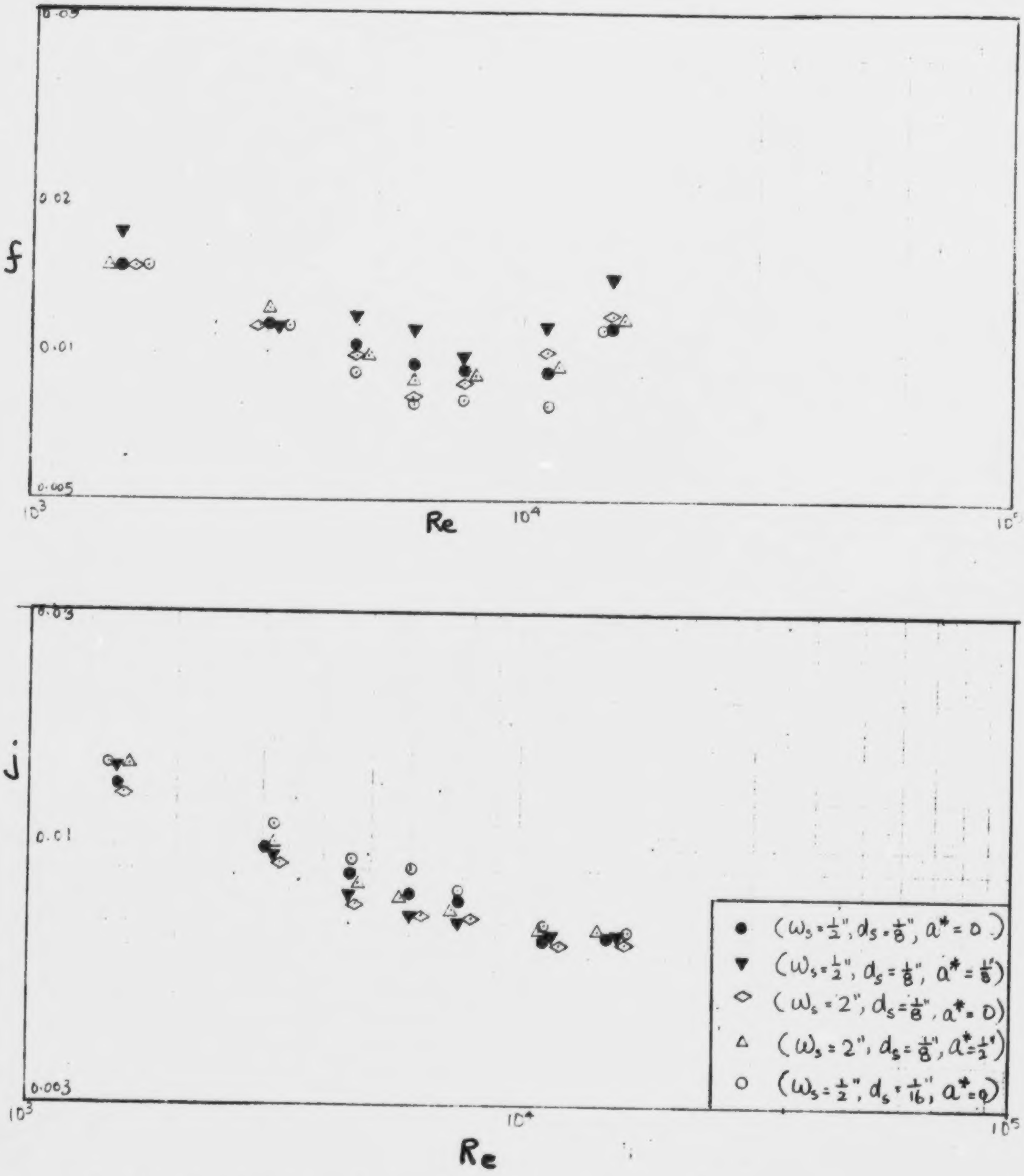

Fig. 23c. f and j versus Re for t/b=0.0665, slots; for σ_s=17.4%.

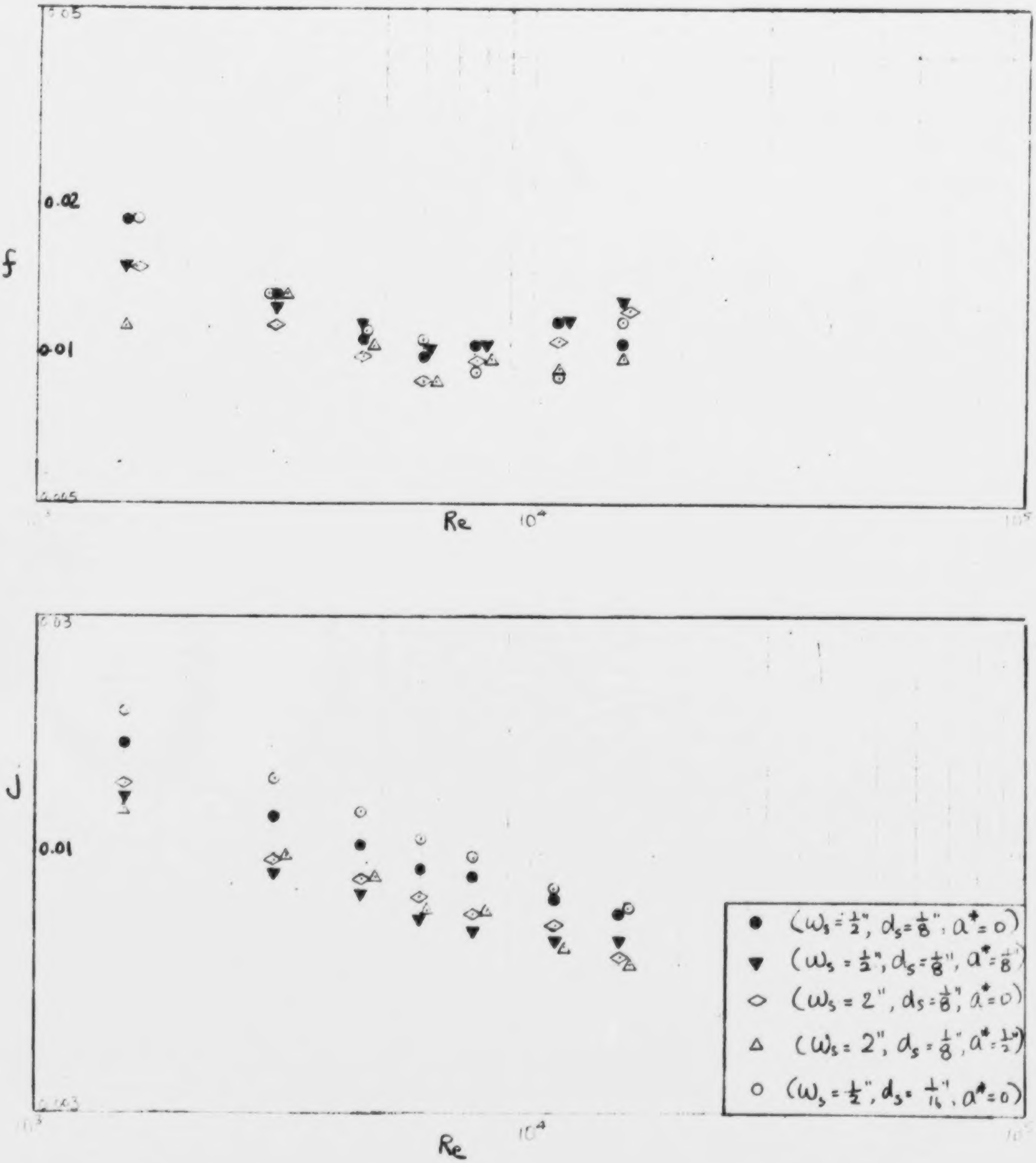

Fig. 23d. f and j versus Re for t/b=0.0665, slots; for σ_s=22.8%.

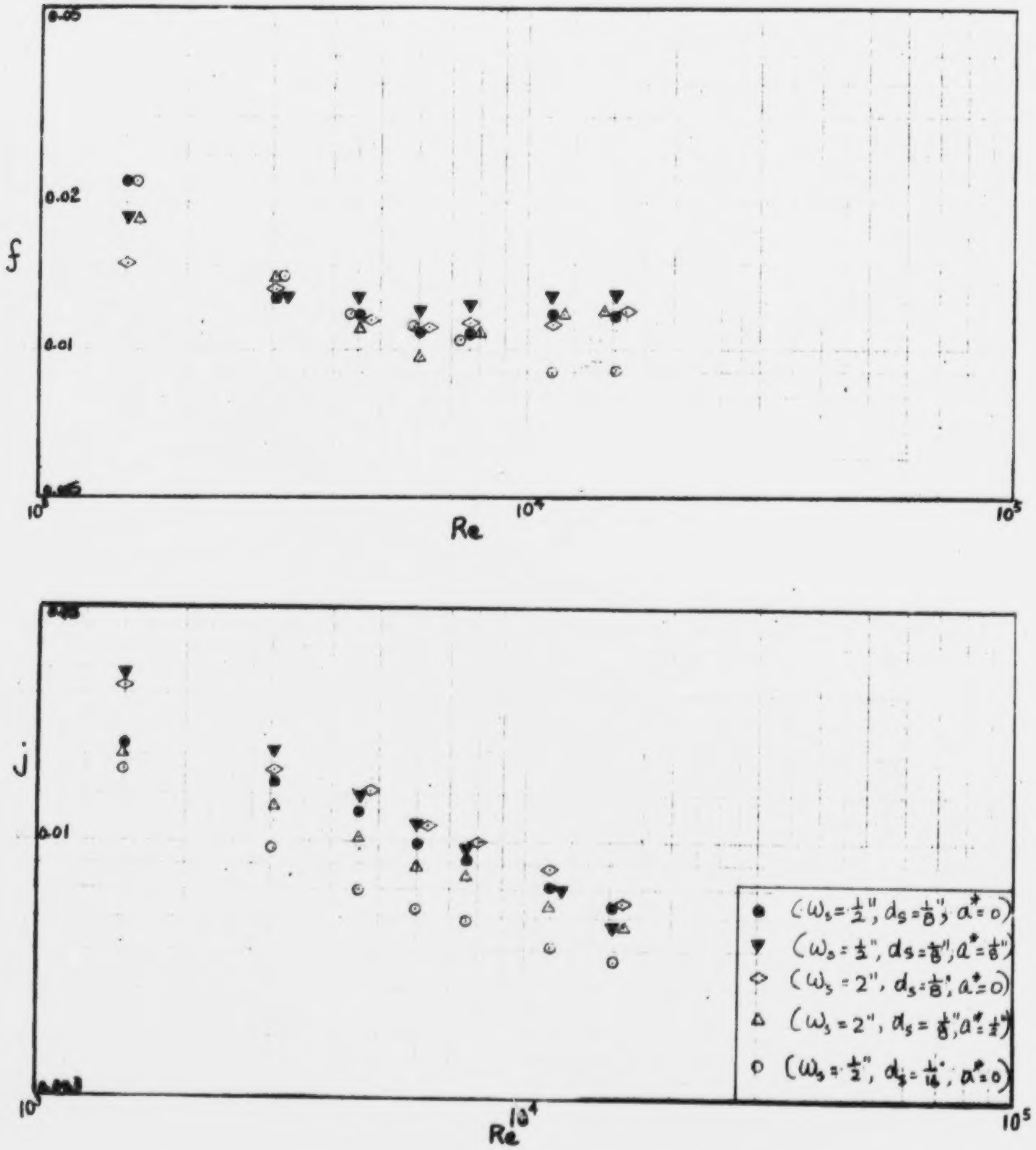

Fig. 23e. f and j versus Re for t/b=0.0665, slots; for σ_s=28.8%.

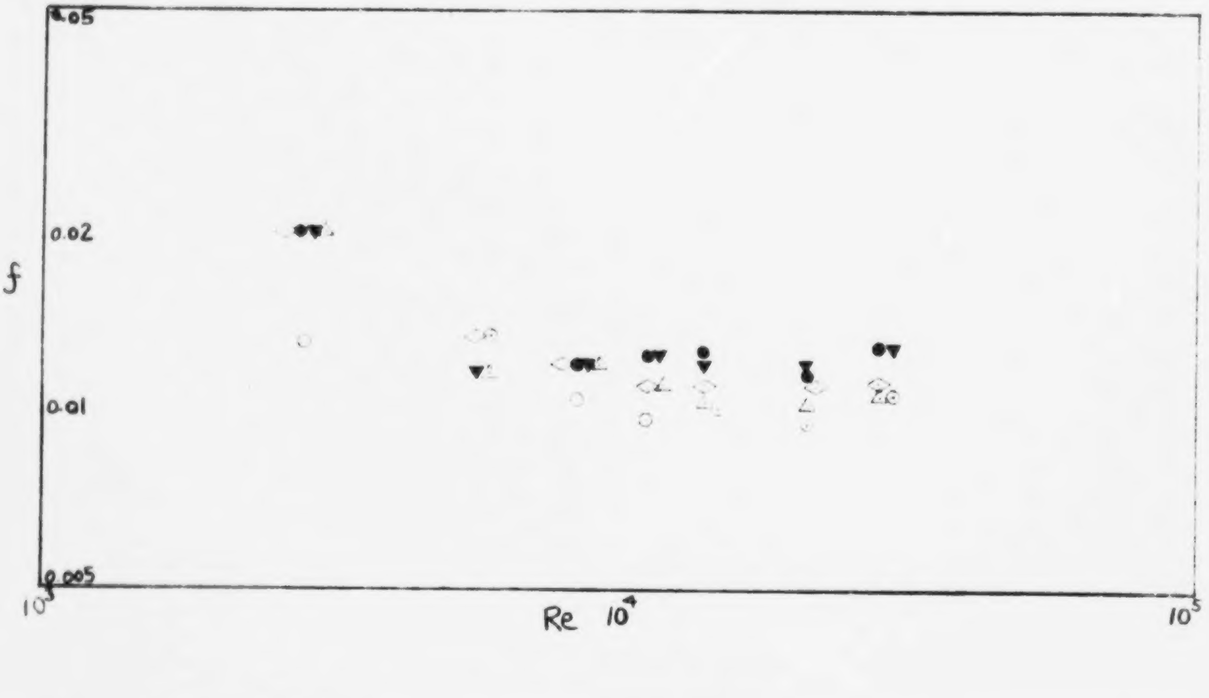

Fig. 24a. f and j versus Re for t/b=0.0321, slots; for σ_s=5.7%.

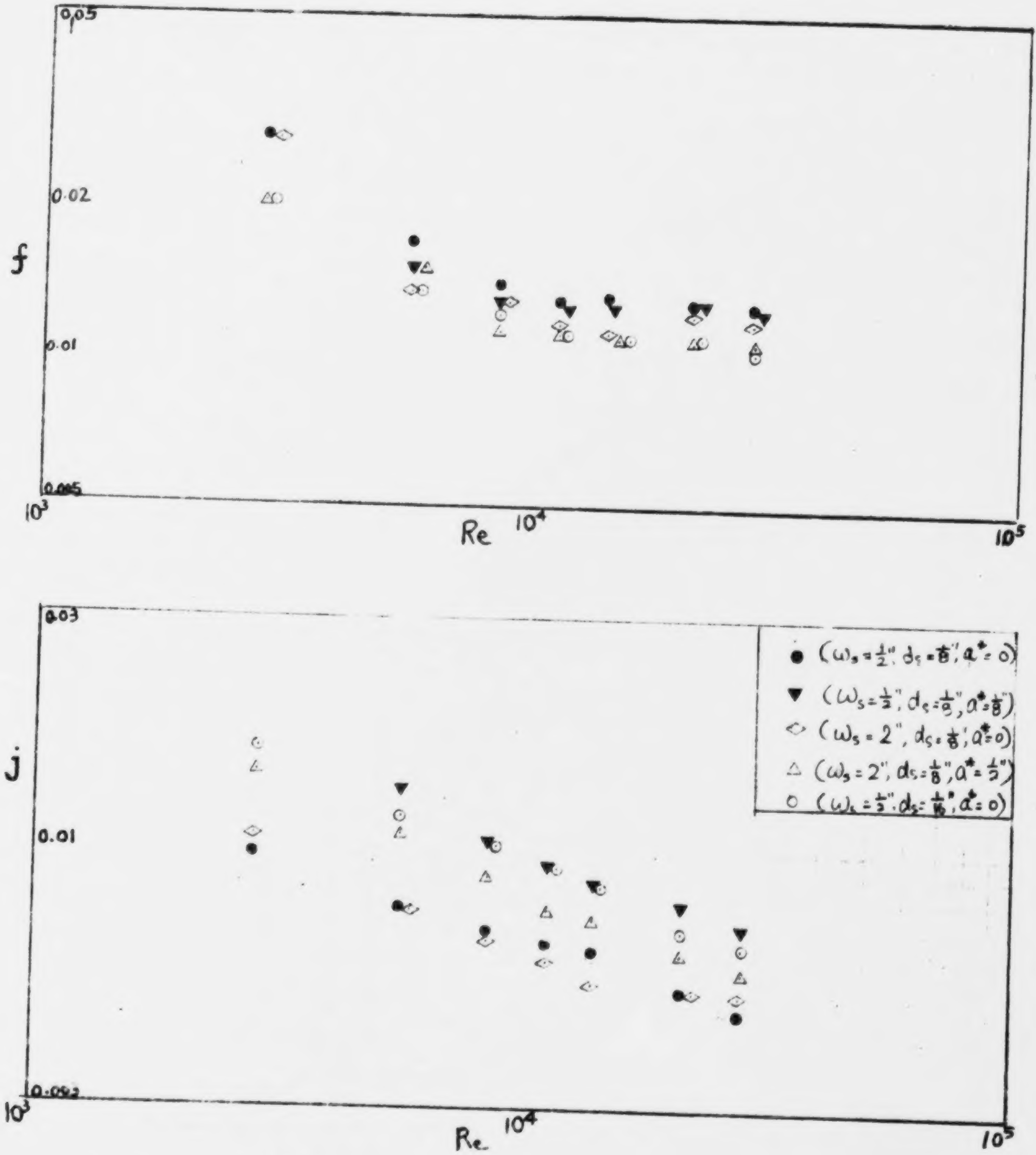

Fig. 24b. f and j versus Re for t/b=0.0321, slots; for σ_s=12.8%.

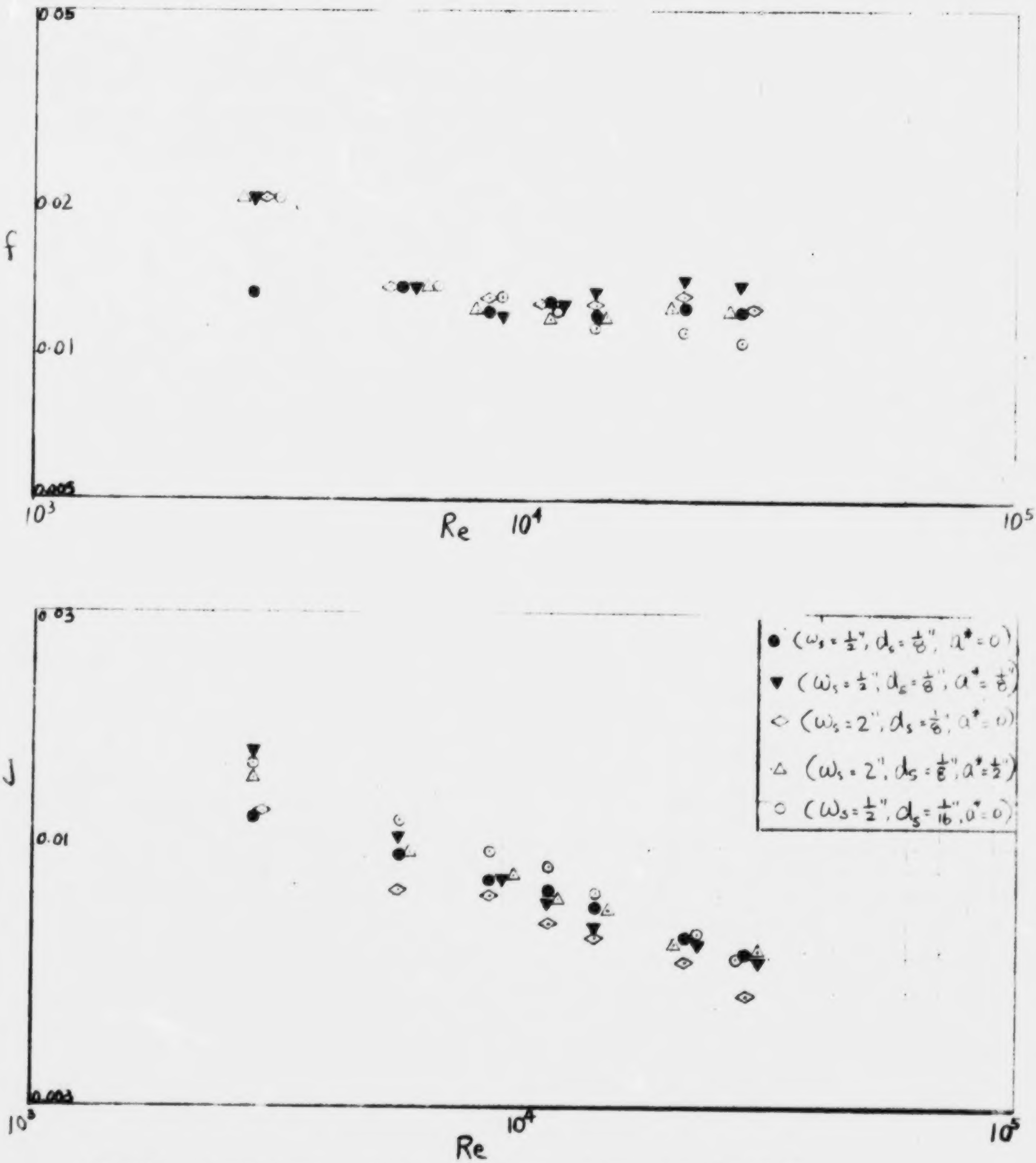

Fig. 24c. f and j versus Re for t/b=0.0321, slots; for σ_s=17.4%.

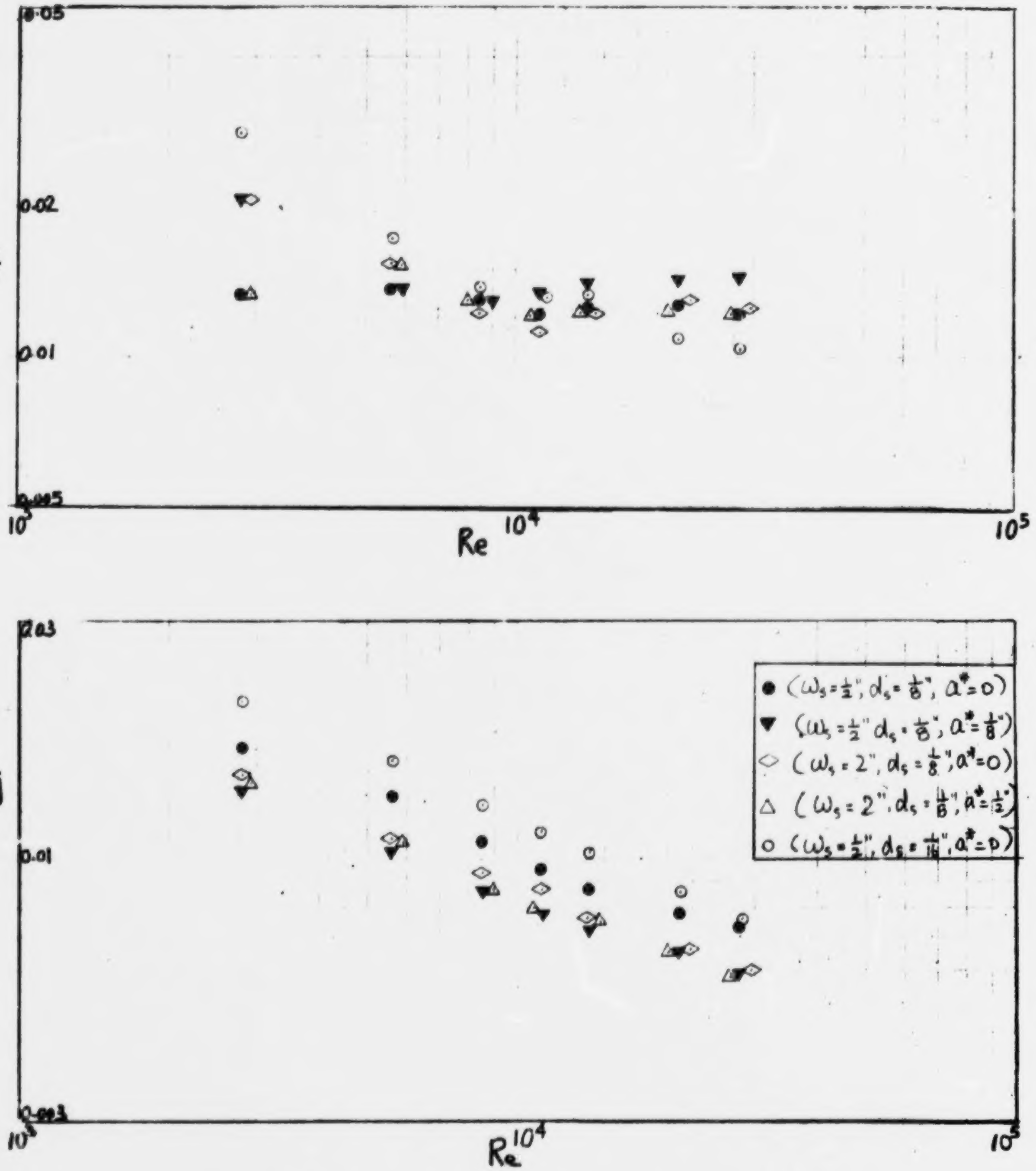

Fig. 24d. f and j versus Re for t/b=0.0321, slots; for σ_s=22.8%.

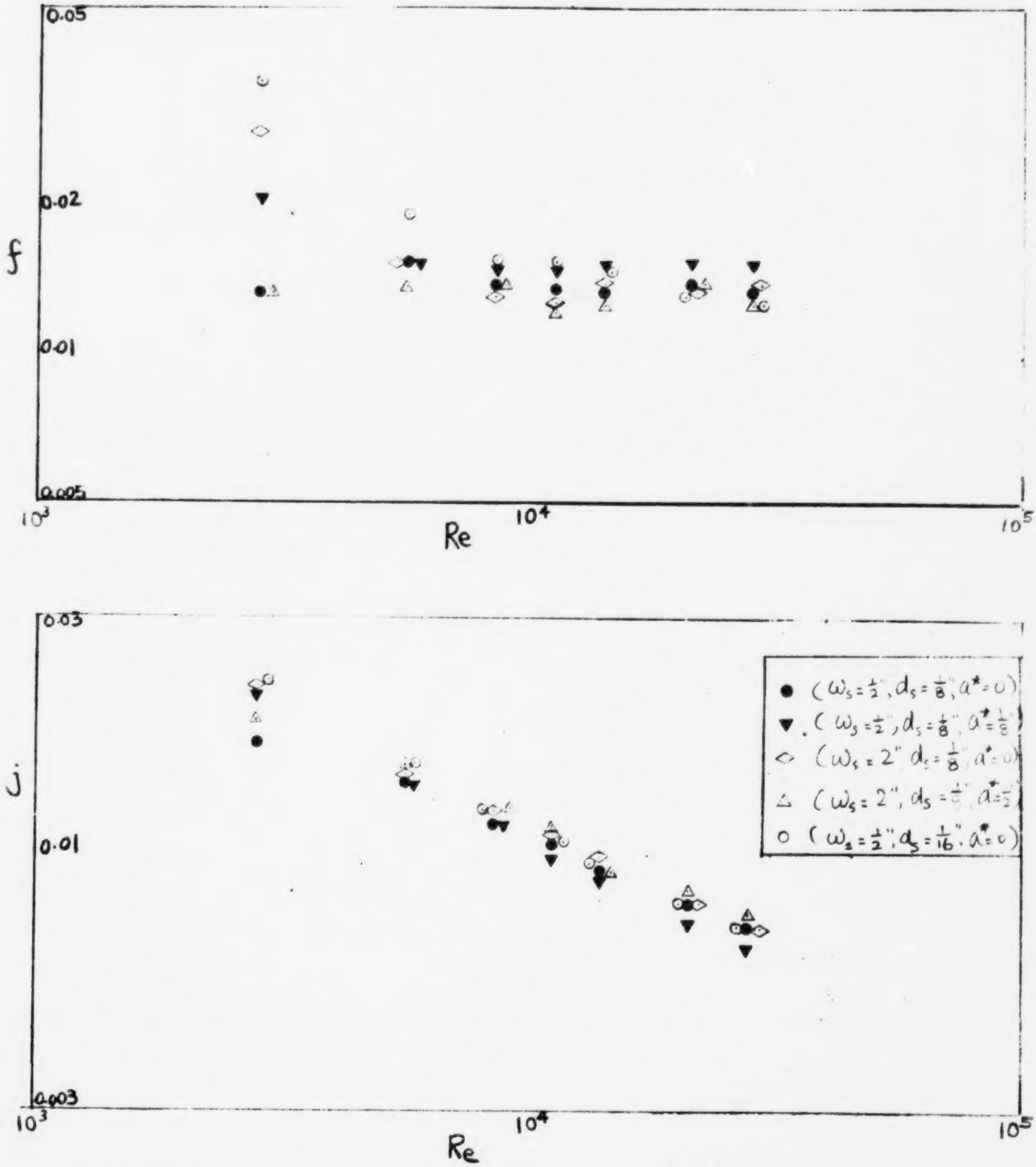

Fig. 24e. f and j versus Re for t/b=0.0321, slots; for σ_s=28.8%.

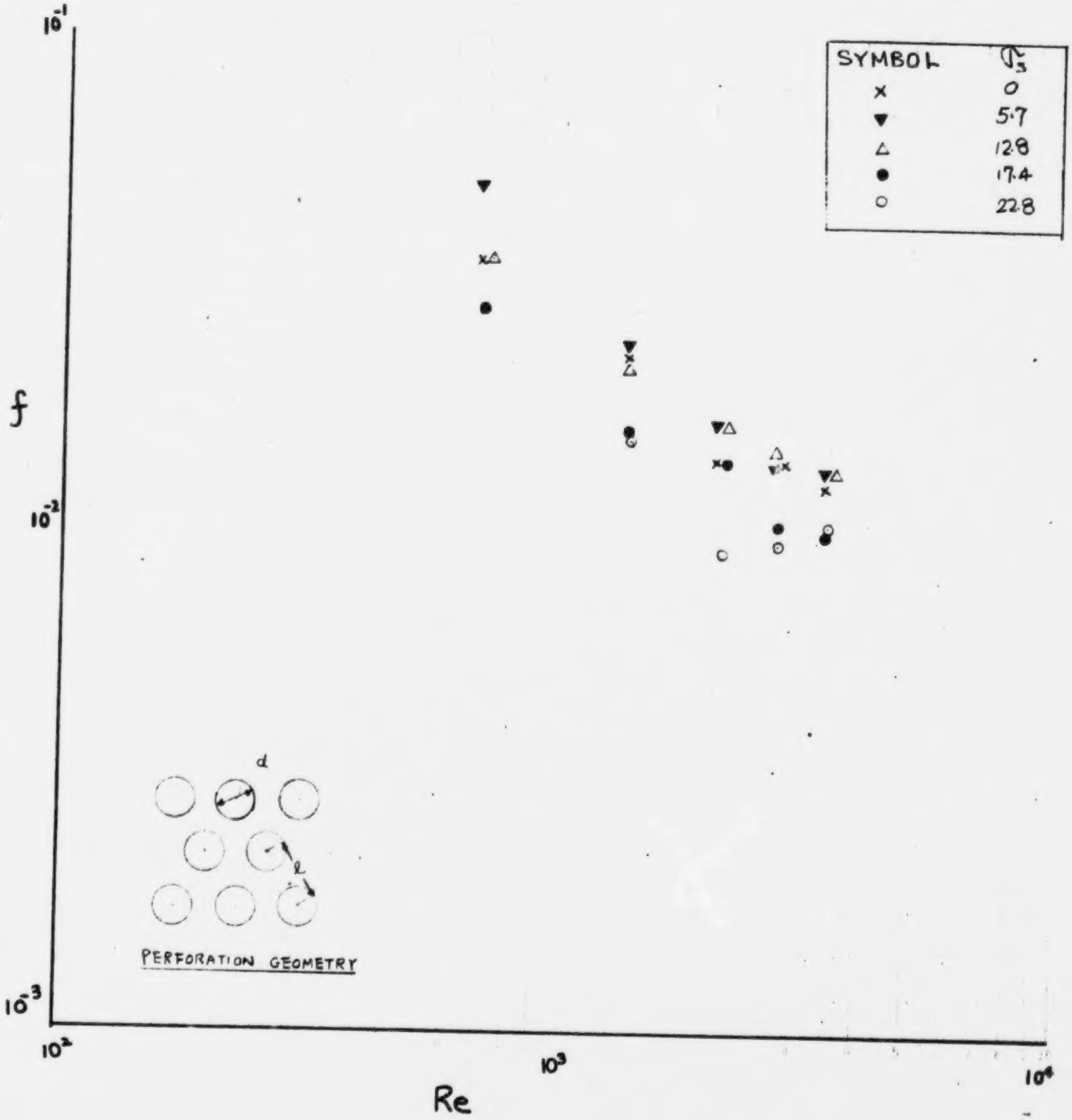

Fig. 25a. f versus Re, for t/b=0.141, staggered round holes.

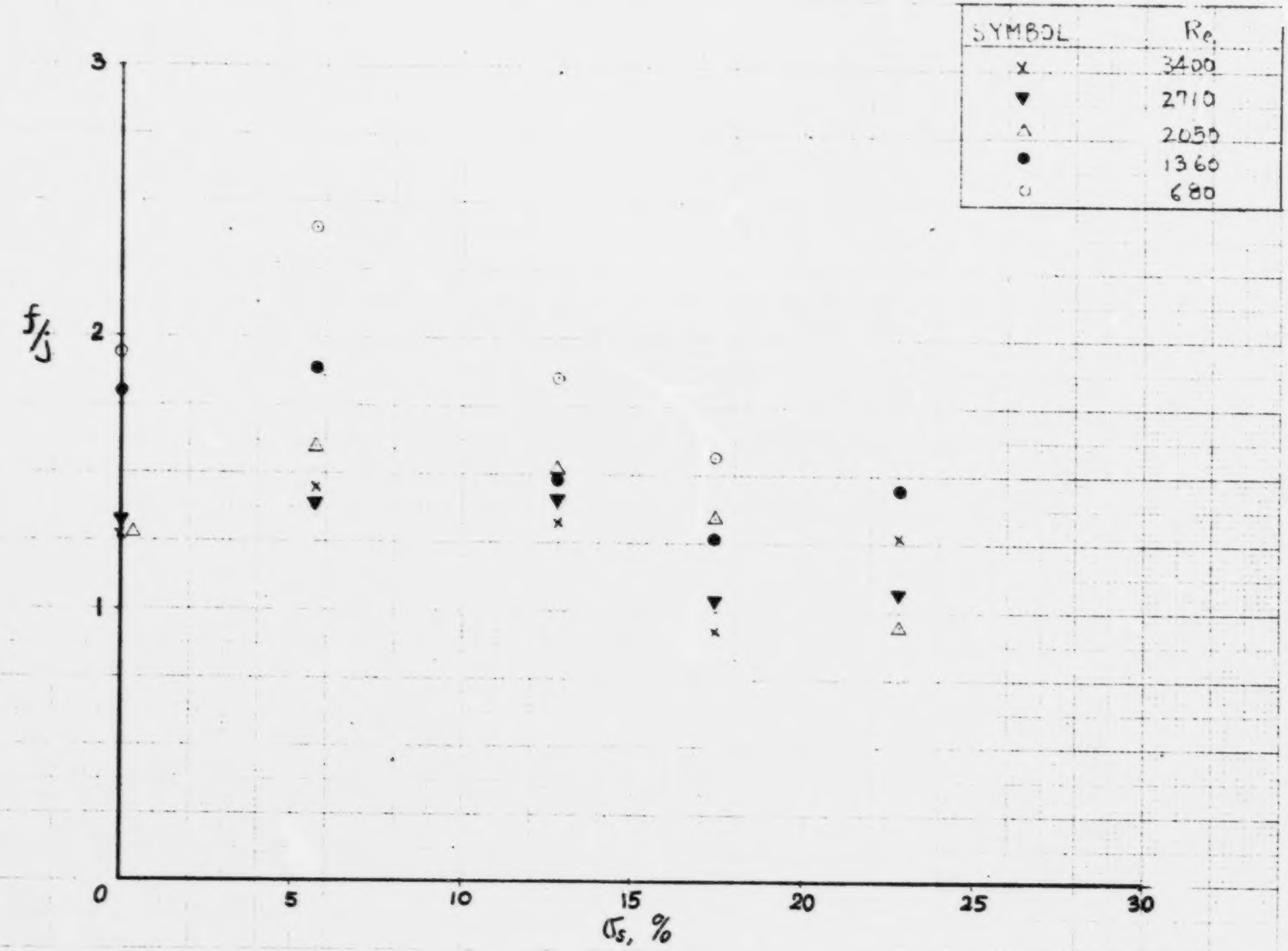

Fig. 25b. f/j versus σ_s, for t/b=0.141, staggered round holes.

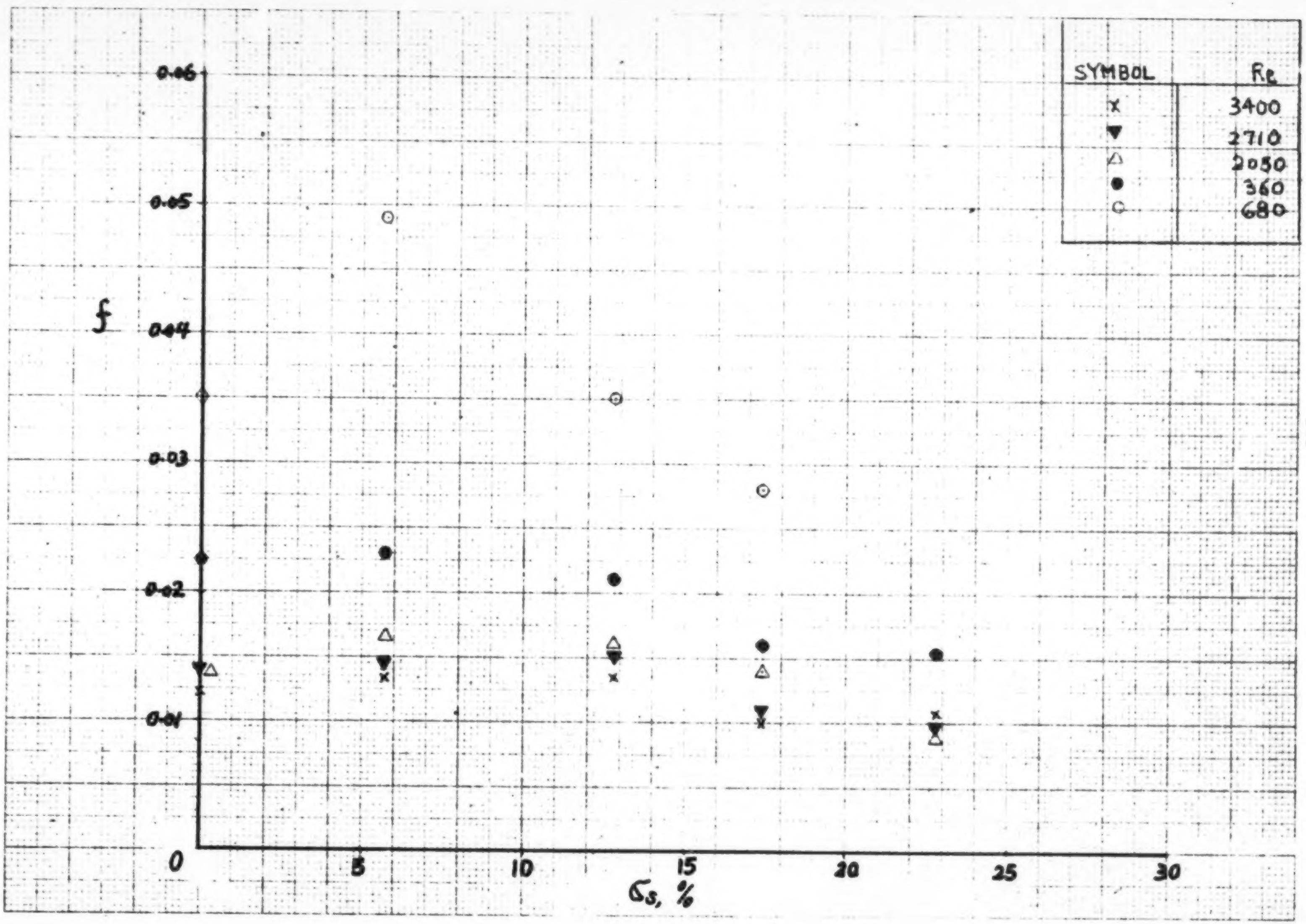

Fig. 25c. f versus σ_s for t/b=0.141, staggered round holes.

20 Squares to the Inch

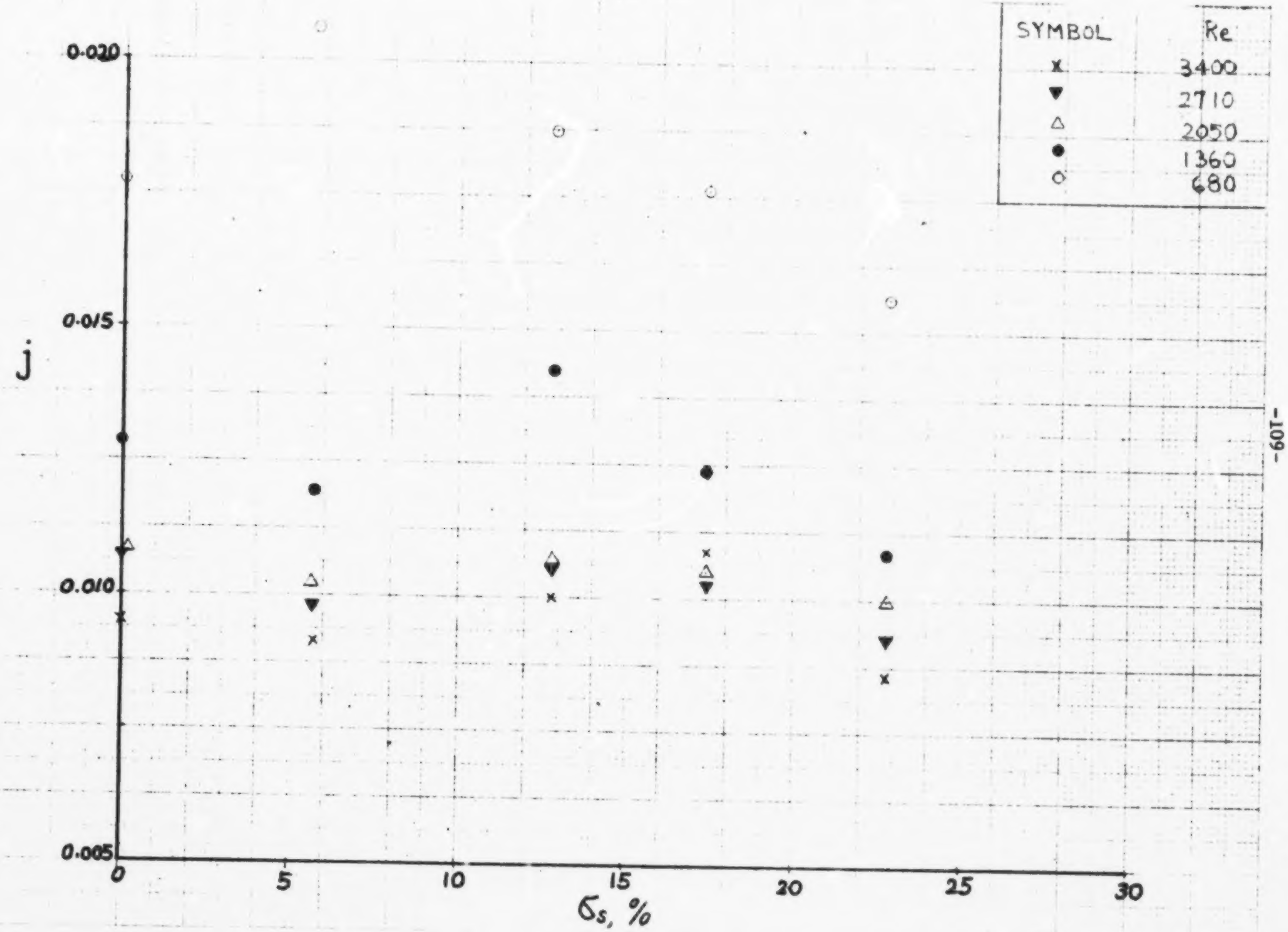

Fig. 25d. j versus σ_s for t/b=0.141, staggered round holes.

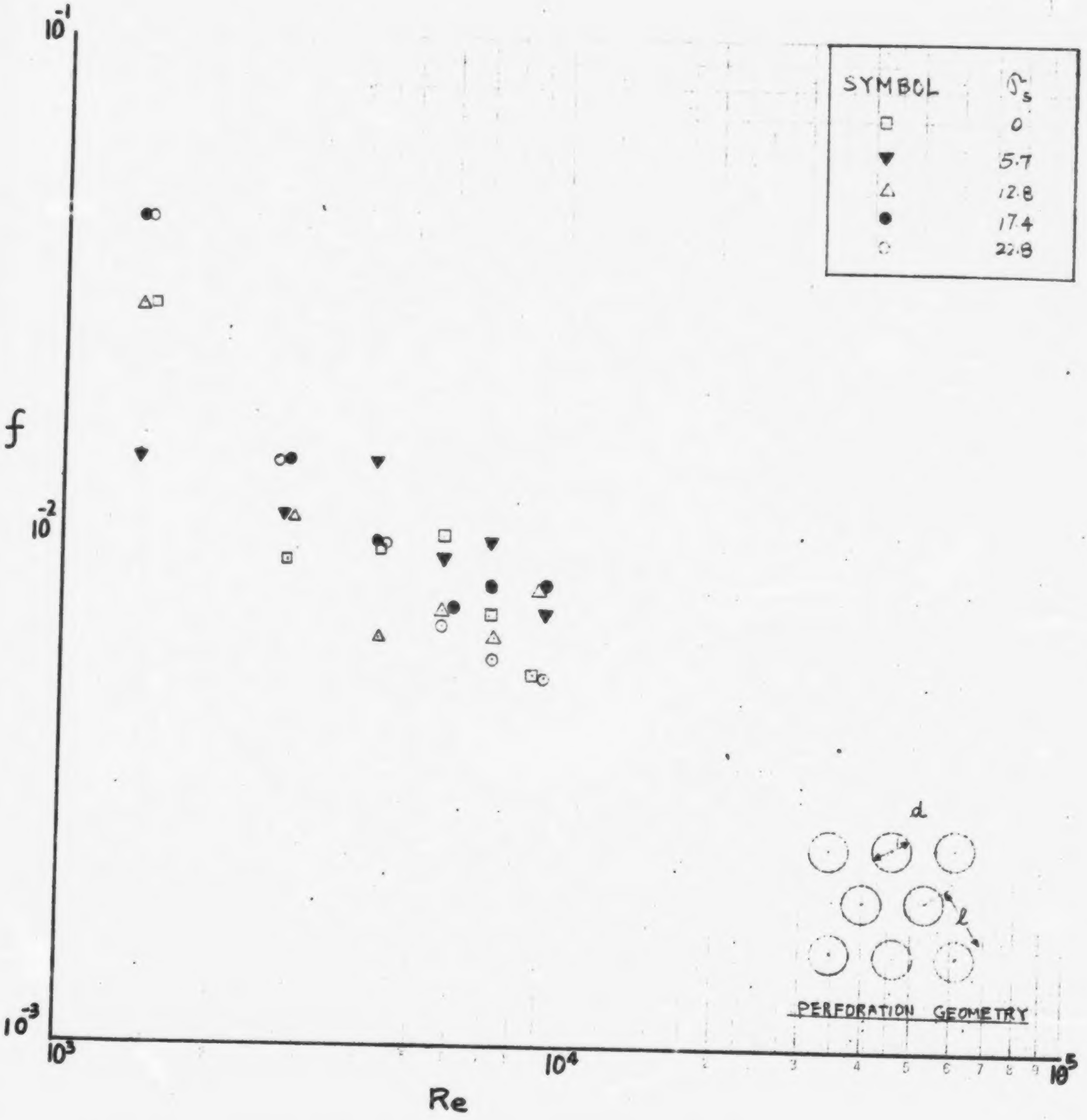

Fig. 26a. f versus Re, for t/b=0.0665, staggered round holes.

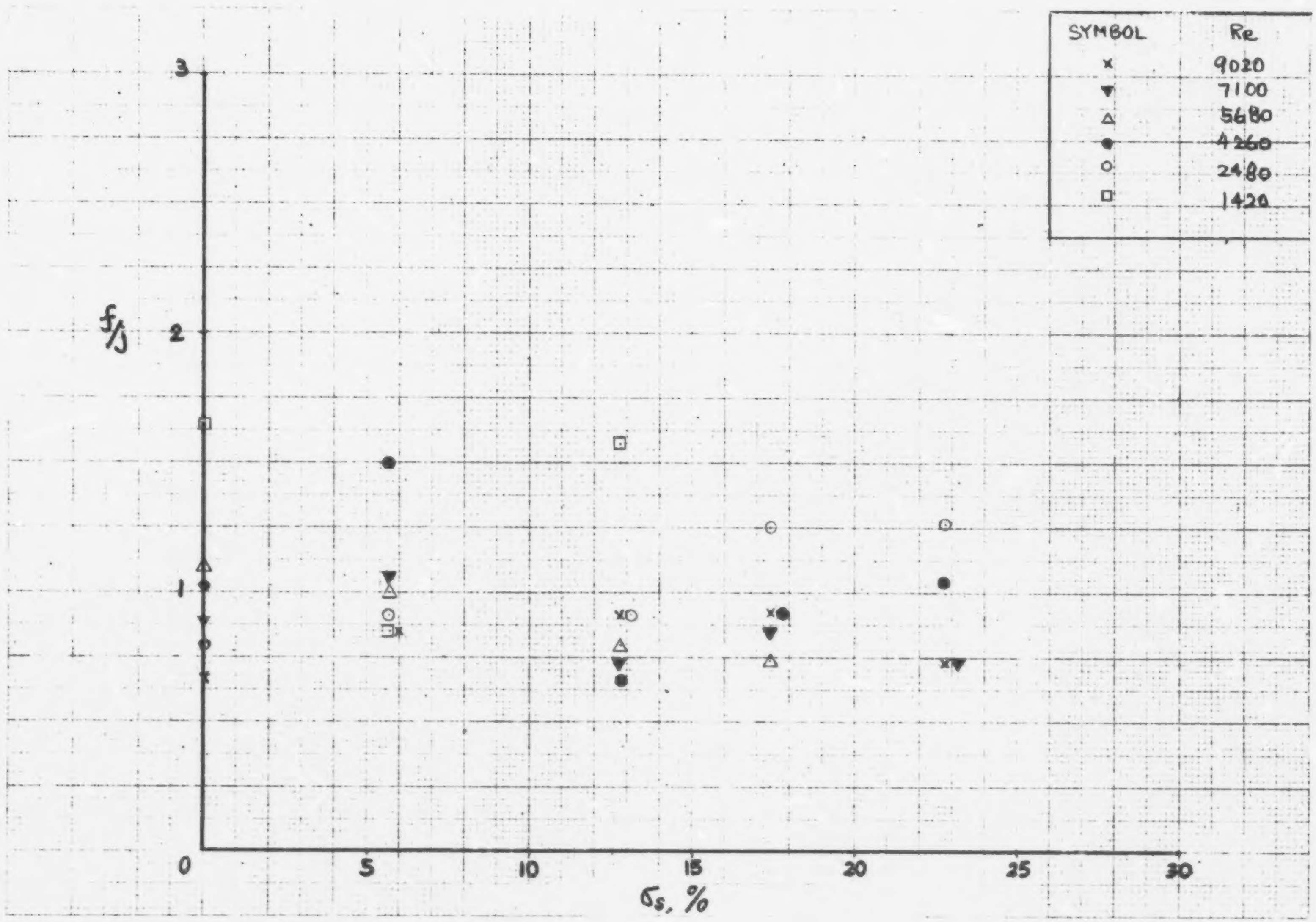

Fig. 26b. f/j versus σ_s, for t/b=0.0665, staggered round holes.

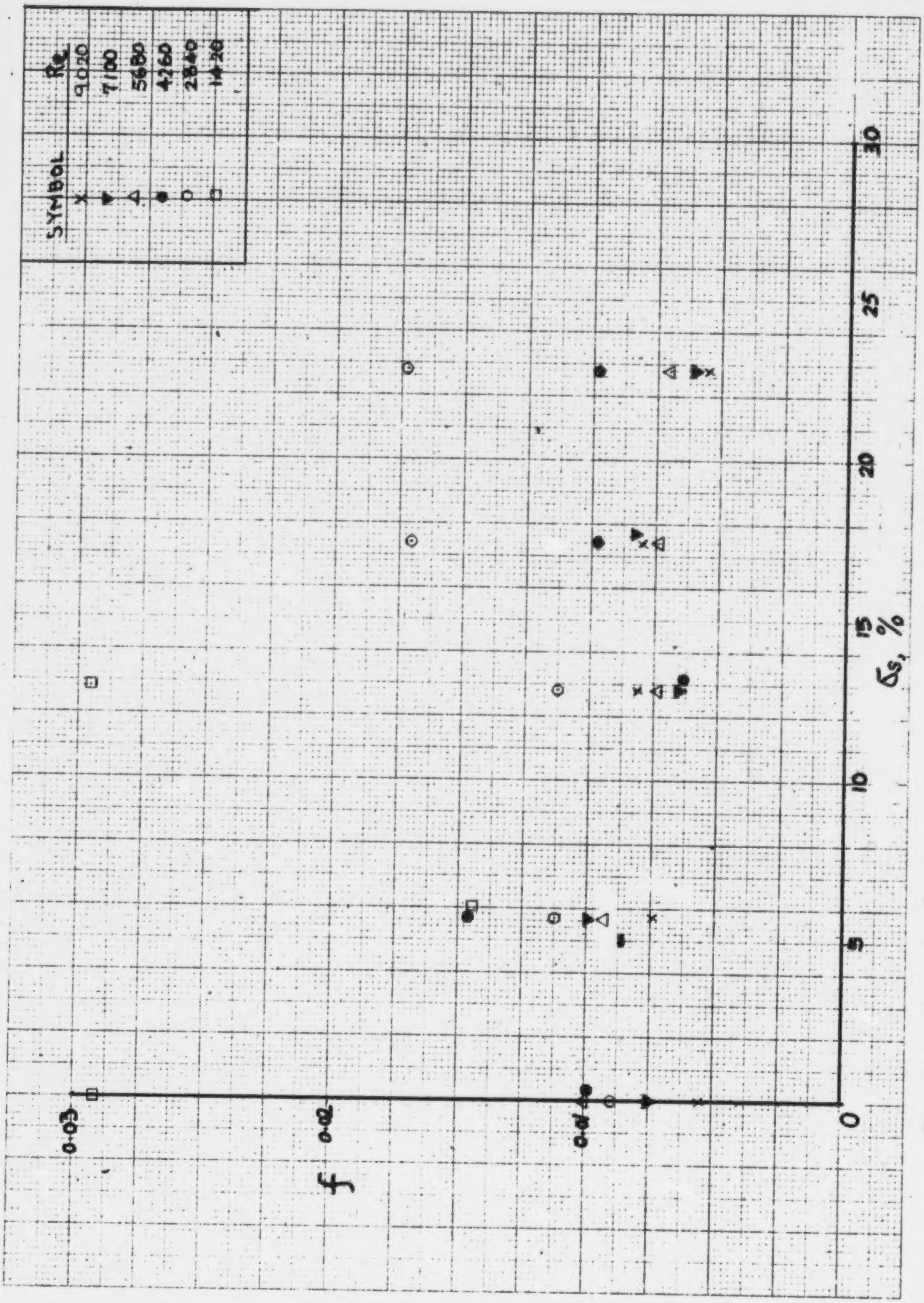

Fig. 26c. f versus σ_s, for t/b=0.0665, staggered round holes.

20 Squares to the Inch

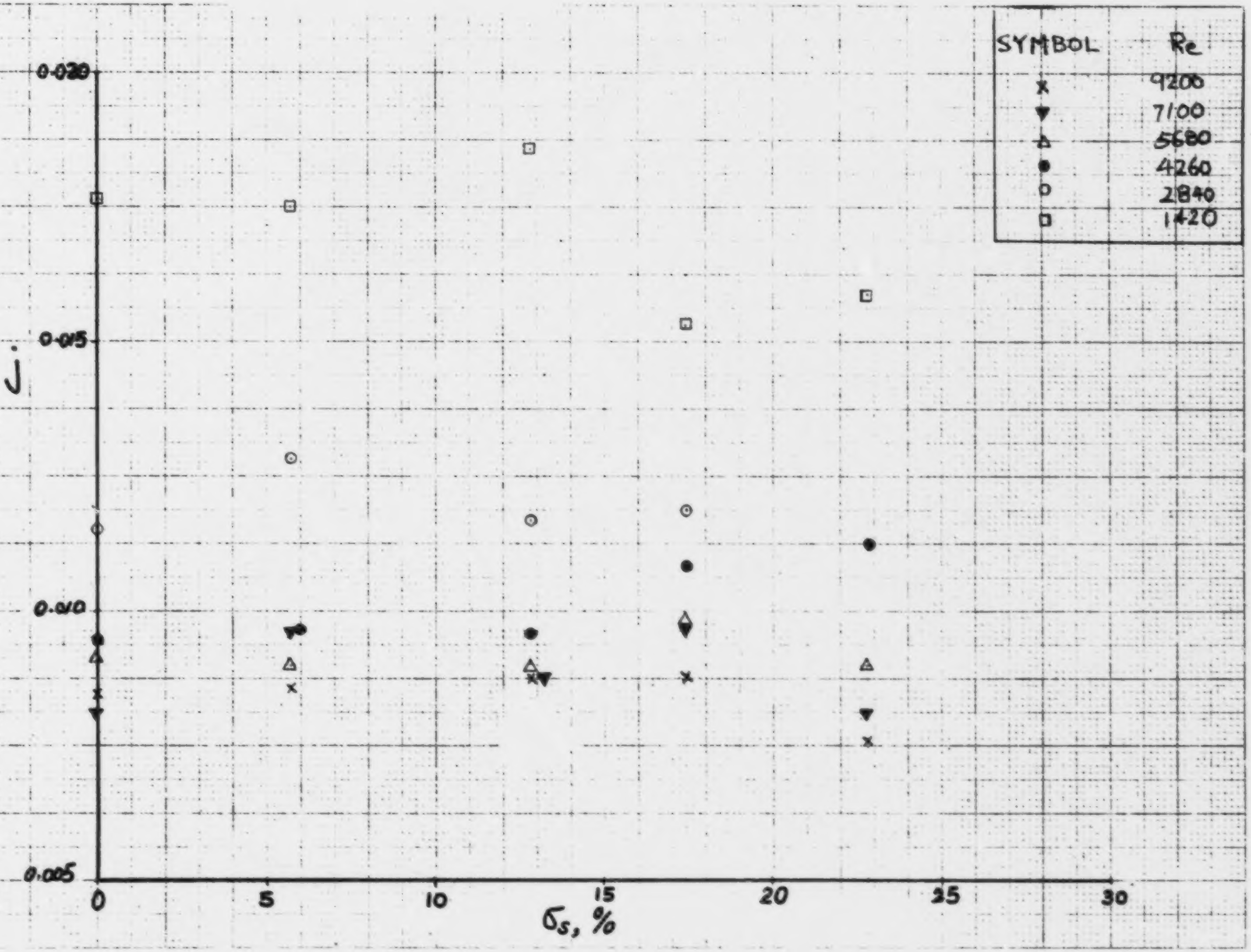

Fig. 26d. j versus σ_s for t/b=0.0665, staggered round holes.

20 Squares to the inch

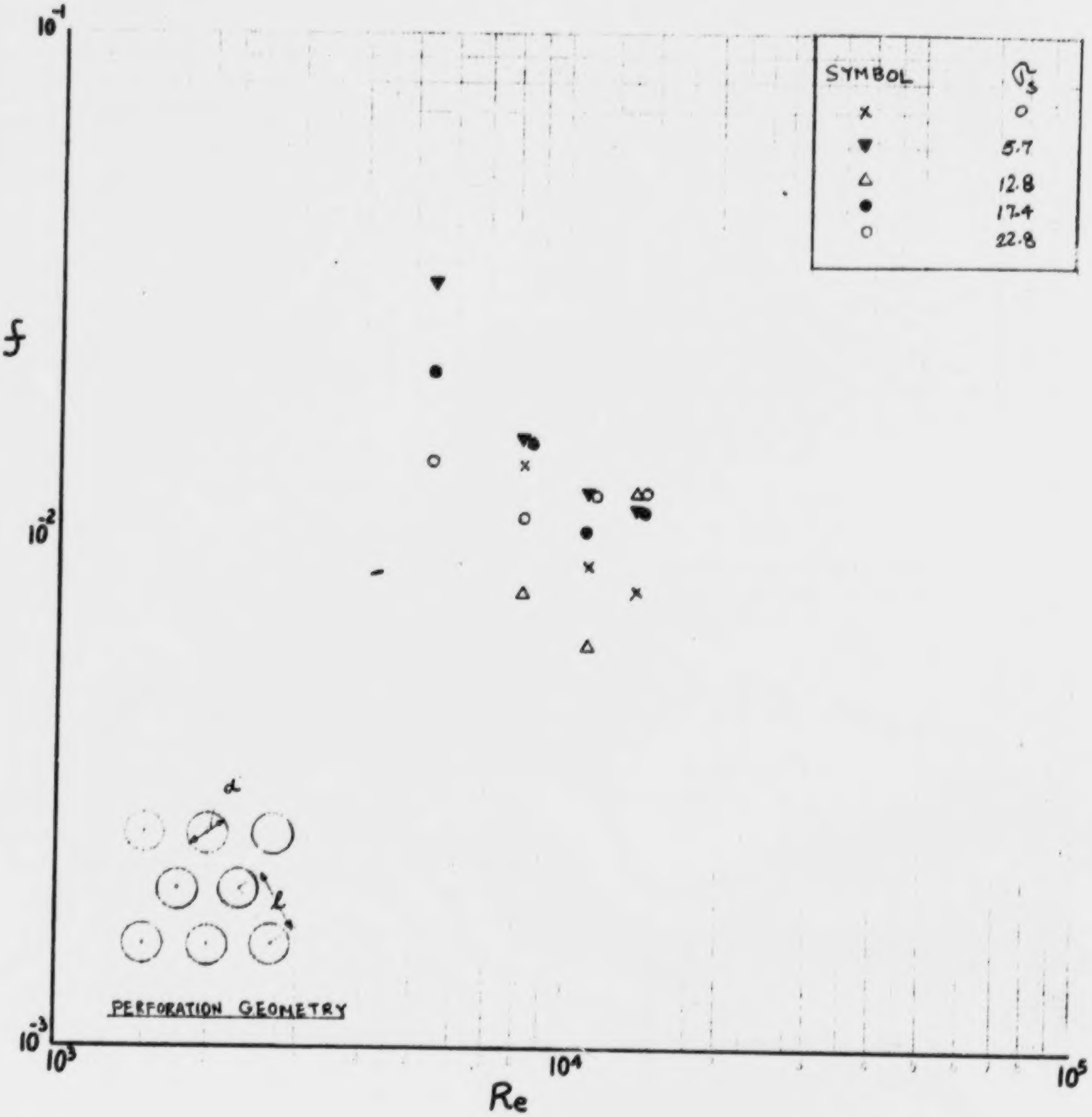

Fig. 27a. f versus Re, for t/b=0.0321, staggered round holes.

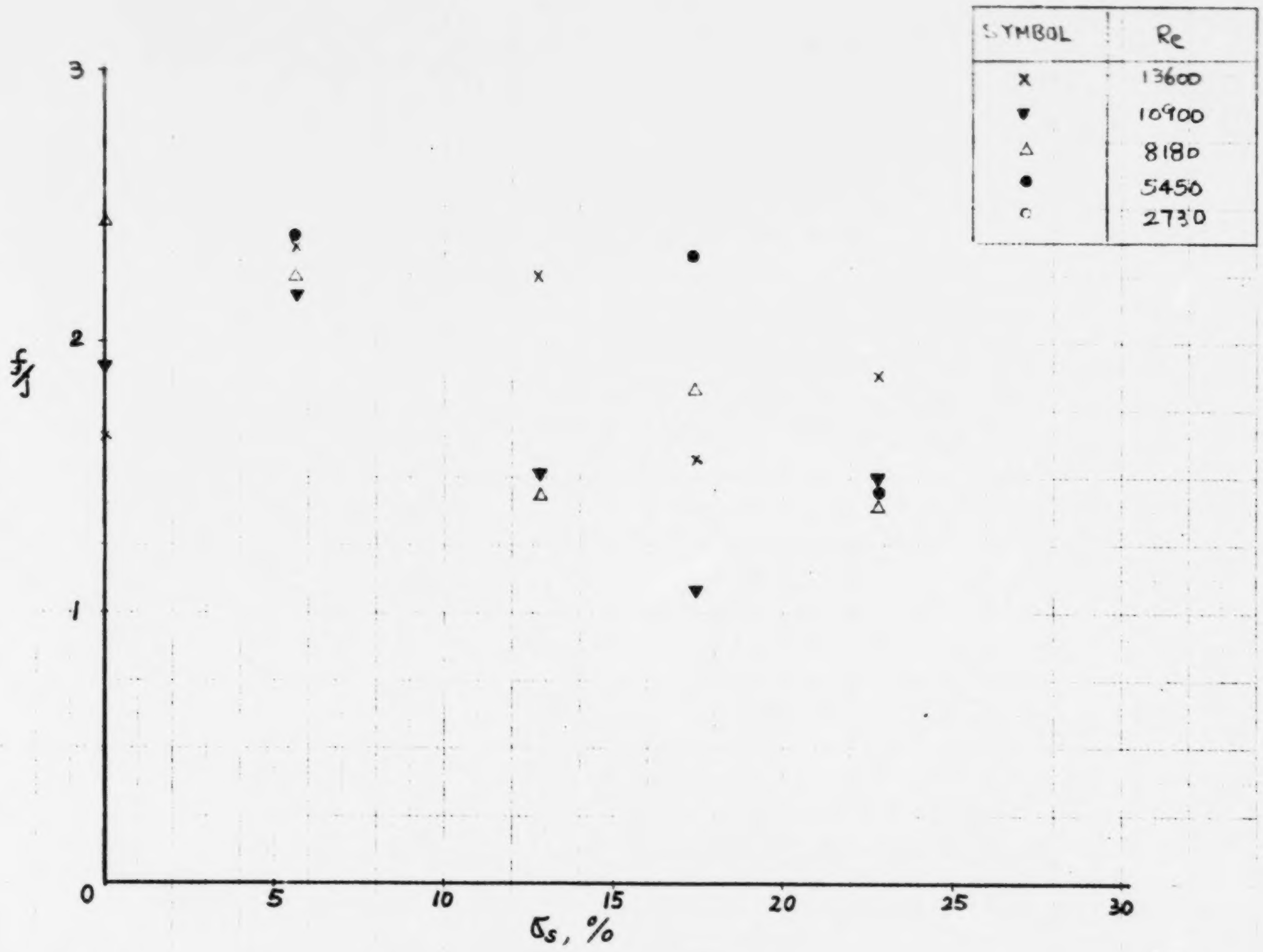

Fig. 27b. f/j versus σ_s, for t/b=0.0321, staggered round holes.

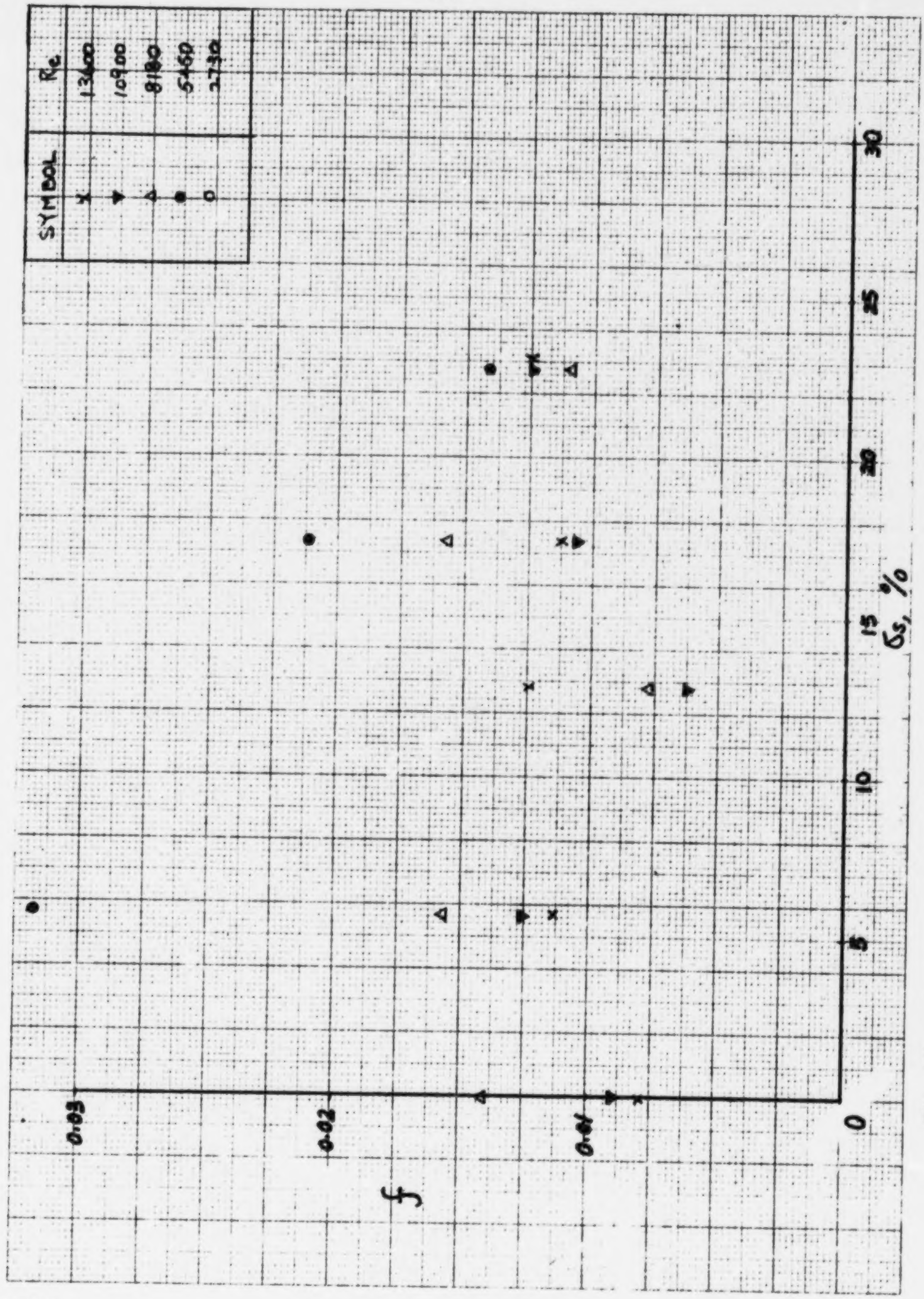

Fig. 27c. f versus σ_s, for t/b=0.0321, staggered round holes.

Squares to the Inch

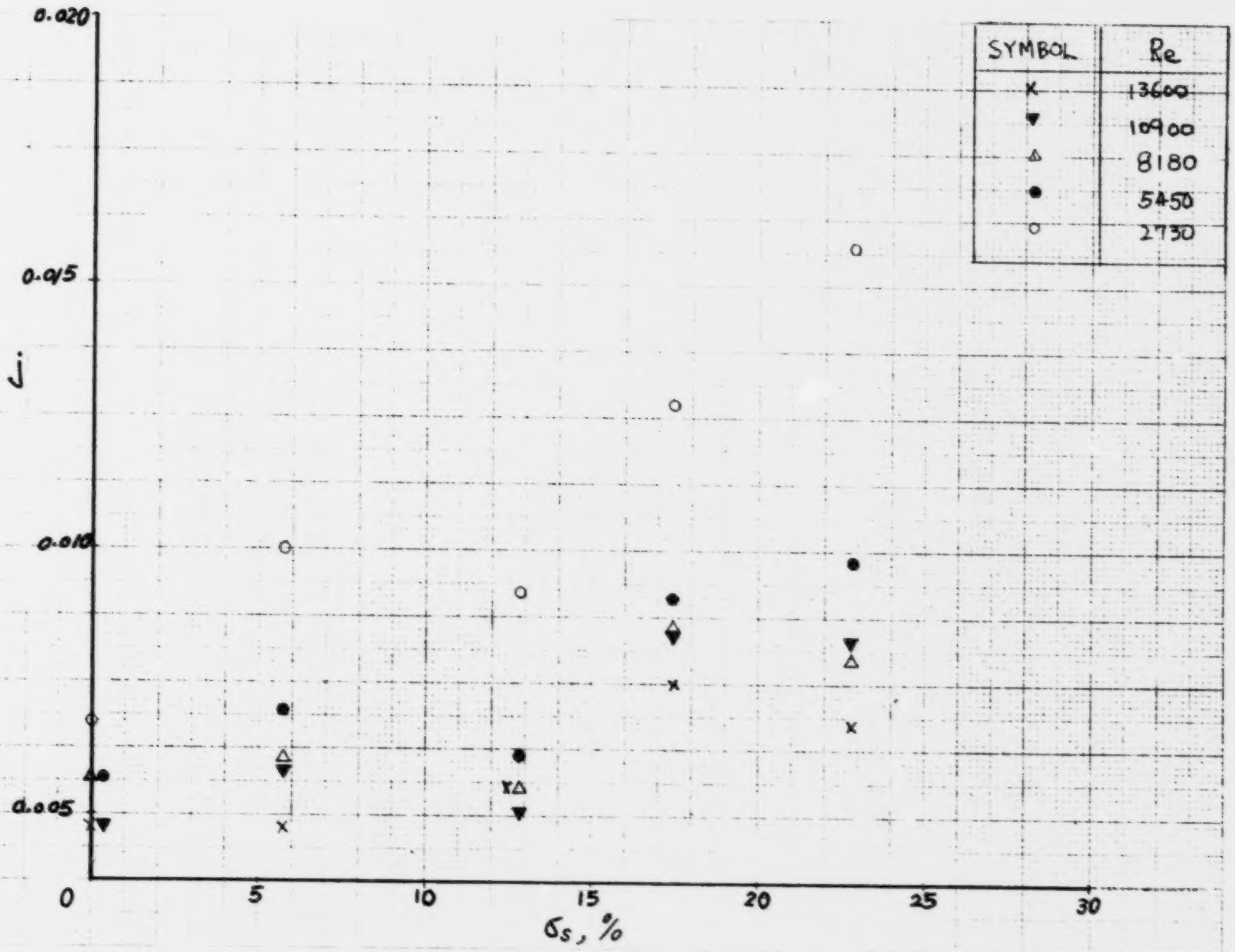

Fig. 27d. j versus σ_s for t/b=0.0321, staggered round holes.

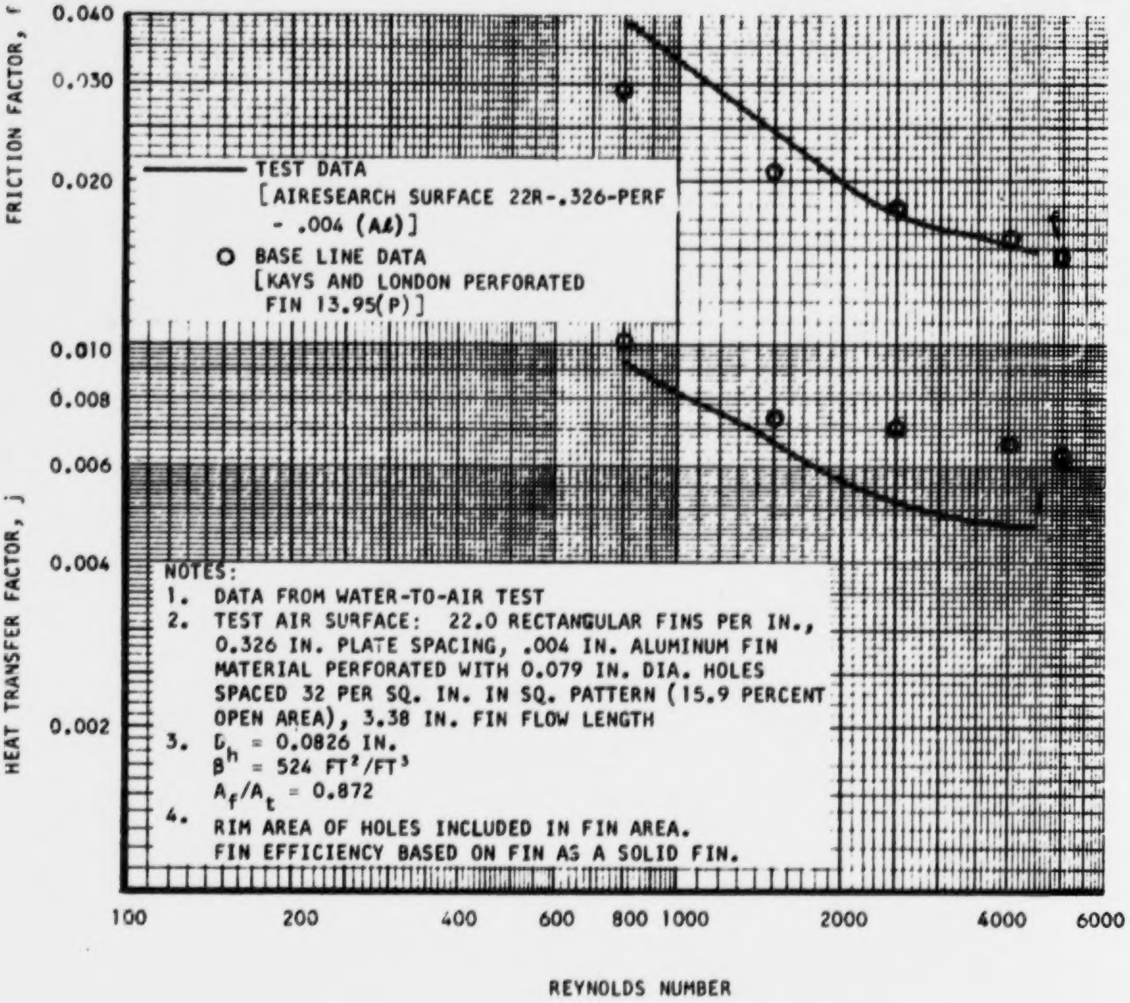

Fig. 28. Performance parameters 22 FPI perforated fin [5].

```
                DIMENSION TP(9),TA(5),FACT(3,4),TT(241),Z(14)
                REAL L16,L25,L34,K,RV(241)
                DATA FACT/.1,.15,.17,.08,.07,.06,.17,.125,.1, .6,.5,.[illegible]/
                READ(5,9230) (Z(I),I=1,14)
                DO 1000 I=1,43
                J=(I-1)*7+1
                [illegible]=J+6
                READ(5,[illegible]) (RV(J),TT(J),J=[illegible],[illegible])
          1000  CONTINUE
          1008  PRINT 9[illegible]
                READ 9000,[illegible]
                GAP=G[illegible]/12.
                PRINT [illegible]
                READ [illegible],(TP(I),I=1,9)
 ①              DO 1017 I=1,9
                CALL STIPE(RV,TT,TP(I))
          1017  CONTINUE
                PRINT 9025
                READ [illegible],(TA(I),I=1,5)
                DO 1020 I=1,5
                CALL STIPE(RV,TT,TA(I))
          1020  CONTINUE
                PRINT 9030
                READ 9000,TI ,RXII,RVIIT,RVOIT,V
                CALL STIPE(RV,TT,TI )
                T=118.
                T=1./384.
 ②              GAP=GAPP-T
                SIGMA=1./(1.+(T/GAPP))
                R=GAP/(AK(.5*LPP))
 ③              RHO=.0172
                VCURR=R/SIG
 ④              PE=4.*RVCURR/[illegible]
                L16=1./64.
                L25=1./12.
                L34=1./8.
                TPA=(.5*(ABS(TP(1)-TP(2))*L16+ABS(TP(2)-TP(3))*L16
 ⑤             1+ABS(TP(3)-TP(4))*L25+ABS(TP(4)-TP(5))*L34
               2+ABS(TP(5)-TP(6))*L34+ABS(TP(6)-TP(7))*L25
               3+ABS(TP(7)-TP(8))*L16+ABS(TP(8)-TP(9))*L16)+TP(2)*L16
               4+TP(3)*L16+TP(4)*L25+TP(5)*L34+TP(6)*L34+TP(7)*L25
               5+TP(8)*L16+TP(9)*L16)/.5
                L=1./768.
 ⑥              RERDD=RVAR(ABS(TP(1)-TP(2))+ABS(TP(8)-TP(9)))/L16
                RIREA=RVOIT*RVOIT*.3412
                RTOTAL=RCURR+RRADI
                IF(GAPP .EQ. 1./48.) AREA=(TA(1)+2.*TA(4)+TA(2))*GAP/4.
                IF(GAPP .EQ. 1./24.) AREA=(TA(1)+2.*TA(4)+3.*TA(2)+2.*TA(5))
 ⑦             1*GAP/8.
                IF(GAPP .EQ. 1./12.) AREA=(TA(1)+2.*TA(4)+3.*TA(2)+6.*TA(5)+
               14.*TA(3))*GAP/16.
 ⑧              TAVT=AREA/GAP
                TBULK=.5*(TI +TOUT)
 ⑨              DELT=TPA-TBULK
                H=2.*RTOTAL/DELT
 ⑩              XU=.761*H/VCURR
                X11=2.76 *RX11
 ⑪              IF(GAPP .EQ. 1./12.) I=1
                IF(GAPP .EQ. 1./24.) I=2
                IF(GAPP .EQ. 1./48.) I=3
```

Reproduced from best available copy.

```
          PERC=(RF-2000.)/8000.
          AKC=FACT(I,1)+(FACT(I,3)-FACT(I,1))*PERC
⑪        AKE=FACT(I,2)+(FACT(I,4)-FACT(I,2))*PERC
          IF(RF .GT. 10000.) AKC=FACT(I,3)
          IF(RF .GT. 10000.) AKE=FACT(I,4)
          PLOSS=.0000000618*(VCORE**2)*(AKC-AKE)
          PCORE=P11-PLOSS
⑫        F=32500000.*PCORE*R/(VCORE**2)
⑬        FJ=F/HJ
          PRINT 9100
          PRINT 9110
          PRINT 9120,TP(1),TP(6),TA(2),PX11
          PRINT 9130,TP(2),TP(7),TA(3),SVOLT
          PRINT 9140,TP(3),TP(8),TA(4),PVOLT
          PRINT 9150,TP(4),TP(9),TA(5),V
          PRINT 9160,TP(5),TA(1),TIN
          PRINT 9100
⑭        PRINT 9300
          PRINT 9310,R,VCORE,RF
          PRINT 9320,TPA,PRADD,POWER
          PRINT 9330,PTOTAL,AREA,TOUT
          PRINT 9340,TBULK,DELT,H
          PRINT 9350,HJ,P11,PLOSS
          PRINT 9360,PCORE,F,FJ
          PRINT 9100
          GO TO 1005
     8000 FORMAT(9H GAP (IN))
     8010 FORMAT(17H TP(1)-TP(9) (MV))
     8020 FORMAT(36H TA(9),TA(10),TA(1),TA(2),TA(3) (MV))
     8030 FORMAT(37H TIN (MV),PX11,SVOLT,PVOLT,V (FT/MIN))
     9000 FORMAT(9F14.5)
     9100 FORMAT(1H1)
     9110 FORMAT(6H INPUT,//)
     9120 FORMAT(1H ,7HTP(1) =,F7.2,2X,7HTP(6) =,F7.2,2X,7HTA(10)=,F7.2,2X,
         17HPX11   =,F10.4)
     9130 FORMAT(1H ,7HTP(2) =,F7.2,2X,7HTP(7) =,F7.2,2X,7HTA(1) =,F7.2,2X,
         17HSVOLT =,F10.4)
     9140 FORMAT(1H ,7HTP(3) =,F7.2,2X,7HTP(8) =,F7.2,2X,7HTA(2) =,F7.2,2X,
         17HPVOLT =,F10.4)
     9150 FORMAT(1H ,7HTP(4) =,F7.2,2X,7HTP(9) =,F7.2,2X,7HTA(3) =,F7.2,2X,
         17HV      =,F10.4)
     9160 FORMAT(1H ,7HTP(5) =,F7.2,2X,7HTA(9) =,F7.2,2X,7HTIN    =,F7.2)
     9220 FORMAT(7(F6.3,F5.0))
     9230 FORMAT(8F6.2,/4F6.2,2F6.4)
     9300 FORMAT(7H OUTPUT,//)
     9310 FORMAT(1H ,8HR       =,F12.4,2X,8HVCORE   =,F12.4,2X,8HRF      =,F12.4)
     9320 FORMAT(1H ,8HTPA     =,F12.4,2X,8HPRADD   =,F12.4,2X,8HPOWER   =,F12.4)
     9330 FORMAT(1H ,8HPTOTAL  =,F12.4,2X,8HAREA    =,F12.4,2X,8HTOUT    =,F12.4)
     9340 FORMAT(1H ,8HTBULK   =,F12.4,2X,8HDELT    =,F12.4,2X,8HH       =,F12.4)
     9350 FORMAT(1H ,8HHJ      =,F12.4,2X,8HP11     =,F12.4,2X,8HPLOSS   =,F12.4)
     9360 FORMAT(1H ,8HPCORE   =,F12.4,2X,8HF       =,F12.4,2X,8HF/HJ    =,F12.4)
          END
```

Reproduced from best available copy.

```
   SUBROUTINE SINTER(MV,TT,TEM)
   REAL MV(231)
   DIMENSION TT(221)
   DO 1000 I=1,231
   IF(TEM .LE. MV(I)) GO TO 1010
1000 CONTINUE
1010 J=I-1
   TEM=TT(J)+(TEM-MV(J))/(MV(I)-MV(J))
   RETURN
   END
                                                  122 LINES PRINTED
```

```
$SIGNON K2E4          T=10          CARDS=750
**LAST SIGNON WAS: 09:15.15    04-22-72
 USER "K2E4" SIGNED ON AT   09:26.40 ON 04-22-72
$LIST DATA
     1        15.5  17.5  15.5  16.0  16.0  19.0  19.0  19.0
     2        19.0  22.0  22.0  44.0  .305  .375
     3         .832  70.  .854  71.  .877  72.  .899  73.  .922  74.  .944  75.  .967  76.
     4         .990  77. 1.012  78. 1.035  79. 1.057  80. 1.080  81. 1.103  82. 1.126  83.
     5        1.148  84. 1.171  85. 1.194  86. 1.217  87. 1.240  88. 1.263  89. 1.286  90.
     6        1.309  91. 1.332  92. 1.355  93. 1.378  94. 1.401  95. 1.424  96. 1.448  97.
     7        1.471  98. 1.494  99. 1.517 100. 1.540 101. 1.563 102. 1.587 103. 1.610 104.
     8        1.633 105. 1.657 106. 1.680 107. 1.704 108. 1.727 109. 1.751 110. 1.774 111.
     9        1.798 112. 1.821 113. 1.845 114. 1.869 115. 1.893 116. 1.916 117. 1.940 118.
    10        1.963 119. 1.987 120. 2.011 121. 2.035 122. 2.059 123. 2.083 124. 2.107 125.
    11        2.131 126. 2.154 127. 2.178 128. 2.202 129. 2.226 130. 2.250 131. 2.274 132.
    12        2.298 133. 2.322 134. 2.346 135. 2.370 136. 2.394 137. 2.418 138. 2.443 139.
    13        2.467 140. 2.491 141. 2.516 142. 2.540 143. 2.565 144. 2.589 145. 2.614 146.
    14        2.638 147. 2.663 148. 2.687 149. 2.711 150. 2.736 151. 2.760 152. 2.785 153.
    15        2.810 154. 2.835 155. 2.859 156. 2.884 157. 2.908 158. 2.933 159. 2.958 160.
    16        2.982 161. 3.007 162. 3.032 163. 3.057 164. 3.082 165. 3.107 166. 3.132 167.
    17        3.157 168. 3.182 169. 3.207 170. 3.232 171. 3.257 172. 3.282 173. 3.307 174.
    18        3.332 175. 3.357 176. 3.382 177. 3.407 178. 3.433 179. 3.458 180. 3.483 181.
    19        3.508 182. 3.534 183. 3.559 184. 3.584 185. 3.610 186. 3.635 187. 3.661 188.
    20        3.686 189. 3.712 190. 3.737 191. 3.762 192. 3.787 193. 3.813 194. 3.839 195.
    21        3.864 196. 3.890 197. 3.915 198. 3.941 199. 3.967 200. 3.993 201. 4.018 202.
    22        4.044 203. 4.070 204. 4.096 205. 4.122 206. 4.148 207. 4.174 208. 4.199 209.
    23        4.225 210. 4.251 211. 4.277 212. 4.303 213. 4.329 214. 4.355 215. 4.381 216.
    24        4.408 217. 4.434 218. 4.460 219. 4.486 220. 4.512 221. 4.538 222. 4.564 223.
    25        4.590 224. 4.617 225. 4.643 226. 4.670 227. 4.696 228. 4.722 229. 4.749 230.
    26        4.775 231. 4.801 232. 4.827 233. 4.854 234. 4.880 235. 4.907 236. 4.934 237.
    27        4.960 238. 4.987 239. 5.014 240. 5.040 241. 5.067 242. 5.094 243. 5.120 244.
    28        5.147 245. 5.174 246. 5.200 247. 5.227 248. 5.254 249. 5.280 250. 5.307 251.
    29        5.334 252. 5.361 253. 5.388 254. 5.415 255. 5.442 256. 5.469 257. 5.496 258.
    30        5.523 259. 5.550 260. 5.577 261. 5.604 262. 5.631 263. 5.658 264. 5.685 265.
    31        5.712 266. 5.739 267. 5.766 268. 5.794 269. 5.821 270. 5.848 271. 5.875 272.
    32        5.903 273. 5.930 274. 5.957 275. 5.985 276. 6.012 277. 6.040 278. 6.067 279.
    33        6.094 280. 6.122 281. 6.149 282. 6.177 283. 6.204 284. 6.232 285. 6.259 286.
    34        6.287 287. 6.314 288. 6.342 289. 6.370 290. 6.397 291. 6.425 292. 6.453 293.
    35        6.481 294. 6.508 295. 6.536 296. 6.564 297. 6.592 298. 6.620 299. 6.647 300.
END OF FILE
```

NOMENCLATURE

TP (9)	temperature of plate at points 1-9	MN, F
TA (5)	temperature of air at points 9,10,1,2,3	MV, F
FACT (3,4)	coefficients of expansion and contraction through an opening	
Z (14)	values read from first two lines of data fill, which have no meaning to program	
TT (231)	temperature readings corresponding to millivolts in MV (231)	F
MV (231)	millivolt readings corresponding to temps in TT (231)	MV
L16	distance between plate thermocouples 1 & 2; 2& 3, 7 & *, and 8 & 9	FT
L25	distance between plate thermocouples 3 & 4; 6 & 7	FT
L34	distance between plate thermocouples 4 & 5; 5 & 6	FT
K	thermal conductivity of plate	BTU/HR-FT-F
GAP	1) center to center distance between plates 2) actual distance between plates	IN FT
GAPP	center to center distance between plates	FT
TIN	inlet temperature of air	MV, F
PX11	pressure at point 1-1	PSIx10^{-1}
SVOLT	shunt voltage	VOLTSx10^{-2}
PVOLT	voltage from power source	VOLTSx10^{-2}
V	velocity	FT/MIN
T	thickness of plate	FT
SIGMA	area reduction factor due to plates in core	
R	hydraulic radius	FT

VCORE	corrected velocity due to area reduction in core	
ANU	viscosity of air	SQFT/MIN
RE	Reynolds number	
TPA	average plate temperature	F
A	cross sectional area of plate	SQFT
PRADD	power added from ends of plate	BTU/HR
POWER	power supplied to plate	BTU/HR
PTOTAL	power supplied to plate plus power from ends	BTU/HR
AREA	area under curve of air temperature vs. gap	F-FT
TOUT	temperature of air at outlet	F
TBULK	average temperature of air	F
DELT	difference between average temperature of plate and average temperature of air	F
H	heat transfer coefficient	BTU/HR-SQFT-F
FJ	ratio of F to HJ	
P11	pressure at point 1-1	"H_2O
PERC	percentage between Reynolds numbers for coefficient of expansion and contraction	
AKC	coefficient of contraction	
AKE	coefficient of expansion	
PLOSS	pressure loss in core	"H_2O
PCORE	core pressure	"H_2O
F	Fanning friction factor	
HJ	heat transfer factor	

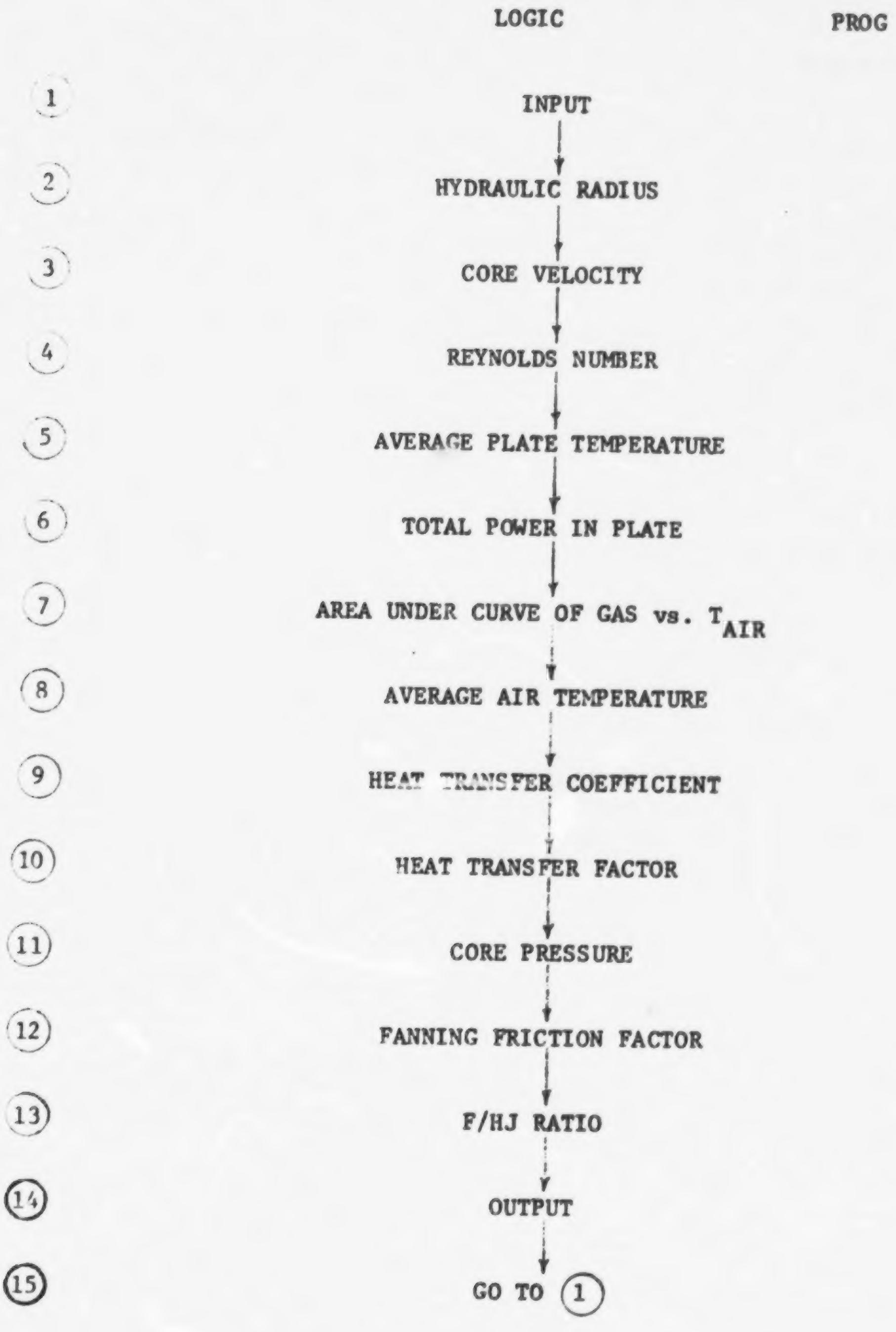
LOGIC
PROG
① INPUT
② HYDRAULIC RADIUS
③ CORE VELOCITY
④ REYNOLDS NUMBER
⑤ AVERAGE PLATE TEMPERATURE
⑥ TOTAL POWER IN PLATE
⑦ AREA UNDER CURVE OF GAS vs. T_{AIR}
⑧ AVERAGE AIR TEMPERATURE
⑨ HEAT TRANSFER COEFFICIENT
⑩ HEAT TRANSFER FACTOR
⑪ CORE PRESSURE
⑫ FANNING FRICTION FACTOR
⑬ F/HJ RATIO
⑭ OUTPUT
⑮ GO TO ①

OPERATING INSTRUCTIONS PROG

(ASSUMES PROG IS STORED IN COMPILED FORM CALLED PROG1; AND FILE 'DATA' IS ALSO STORED)

(ASSUMED OPERATOR HAS WORKING KNOWLEDGE OF TELETYPE AND MICHIGAN TERMINAL SYSTEM)

① SIGN ON TO TELETYPE

② WHEN TERMINAL IS READY TYPE THE FOLLOWING:

```
#RUN PROG1  5 = DATA
```

③ TERMINAL WILL TYPE:

```
#EXECUTION BEGINS
        GAP (IN)*
```

④ USER WILL TYPE IN A GAP AND HIT 'RETURN' BUTTON. TERMINAL WILL TYPE:

```
TP(1)-TP(9)  (MV)
```

⑤ USER WILL TYPE IN TP(1)-TP(9) IN MILLIVOLTS, WITH A COMMA BETWEEN EACH PIECE OF DATA. THIS WILL ALLOW THE USER TO AVOID FORMATTED INPUT. USER WILL THEN HIT 'RETURN'.

⑥ THE REMAINING DATA IS TYPED IN AS THE TERMINAL ASKS FOR IT. WHEN ALL THE DATA IS IN, THE TERMINAL WILL PRINT THE OUTPUT AND RETURN TO ASK FOR A NEW GAP AND MORE DATA.

⑦ IF THERE IS MORE DATA, INPUT IT: IF NOT, HIT 'BREAK', AFTER MESSAGE, HIT 'BRK-RLS', THEN SIGN OFF.

---

* ALL DATA IS REAL, AND DECIMAL POINTS MUST BE TYPED.

DATA FILES PROG

① DATA

The first two lines of 'DATA' contain information used for another program. They have no use here, but are bypassed by reading into array Z by the following format:

```
FORMAT (8F6.2,/4F6.2, 2F6.4)
```

The rest of the file contains a conversion chart for changing millivolt readings of temperature to Fahrenheit. All temperatures inputted are done so in millivolts, and the program converts them to °F. The chart starts at 70°F and goes to 300°F. Each line is stored in the following format:

```
                MV    °F
                ↓     ↓
FORMAT (7(F6.3, F5.0))
```

There are 33 lines in this chart and 35 in the complete file.

EXPLANATION OF LOGIC PROG

① INPUT

The program begins by setting up the array FACT and then reads the file 'DATA'. The program will then ask for the following information which should be typed on separate lines.

1) GAP (IN)
2) TP(1)-TP(9) (MV)
3) TA(9), TA(10), TA(1), TA(2), TA(3) (MV)
4) TIN(MV), PX11, SVOLT, PVOLT, V(FT/MIN)

The information is read in and all temperatures are converted to °F.

② HYDRAULIC RADIUS (R)

1) K=118. BTU/HR-FT-F
2) T=1/384. FT
3) GAP=GAPP-T FT
4) SIGMA=1/(1+T/GAP)
5)

$$4R = \frac{4*W*GAP}{2*(W+GAP)}, \quad W=.5 \text{ FT}$$

$$R = \frac{GAP}{4*(.5+GAP)} \qquad \text{FT}$$

③ CORE VELOCITY (VCORE)

1) $ANU = .17 \times 10^{-3} \frac{FT^2}{SEC} \times \frac{60SEC}{MIN} = .0102 \quad \frac{FT^2}{MIN}$

2) $VCORE = \frac{V}{SIGMA}$ FT/MIN

④ REYNOLDS NUMBER

1) $Re = \frac{4*R*VCORE}{ANU}$

⑤ AVERAGE PLATE TEMPERATURE

TPA is calculated taking the area under the curve of TP(9) VS. LENGTH of plate, and dividing it by the length of the plate.

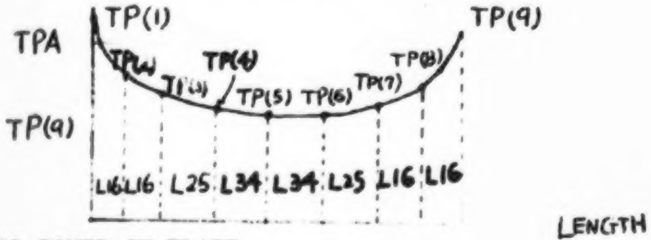

⑥ TOTAL POWER IN PLATE

1) A=T*L=.(1/384)*(1/2)=1/768 FT^2

2) PRADD=K*A*(LTP(1)-TP(2)/+/TP(8)-TP(9)/)/L16

$$=\frac{BTU^*}{HR} \qquad BTU/HR$$

3) POWER=PVOLT*SVOLTX.3412

$$= \frac{VOLT\times10^{+2}\times VOLT\times10^{+2}}{10^{+5}OHM} \times 3.412 \frac{BTU}{HR\ WATT} = \frac{BTU}{HR}$$

4) PTOTAL=POWER + PRADD $\frac{BTU}{HR}$

⑦ AREA UNDER CURVE OF GAP VS. T_{AIR}

1) IF GAPP=1/48 FT (t/b=0.141)

AREA = (TA(1) + 2TA(4) + TA(2)) * GAP/4. FT-F

IF GAPP=1/24 FT (t/b=0.0665)

AREA + (TA(1) + 2TA(4) + 3TA(2) + 2TA(5)) * GAP/8 FT-F

IF GAPP=1/12 FT (t/b=0.0321)

AREA =(TA(1) + 2TA(4) + 3TA(2) +6TA(5) +4TA(3))x GAP/16 FT-F

⑧ AVERAGE AIR TEMPERATURE

1) TOUT = AREA/GAP F

2) TBULK = (TOUT + TIN) x .5 F

⑨ HEAT TRANSFER COEFFICIENT

1) DELT=TPA-TBULK F

2) $H=PTOTAL/(A*DELT)$, $A=L^2*2$, $L=.5$

$$H= \frac{2*PTOTAL}{DELT} \quad \frac{BTU}{FT^2 HR°F} \qquad BTU/HR\text{-}FT^2\text{-}F$$

⑩

1) $$HJ= \frac{(PR)^{2/3}}{\rho C_p} \frac{H}{VCORE}, \quad PR=.72 \quad \rho=.074 \quad LBM/FT^3, \quad C_p=.24 \quad BTU/LBM°F$$

$$= \frac{(.72)^{2/3}}{.074x.24x60} \frac{H}{VCORE}$$

⑪ CORE PRESSURE

1) P11=2.768xPX11x "H_2O "H_2O

2) PLOSS=.0000000618 x (VCORE**2) * (AKC-AKE) "H_2O

3) PCORE=P11-PLOSS "H_2O

⑫

1) $$F = \frac{PCORE}{1/2Gx \rho xVCORE^2 (\frac{L}{R})}, \quad L=.5\ FT, \quad G=32.2\ LBMxFT/LBFxSEC^2$$

$$= \frac{PCORExRx64.4}{.074x.5x(VCORE**2)} \qquad \frac{"H2O\ x\ FT^2\ x\ MIN}{LBFxSEC^2}$$

$$= \frac{64.4x3600x144xPCORExR}{7.4x5.x2.768x(VCORE**2)}$$

$$= \frac{32500000.*PCORE*R}{(VCORE**2)}$$

⑬

1) FJ = F/HJ

⑭ OUTPUT

Program prints output sheet showing input and answers.